AD NUMBER

ADB019978

LIMITATION CHANGES

TO:

Approved for public release; distribution is unlimited.

FROM:

Distribution authorized to U.S. Gov't. agencies only; Test and Evaluation; NOV 1976. Other requests shall be referred to Air Force Armament Lab., Eglin AFB, FL.

AUTHORITY

AFATL ltr 23 Oct 1979

AFATL-TR-76-132, VOLUME III

DIGITAL GUIDED WEAPONS TECHNOLOGY VOLUME III: PROGRAMMABLE DIGITAL AUTOPILOT

MISSILE SYSTEMS DIVISION
HUGHES AIRCRAFT COMPANY
CANOGA PARK, CALIFORNIA 91304

NOVEMBER 1976

FINAL REPORT: AUGUST 1974-NOVEMBER 1976

AIR FORCE ARMAMENT LABORATORY
AIR FORCE SYSTEMS COMMAND • UNITED STATES AIR FORCE
EGLIN AIR FORCE BASE, FLORIDA

UNCLASSIFIED

SECURITY CLASSIFICATION OF THIS PAGE (When Data Entered)

REPORT DOCUMENTATION PAGE

READ INSTRUCTIONS BEFORE COMPLETING FORM

1. REPORT NUMBER: AFATL-TR-76-132-Volume III	2. GOVT ACCESSION NO.: -3
3. RECIPIENT'S CATALOG NUMBER:	
4. TITLE (and Subtitle): Digital Guided Weapons Technology, Volume III. Programmable Digital Autopilot,	5. TYPE OF REPORT & PERIOD COVERED: Final Report: August 1974 - to November 1976
	6. PERFORMING ORG. REPORT NUMBER: DGWT-0230-1-Vol-3
7. AUTHOR(s): J. A. Drgon, L. Pivar	8. CONTRACT OR GRANT NUMBER(s): F08635-75-C-0014
9. PERFORMING ORGANIZATION NAME AND ADDRESS: Missile Systems Division, Hughes Aircraft Company, Canoga Park, CA 91304 — 94 p.	10. PROGRAM ELEMENT, PROJECT, TASK AREA & WORK UNIT NUMBERS: Project No. 670B, Task No. 05, Work Unit No. 001
11. CONTROLLING OFFICE NAME AND ADDRESS: Air Force Armament Laboratory, Armament Development and Test Center, Eglin Air Force Base, Florida 32542	12. REPORT DATE: November 1976
	13. NUMBER OF PAGES: 98
14. MONITORING AGENCY NAME & ADDRESS (if different from Controlling Office): 670B 05	15. SECURITY CLASS. (of this report): UNCLASSIFIED
	15a. DECLASSIFICATION/DOWNGRADING SCHEDULE

16. DISTRIBUTION STATEMENT (of this Report)

Distribution limited to U.S. Government agencies only; this report documents test and evaluation; distribution limitation applied November 1976. Other requests for this document must be referred to the Air Force Armament Laboratory (DLMM), Eglin Air Force Base, Florida 32542.

17. DISTRIBUTION STATEMENT (of the abstract entered in Block 20, if different from Report)

18. SUPPLEMENTARY NOTES

Available in DDC.

19. KEY WORDS (Continue on reverse side if necessary and identify by block number)

Programmable Digital Autopilot
Pave Strike
Digital Guided Weapons Technology
GBU-15(V) Analog Autopilot

20. ABSTRACT (Continue on reverse side if necessary and identify by block number)

This report describes how current technology was used to produce a programmable digital autopilot (PDAP) capable to satisfying the requirements for three configurations of the Pave Strike glide weapon (GBU-15(V)).

A digital design for the three GBU-15(V) analog autopilots was produced. From this design, the requirements for a common PDAP were determined. Two Brassboard PDAPs were then built and evaluated--one in the Hybrid Simulation Laboratory at Eglin Air Force Base and one in a similar simulation ~ over

DD FORM 1 JAN 73 1473 EDITION OF 1 NOV 65 IS OBSOLETE

403 848

UNCLASSIFIED

SECURITY CLASSIFICATION OF THIS PAGE (When Data Entered)

20. ABSTRACT (Concluded)

at Hughes Aircraft Company.

The simulation validated the design concept.

PREFACE

This report was prepared by the Missile Systems Division, Hughes Aircraft Company, Canoga Park, California 91304, under Contract No. F08635-75-C-0014 with the Air Force Armament Laboratory, Armament Development and Test Center, Eglin Air Force Base, Florida. Major Robert L. Haney (DLMM) monitored the program for the Armament Laboratory. This effort was conducted during the period from August 1974 to November 1976.

This report consists of three volumes. Volume I contains Digital Processor System Studies. Volume II is concerned with System Simulations. Volume III deals with Programmable Digital Autopilot. This is Volume III.

This technical report has been reviewed and is approved for publication.

FOR THE COMMANDER:

CLIFFORD H. ALLEN, JR., Colonel, USAF
Chief, Guided Weapons Division

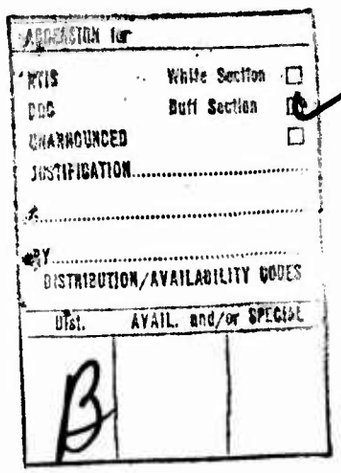

(The reverse of this page is blank.)

TABLE OF CONTENTS

LIST OF FIGURES

LIST OF FIGURES (Continued)

LIST OF FIGURES (Concluded)

LIST OF TABLES

(The reverse of this page is blank.)

SECTION I
SUMMARY

This report describes how current technology was used to produce a programmable digital autopilot (PDAP) capable of satisfying the requirements for three configurations of the Pave Strike glide weapon (GBU-15(V)).

To determine the requirements for a multiconfiguration PDAP, a digital design was produced for the three existing GBU-15(V) analog autopilots. From the digital design, the requirements for a digital autopilot processor were determined.

The PDAP design provides the autopilot control laws for three different aerodynamic configurations of the GBU-15(V) weapon system. These configurations are the large and the small wing cruciform airframes developed by Rockwell and the planar wing airframe developed by Celesco. (At the initiation of the PDAP program, the small winged version was a part of the GBU-15 family. It has now been dropped in favor of the large winged version. Also since the initiation of the program, Celesco has been acquired by Brunswick and Hughes has taken over their responsibility for the planar wing airframe system integration.) The autopilot control laws accept inputs from the autopilot sensors and generate the appropriate fin deflection commands for the actuators.

PDAP also provides the midcourse and terminal guidance laws, integrating the various seekers and sensors. For midcourse it receives steering signals from the distance measuring equipment (DME) and/or data link (D/L) guidance receivers, as well as information from the vehicle sensors used for midcourse control. It also receives signals from the electro-optical (EO) seeker (and in the future from the infrared (IR) imaging and laser seekers) and generates the appropriate terminal steering laws. The DME will also generate terminal guidance signals.

To provide the necessary integration of all of the guidance and control modes, PDAP performs all of the mode switching and timing functions. Figure 1 illustrates the principal PDAP functions and GBU-15(V) interfaces.

A brassboard of the PDAP was fabricated and delivered to the Air Force, along with the software required to implement the three different GBU-15(V) autopilots, in February 1975. Since then PDAP design characteristics for both the cruciform wing module (CWM) and the planar wing module (PWM) configurations have been evaluated in the Air Force Hybrid Simulation Laboratory at Eglin Air Force Base. A second brassboard underwent evaluation at Hughes Aircraft Company in a similar simulation. PDAP and analog autopilot comparison runs have been made for both trajectory runs

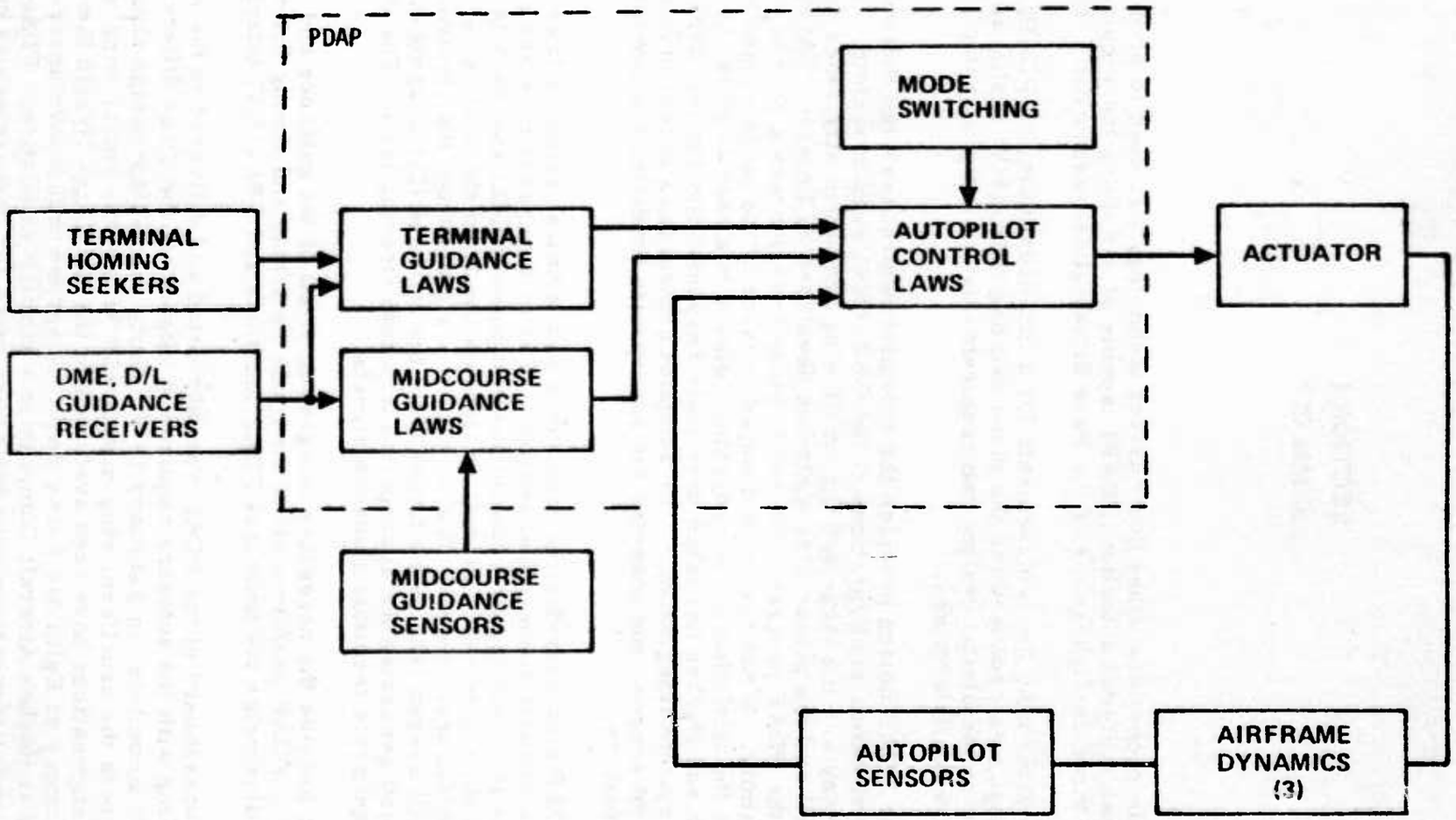

Figure 1. PDAP Functions and GBU-15 Interfaces

and step response inputs. The majority of the cases have compared favorably. The PWM gain margin comparisons were all within acceptable close agreement. The present PDAP hardware has three autopilot configurations programmed in software which demonstrate the modular weapon capability. The input and output interface for each of these autopilot configurations is the same. The PDAP software provides the desired autopilot configuration by means of missile identification through discrete logic inputs. The PDAP design requirements selected for the engineering development phase initiated in May 1975, were as follows:

• Iteration rates	
• High speed loops	400 Hz
• Slow speed loops	50 Hz
• Computation transport lag (including A/D and D/A)	0.6 ms
• Analog-to-digital converter quantization	12 bits
• Digital-to-analog converter quantization	9 bits
• Computation word length	16 bits
• Variable data memory	256 words
• Constant data memory	512 words
• Program memory	1024 words
• Instruction speed	
• Short	440 K OPS/sec
• Multiply/Divide	16 K OPS/sec

In each selection, the more conservative alternate was chosen for the design. Specifically, the 400 Hz sample rate was selected to allow margin for potential flexible airframe problems. A reduction to 200 Hz may be possible after these effects have been evaluated. Also the digital-to-analog quantization may possible be reduced to save cost, but tests with actual hardware are necessary before this change can be considered.

The memory requirements shown on the table are greater than the amount of memory actually used for the three autopilot configurations in PDAP. Since memory is purchased in blocks, the actual requirements were increased to the next largest block. Thus there is memory margin implied in these requirements.

The instruction speed shown is based on the program statement count for the actual program used in the PDAP software.

As a result of this part of the DGWT program the PDAP modular weapon capability has been demonstrated and a production design effort has been inititated for a programmable digital autopilot to be used on both the CWM and the PWM version of the GBU-15(V) vehicle.

SECTION II

INTRODUCTION

At Design Review 1 in October 1974, a preliminary set of functional requirements was presented for review. These requirements were based on preliminary and limited data about the GBU-15(V) vehicles. However, to meet the February delivery date for the PDAP hardware, the requirements were used as a basis for the hardware design. The description of the hardware is documented in Report Number DGWT 0150-1.

Four PDAP design requirements areas will be discussed in this report. First, the functional designs of the Rockwell and Celesco autopilots will be presented. Next, the definition of the functional interfaces between PDAP and the GBU-15(V) will be identified. Following this, the specific requirements for the input/output functions and the processor functions will be described. (For a complete description of the PDAP software development effort, see Report No. DGWT 0160-1).

Two PDAP brassboards have been fabricated. One was delivered to AFATL/DLMA to be integrated with their hybrid simulation facility. The other was retained at Hughes to be integrated with a similar hybrid simulator. In general, the two simulation studies validated the initial design requirements and only minor updating of the requirements was necessary.

Design validation was achieved by conducting hybrid simulation studies to obtain data for:

- Making analog and PDAP trajectory comparisons
- Determining dynamic response of autopilot modes
- Determining wordlength sensitivity

  (Analog-to-digital, digital-to-analog, computational)
- Making noise comparisons
- Making gain margin comparisons
- Measuring transport lag

PDAP hybrid six-degree-of-freedom simulation studies were conducted at both Hughes, Canoga Park and Eglin Air Force Base, Florida. Both simulation configurations are similar. Figure 2 shows a simplified block diagram representation of the hybrid simulation. The simulation at Eglin Air Force Base evaluated the first PDAP hardware which was delivered in February; the simulation at Hughes evaluated the second PDAP hardware system. Both simulations employed a PDAP system with an equivalent analog autopilot representation placed in parallel to the PDAP input-output interface. Sensor input information and the discrete input signals were sent to both autopilots simultaneously. Closed loop control of the system dynamics was provided by connecting the PDAP or analog autopilot flipper command signals to the fin servo inputs. The fin servo block shown in Figure 2 consists of four individual actuator models implemented with analog computer components. The equations associated with system dynamics include aero loading on the missile, sensor input variables, inertial reference equations, geometry equations, etc. These equations are implemented with both analog computer facilities and digital computer facilities. The hybrid simulation at Hughes also includes closed-loop EO steering signals which can be used with the different autopilot configurations.

The PDAP software tape contains both the PWM autopilot design representing the MGGB-II (Phase 1) configuration and the CWM autopilot design presently defined. Either of these autopilot configurations is available within the PDAP software and can be selected by means of discrete logic inputs (PWM or LWP). The equivalent analog autopilot representations are also available and are mechanized on separate analog computer boards. Input information for flight conditions (Mach, altitude, target location, in-flight mode switching time, etc.) are transmitted to the hybrid digital computer facility with punched card inputs. Output information from the hybrid simulation includes four strip chart recorders and digital printout as a function of flight time for such items as Mach, altitude, inertial missile position coordinates, etc.

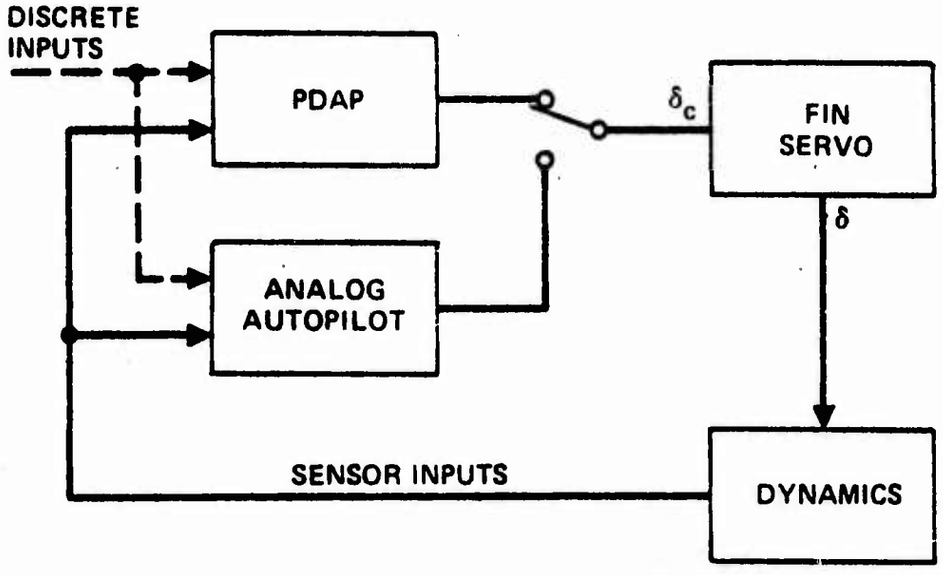

Figure 2. Hybrid Simulation Study Configuration

SECTION III

PDAP DESIGN REQUIREMENTS

GBU-15(V) AUTOPILOT

In order to meet the February PDAP delivery date, a firm autopilot functional design was required in early January so that the software could be developed and checked out. At that time, the autopilot information available to Hughes was for the Rockwell International Corporation (RIC) Preliminary Design Review (PDR) configuration of the CWM and the Celesco Phase I configuration of the PWM. The RIC PDR autopilot design was for an early aerodynamic configuration. Both airframe and autopilot have subsequently been changed. The Celesco Phase I autopilot design is for programmed vehicles only and has no terminal guidance. The design effort for the Phase II, or production autopilot, had not been initiated. Consequently, the software programmed in the PDAP brassboards reflects these earlier autopilot configurations. The new designs, however, are not expected to appreciably alter the PDAP design requirements. The Hughes defined common autopilot is shown in Figures 3 through 5 and the associated logic statements implemented in the logic control section are depicted by Boolean Algebra in Figures 6 through 8.

PDAP FUNCTIONAL INTERFACE

Figures 9, 10, and 11 define the PDAP functional interfaces. The block diagram has been updated slightly from the one presented in Design Review 1. The interfaces shown are for the autopilot functions only; insufficient information was available to permit a detailed identification of the interfaces required for the other non-autopilot functions.

Sixteen analog input signals have been identified for the autopilot and are listed in Tables 1 and 2 with the scale factors applicable to the GBU-15(V) and the simulator, respectively. These signals are the ones provided by the common sensor package, terminal seeker, and DME module. One growth signal has also been included. This is the roll command signal from the Laser seeker, which is used in conjunction with the Pave Tack pod. Three analog output signals are required as listed in Tables 3 and 4. These are the three fin deflection command signals.

Eleven discrete logic input signals as listed in Table 5 are used by the autopilot in order for it to generate the necessary mode switching logic.

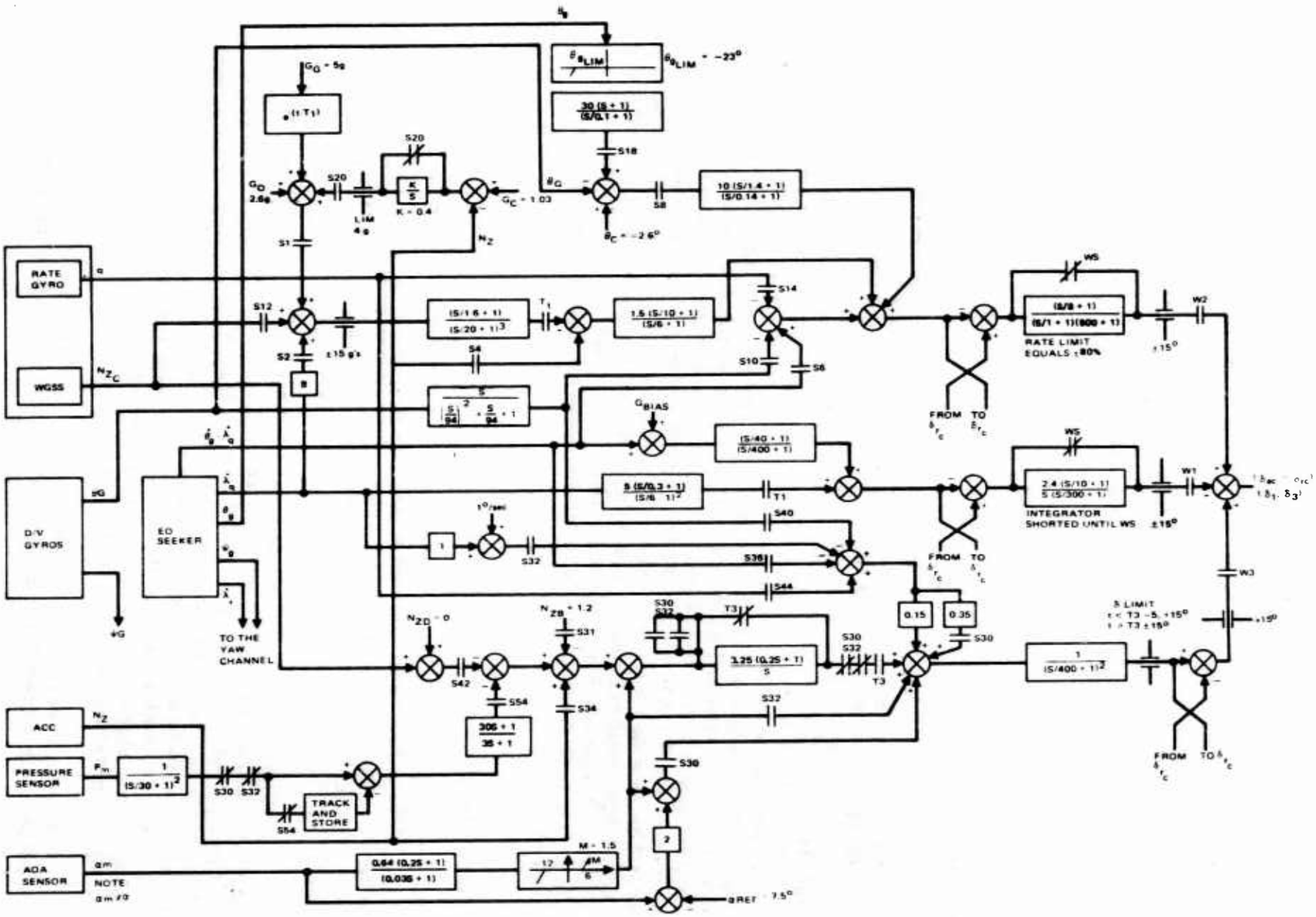

Figure 3. Pave Strike Autopilot - Pitch Channel

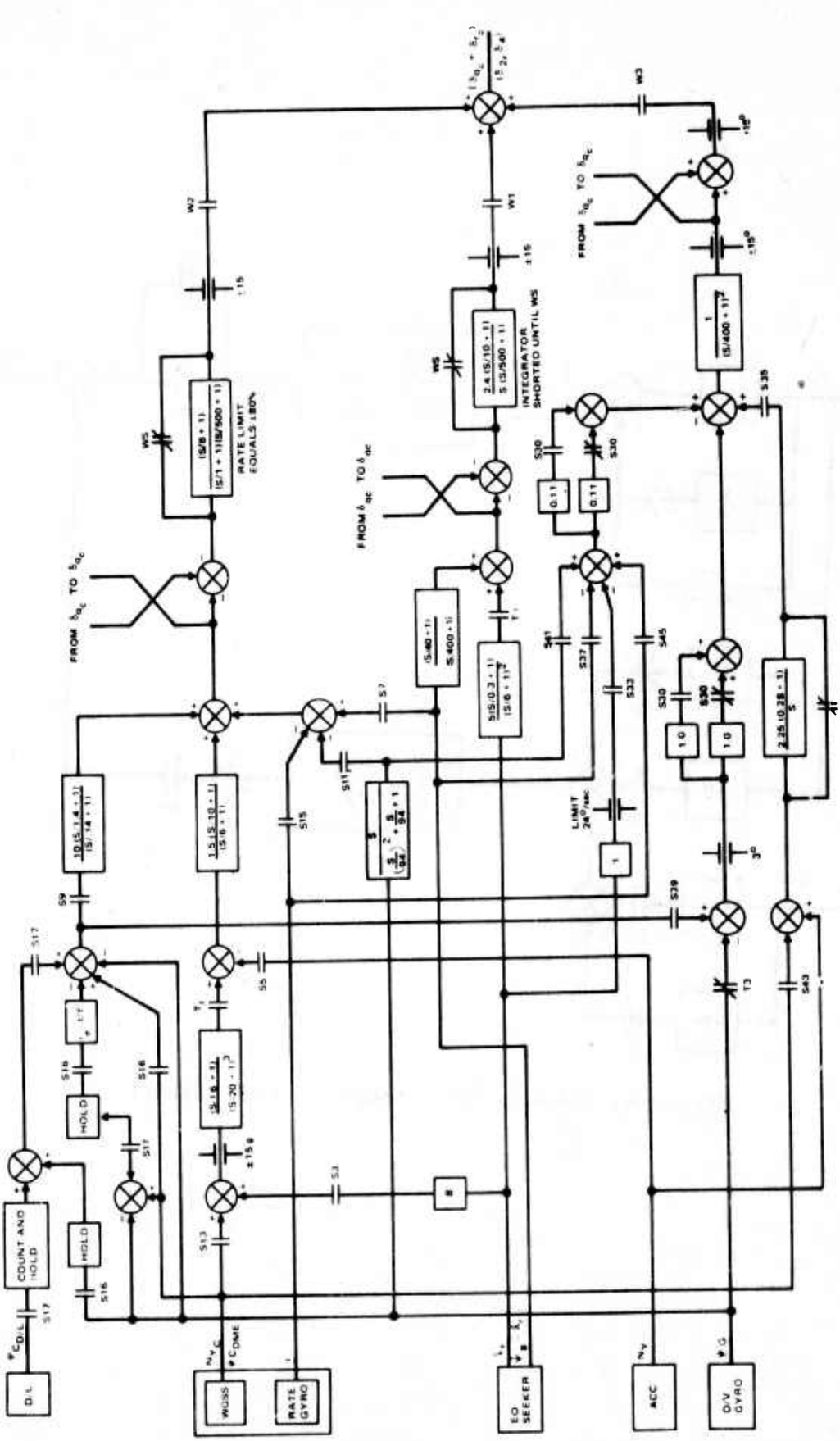

Figure 4. Pave Strike Autopilot - Yaw Channel

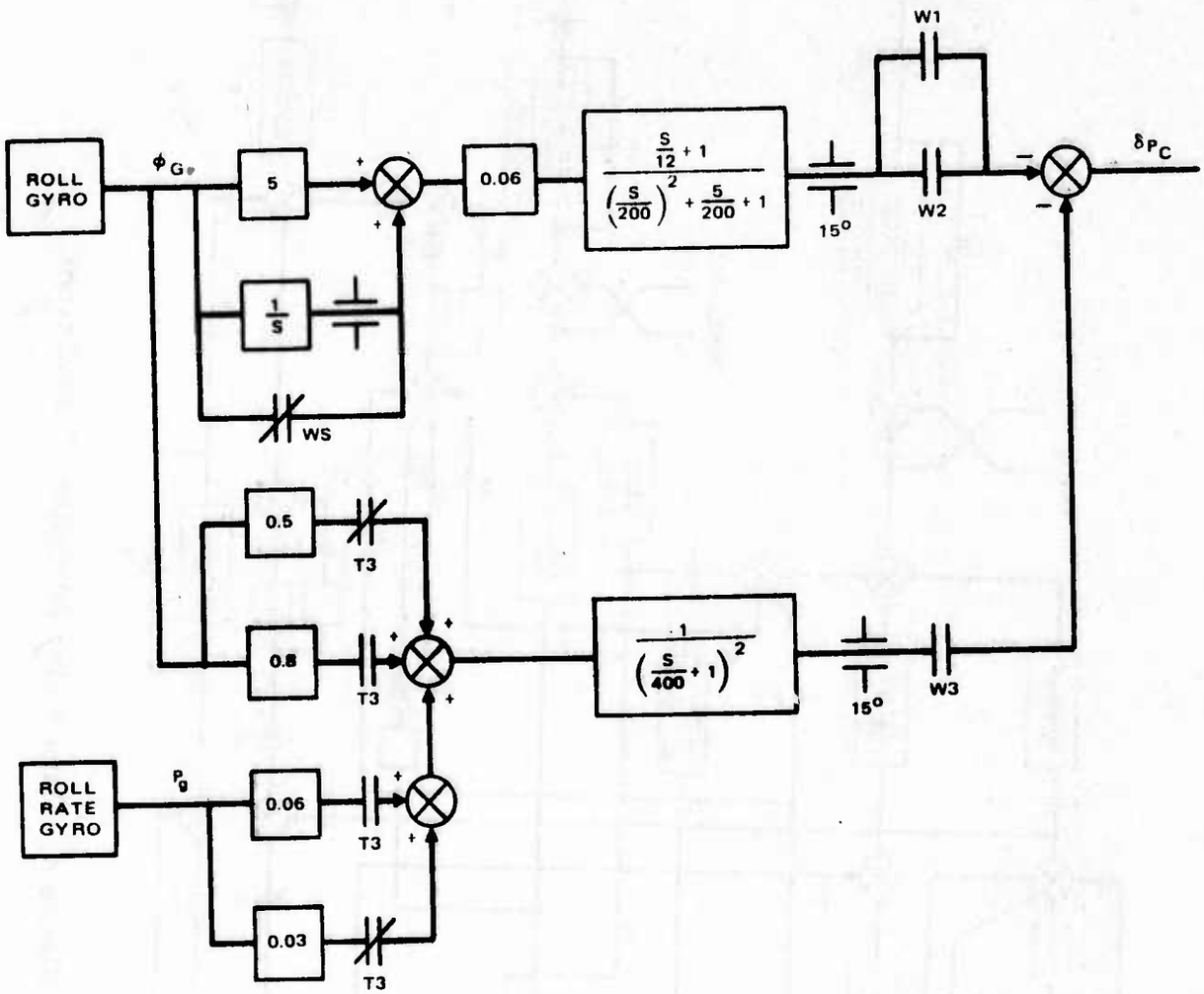

Figure 5. Pave Strike Autopilot - Roll Channel

LOGIC EVENTS	LOGIC STATEMENTS
EO TERMINAL ENABLE	EOT = $\overline{\text{DMET}}$ ● (EOT + LOSC + EOT COMMAND + LOBL)
TRANSITION MODE ENGAGE	TE = TE + (TRANSITION ENABLE ● $\overline{\text{DMET}}$)
TRANSITION TO TERMINAL SWITCH	LOSC = TE ● (LWP ● [$\dot{n}_g \angle -2.5\%$] + PWM ● [$\theta_g \leq -23°$])
D/L CONTROL	S17 = EO TAKEOVER + $\overline{\text{S16}}$ ● S17
DME CONTROL	S16 = $\overline{\text{EOT}}$ ● $\overline{\text{TE}}$ ● ($\overline{\text{EO TAKEOVER}}$ + DMEI ● $\overline{\text{S17}}$)
DME TERMINAL LATCH	DMET = S16 ● (EO INHIBIT COMMAND) + DMET
DME PITCHOVER	DMEP = DMET ● (PITCHOVER COMMAND) + DMEP
WEAPON SEPARATION	WS = ($\tau \geq 0$)

DISCRETE LOGIC INPUT READ ONLY FLAGS

EOT COMMAND

PITCHOVER COMMAND

LOBL

TRANSITION ENABLE

LWP

PWM

EO TAKEOVER

EO INHIBIT COMMAND

DMEI

Figure 6. Common Autopilot Logic

LOGIC EVENTS	LOGIC STATEMENTS
HEADING HOLD ENGAGED	$S9 = (t \geq 1.75) \bullet \overline{S3} \bullet \overline{DMEP}$
YAW ACCELERATION FEEDBACK	$S5 = (t \geq 1.75) \bullet (S3 + DMEP)$
YAW EO STEERING	$S3 = (t \geq 1.75) \bullet (EOT + TE)$
PITCH EO STEERING	$S2 = (t \geq 1.75) \bullet EOT$
PITCH ACCELERATION BIAS	$S1 = (t \geq 1.75) \bullet \overline{DMEP} \bullet (EOT + \overline{S8})$
PITCH ACCELERATION FEEDBACK	$S4 = (t \geq 1.75) \bullet (S1 + DMEP)$
PITCH ACCELERATION TRIM BIAS	$S20 = (t \geq 1.75) \bullet \overline{EOT}$
DME TERMINAL STEERING	$(S12, S13) = (t \geq 1.75) \bullet DMEP$
PITCH HOLD ENGAGE	$S8 = (t \geq 1.75) \bullet \overline{EOT} \bullet \overline{DMEP} \bullet [(\theta_G \leq -5°) + S8 + (t \geq 35\ SEC)]$
SEEKER LOOK ANGLE HOLD ACTIVATE	$S18 = (t \geq 1.75) \bullet \overline{EOT} \bullet TE \bullet [(\theta_G \leq -5°) + S8 + (t \geq 35\ SEC)]$
GUIDANCE LOOPS ACTIVATED	$T1 = 1.75\ SEC$
CWW AUTOPILOT ACTIVATION	$W1 = LWP$
SMALL WING PLAN AUTOPILOT ACTIVATED	$W2 = SWP$
PITCH AND YAW RATE GYRO	$(S14, S15) = DMEI$
PITCH AND YAW D/V GYRO DERIVED RATE	$(S10, S11) = \overline{DMEI} \bullet \overline{EOT} \bullet \overline{TE}$
PITCH AND YAW SEEKER DERIVED RATE	$(S6, S7) = \overline{DMEI} \bullet (EOT + TE)$

Figure 7. CWM Logic

LOGIC EVENTS	LOGIC STATEMENTS
HEADING HOLD ENGAGED	$S39 = (t \geq 2) \bullet \overline{S33} \bullet \overline{DMEP}$
YAW ACCELERATION CONTROL	$S35 = (t \geq 2) \bullet DMEP$
DME TERMINAL STEERING	$(S42, S43) = (t \geq 2) \bullet DMEP$
PITCH ACCELERATION FEEDBACK	$S34 = (t \geq 2) \bullet \overline{S30} \bullet \overline{S32}$
PITCH ACCELERATION BIAS	$S31 = (t \geq 2) \bullet \overline{S30} \bullet \overline{S32} \bullet \overline{DMEP}$
PITCH EO STEERING SIGNAL	$S32 = (t \geq 5) \bullet EOT$
YAW EO STEERING SIGNAL	$S33 = (t \geq 5) \bullet (EOT + TE)$
ANGLE OF ATTACK HOLD	$S30 = [(t \geq 5) \bullet [(\alpha \geq \alpha_0$ FOR 0.3 SEC) + S30] $\bullet \overline{DMEP} \bullet \overline{EOT}$
PRESSURE HOLD ENGAGED	$S54 = [(P \geq P_0$ AT t = 12SEC) + S54 + $(t \geq 28)] \bullet \overline{EOT} \bullet \overline{DMEP} \bullet \overline{S30}$
GUIDANCE LOOPS ACTIVATED	T3 = 2.0 SEC
PWW AUTOPILOT ACTIVATION	W3 = PWM
PITCH AND YAW RATE GYRO	(S44, S45) = DMEI
PITCH AND YAW D/V GYRO DERIVED RATE	$(S40, S41) = \overline{DMEI} \bullet EOT \bullet TE$
PITCH AND YAW SEEKER DERIVED RATE	$(S46, S47) = \overline{DMEI} \bullet (EOT + TE)$

Figure 8. PWM Logic

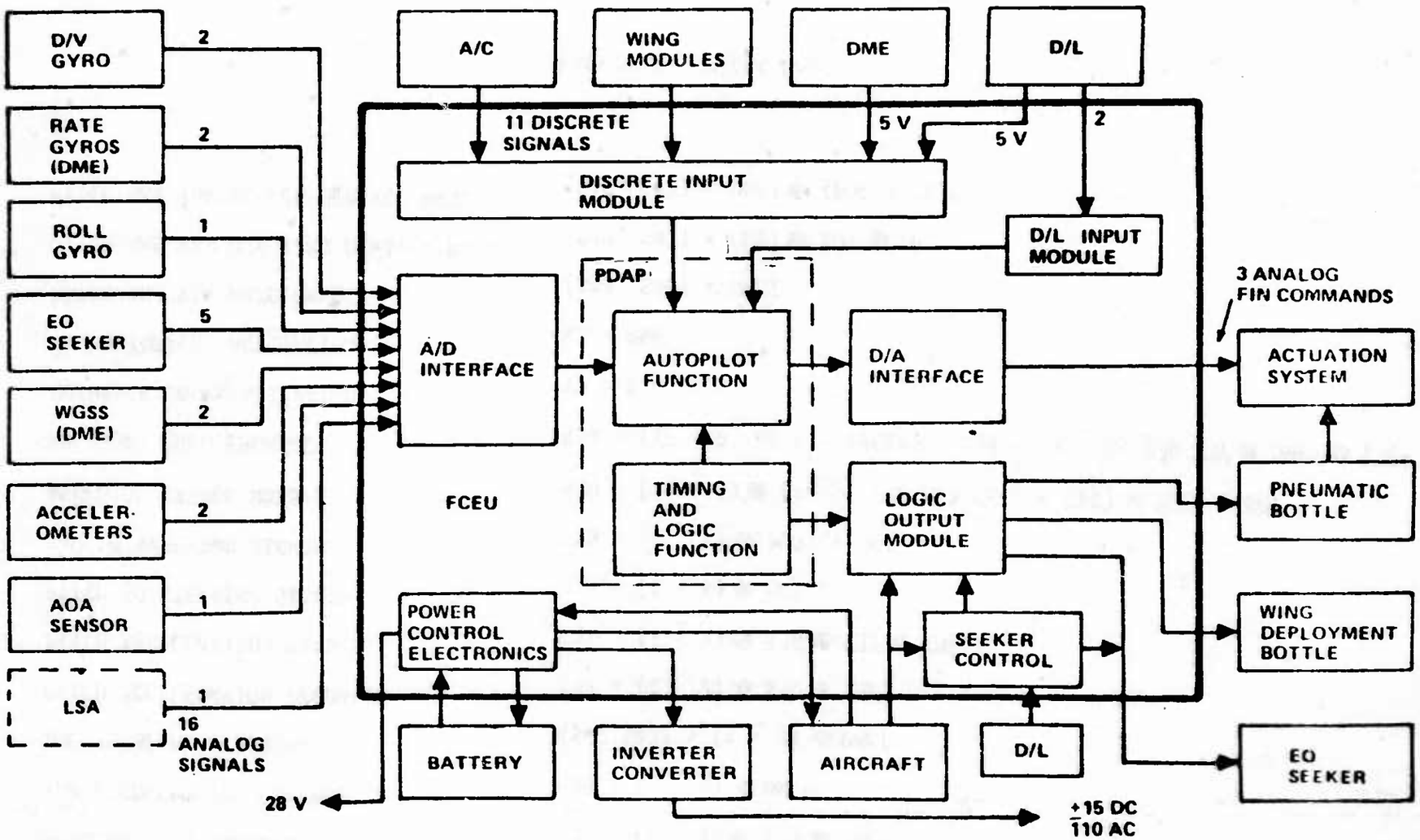

Figure 9. PDAP Functional Interface Diagram

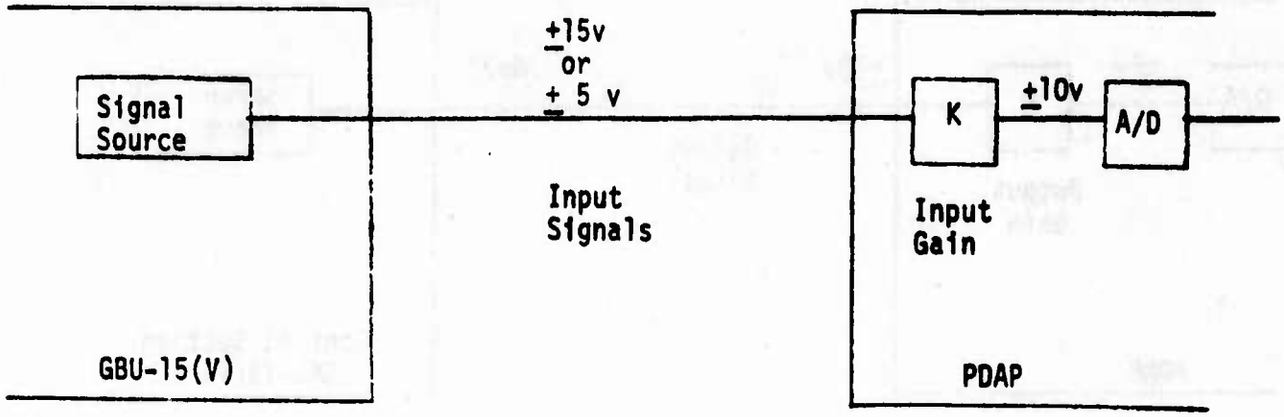

(a) GBU-15(V) INTERFACE

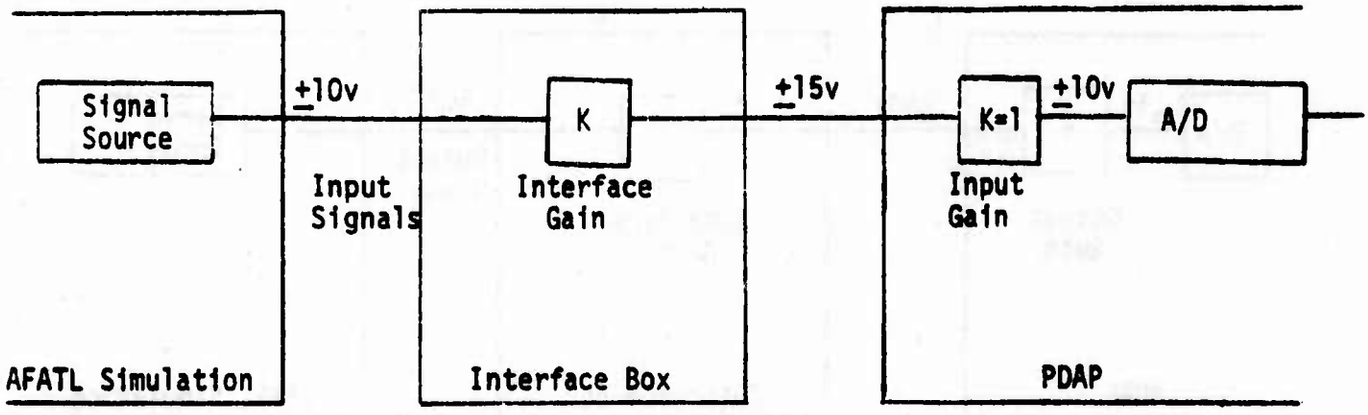

(b) HYBRID SIMULATION INTERFACE

Figure 10. PDAP Analog Input Signals

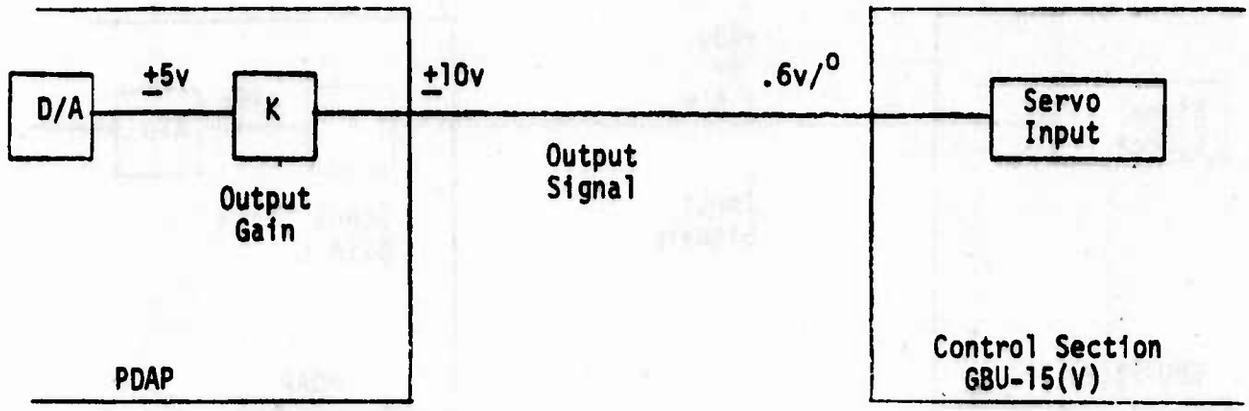

(a) GBU-15(V) INTERFACE

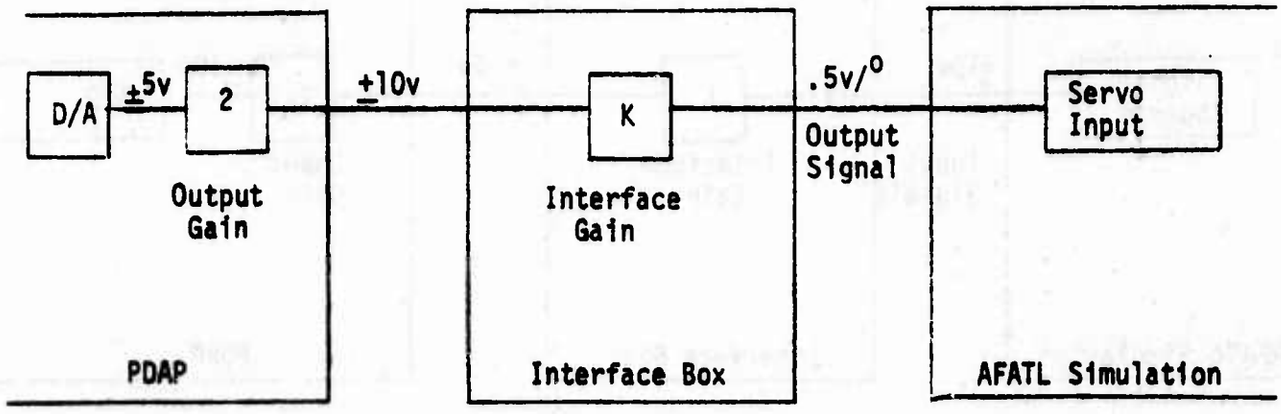

(b) AFATL HYBRID SIMULATION INTERFACE

Figure 11. PDAP Analog Output Signals

TABLE 1. PDAP ANALOG INTERFACE - GBU-15(V) INPUT SIGNALS

SIGNAL DESCRIPTION	SYMBOL	SCALE FACTOR	RANGE		PHASING	INPUT GAIN	A/D RANGE	LSB
			volts	FUNCTION				
PITCH SEEKER STEERING SIGNAL	$\dot{\lambda}_q$	0.283 v/deg/sec	±15	53 deg/sec	$+\dot{\lambda}_q$ +v UP COMMAND	1	35.33 deg/sec	0.0173 deg/sec
YAW SEEKER STEERING SIGNAL	$\dot{\lambda}_r$	0.283 v/deg/sec	±15	53 deg/sec	$+\dot{\lambda}_r$ −v RIGHT COMMAND	1	35.33 deg/sec	0.0173 deg/sec
PITCH SEEKER DERIVED RATE	$\dot{\theta}_g$	0.333 v/deg/sec	±15	45 deg/sec	$-\dot{\theta}_g$ +v NOSE UP	10/15 = 0.667	45 deg/sec	0.0220 deg/sec
YAW SEEKER DERIVED RATE	$\dot{\psi}_g$	0.333 v/deg/sec	±15	45 deg/sec	$-\dot{\psi}_g$ −v NOSE RIGHT	10/15	45 deg/sec	0.0220 deg/sec
PITCH RATE GYRO	q_g	0.333 v/deg/sec	±15	45 deg/sec	$+q_g$ +v NOSE UP	10/15	45 deg/sec	0.0220 deg/sec
YAW RATE GYRO	r_g	0.333 v/deg/sec	±15	45 deg/sec	$+r_g$ −v NOSE RIGHT	10/15	45 deg/sec	
PITCH ACCELEROMETER	N_z	2.0 v/g	±15	7.5 g	$+N_z$ −v ACCELERATES UP	10/15	7.5 g	0.0037 g
YAW ACCELEROMETER	N_y	2.0 v/g	±15	7.5 g	$+N_y$ +v ACCELERATES RIGHT	10/15	7.5 g	
PITCH ATTITUDE D/V GYRO	θ_G	0.167 v/deg	±15	90 deg	$+\theta_G$ −v NOSE UP	10/15	90 deg	0.0439 deg
YAW ATTITUDE D/V GYRO	ψ_G	0.167 v/deg	±15	90 deg	$+\psi_G$ +v NOSE RIGHT	10/15	90 deg	
ROLL GYRO	ϕ_G	0.0848 v/deg	±15	177 deg	$+\phi_G$ −v ROLL CW	1	118 deg	0.0576 deg
PITCH GIMBAL ANGLE	θ_g	0.4 v/deg	±15	37.5 deg	$+\theta_g$ −v LOOK-UP	10/15	37.5 deg	0.0183 deg
DME PITCH GUIDANCE COMMAND	N_{zc}	0.25 v/g	±5	20 g	$+N_{zc}$ +v UP COMMAND	1	40 g	0.0196 g
DME YAW GUIDANCE COMMAND	N_{yc} ψ_c	0.25 v/g 0.167 v/deg	±5	20 g 30 deg	$+N_{yc}$ −v RIGHT COMMAND $+\psi_c$	1	40 g 60 deg	0.0196 g 0.0293 deg
ANGLE OF ATTACK SENSOR	α	0.6 v/deg	±15	25 deg	TBD	10/15	25 deg	0.0122 deg
PAVE TACK ROLL COMMAND	ϕ_c	TBD	TBD	TBD	TBD	TBD	TBD	TBD

TABLE 2. PDAP ANALOG INTERFACE - AFATL SIMULATION INPUT SIGNALS

SIGNAL DESCRIPTION	SYMBOL	SCALE FACTOR	RANGE (±10 v)	PHASING	INTERFACE GAIN	ANALOG-TO-DIGITAL RANGE
PITCH SEEKER STEERING SIGNAL	$\dot{\lambda}_q$	1.0 v/deg/sec	10 deg/sec	$+\dot{\lambda}_q$ +v UP COMMAND	10/35.33 = 0.283	35.33*
YAW SEEKER STEERING SIGNAL	$\dot{\lambda}_r$	1.0 v/deg/sec	10 deg/sec	$+\dot{\lambda}_r$ +v RIGHT COMMAND	10/35.33 = 0.283	35.33*
PITCH SEEKER DERIVED RATE	$\dot{\theta}_g$	0.1 v/deg/sec	100 deg/sec	$-\dot{\theta}_g$ +v NOSE UP	100/45 = 2.22	45 deg/sec
YAW SEEKER DERIVED RATE	$\dot{\psi}_g$	0.1 v/deg/sec	100 deg/sec	$+\dot{\psi}_g$ −v NOSE RIGHT	100/45 = 2.22	45 deg/sec
OR ROLL RATE GYRO	p_g	$0.0499 = \frac{10}{(3.5)(57.3)} \frac{v}{deg/sec}$	3.5 rad/sec	$+p_g$ −v ROLL CW	100/45 = 2.22	90.24 deg/sec
PITCH RATE GYRO	q_g	$0.0873 = \frac{(10)}{(2)(57.3)}$ v/deg/sec	2 rad/sec	$+q_g$ −v NOSE UP	$\frac{(2)(57.3)}{(45)} = 2.547$	45 deg/sec
YAW RATE GYRO	r_g	$0.0873 = \frac{(10)}{(2)(57.3)}$ v/deg/sec	2 rad/sec	$+r_g$ −v NOSE RIGHT	$\frac{(2)(57.3)}{(45)} = 2.547$	45 deg/sec
PITCH ACCELEROMETER	N_z	0.5 v/g	20 g	$+N_z$ −v ACCELERATES UP	20/7.5 = 2.67	7.5 g
YAW ACCELEROMETER	N_y	0.5 v/g	20 g	$+N_y$ −v ACCELERATES RIGHT	20/7.5 = 2.67	7.5 g
PITCH ATTITUDE D/V GYRO	θ_G	0.05 v/deg	200 deg	$+\theta_G$ +v NOSE UP	200/90 = 2.22	90 deg
YAW ATTITUDE D/V GYRO	ψ_G	0.05 v/deg	200 deg	$+\psi_G$ +v NOSE RIGHT	200/90 = 2.22	90 deg
ROLL GYRO	ϕ_G	0.222 v/deg	45 deg	$+\phi_G$ −v ROLL CW	0.382	118 deg*
PITCH GIMBAL ANGLE	θ_g	0.05 v/deg	200 deg	$+\theta_g$ +v LOOK UP	200/37.5 = 5.33	37.5 deg
DME PITCH GUIDANCE COMMAND	N_{zc}	0.5 v/g	20 g	$+N_{zc}$ +v UP COMMAND	0.5	40 g*
DME YAW GUIDANCE COMMAND	N_{yc}	0.5 v/g	20 g	$+N_{yc}$ +v RIGHT COMMAND	0.5	40 g*
	ψ_c	0.333 v/deg	30 deg	$+\psi_c$		60 deg*
ANGLE OF ATTACK SENSOR	α	0.3125 v/deg	32 deg	$+\alpha$ +v ℄ ABOVE VELOCITY	32/25 = 1.28	25 deg
PRESSURE SENSOR	P	0.3125 v/psi	32 psi	+p +v POS. PRESS.	1	32 psi

*ALTERNATE SCALE FACTORS DESIRED

TABLE 3. PDAP ANALOG OUTPUT SIGNALS - GBU-15(V) INTERFACE

SIGNAL DESCRIPTION	SYMBOL	SCALE FACTOR	RANGE		PHASING	OUTPUT GAIN	D/A RANGE	LSB
			volts	FUNCTION				
YAW/PITCH NO. 1 FIN COMMAND	$\delta_{q_c} + \delta_{r_c}$	0.6 v/deg	±9 (LIMITED)	15 deg	+ $(\delta_{q_c} + \delta_{r_c})$ +v PITCH DN, YAW LEFT	1.8	±15 deg	0.0293
YAW/PITCH NO. 2 FIN COMMAND	$\delta_{q_c} - \delta_{r_c}$	0.6 v/deg	±9 (LIMITED)	15 deg	+ $(\delta_{q_c} - \delta_{r_c})$ +v PITCH DN, YAW RIGHT	1.8	±15 deg	0.0293
ROLL COMMAND	δ_{p_c}	0.6 v/deg	±9 (LIMITED)	15 deg	+ δ_{p_c} –v ROLL CW	1.8	±15 deg	0.0293

TABLE 4. PDAP ANALOG OUTPUT SIGNALS -- AFATL SIMULATION INTERFACE

SIGNAL DESCRIPTION	SYMBOL	SCALE FACTOR	RANGE (±10 volts)	PHASING	INTERFACE GAIN	DIGITAL-TO-ANALOG RANGE	LSB
YAW/PITCH NO. 1 FIN COMMAND	$\delta_{q_c} + \delta_{r_c}$	0.5 v/deg	20 deg	+ $(\delta_{q_c} + \delta_{r_c})$ +v PITCH DN, YAW LEFT	0.75	15 deg	0.0293
YAW/PITCH NO. 2 FIN COMMAND	$\delta_{q_c} - \delta_{r_c}$	0.5 v/deg	20 deg	+ $(\delta_{q_c} - \delta_{r_c})$ +v PITCH DN, YAW RIGHT	0.75	15 deg	0.0293
ROLL COMMAND	δ_{p_c}	0.5 v/deg	20 deg	+ δ_{p_c} –v ROLL CW	0.75	15 deg	0.0293

TABLE 5. PDAP DISCRETE LOGIC INPUTS

DISCRETE TYPE OF SIGNAL	SIGNAL DESCRIPTION	VOLTAGE LEVEL, volts	SIGNAL SOURCE WITHIN THE MISSILE
DISCRETE LOGIC	PWM INSTALLED	28	PLANAR WING MODULE
	LWP INSTALLED	28	LARGE WING MODULE
	SWP INSTALLED	28	SMALL WING MODULE
	DME GUIDANCE MODULE INSTALLED	28	DME GUIDANCE MODULE
	WEAPON SEPARATION	28	UMBILICAL
	EO LOCK ON (LOBL)	28	UMBILICAL
	TRANSITION ENABLE	5	D/L
	EO TAKEOVER	5	D/L
	EO TERMINAL	5	D/L
	DME PITCHOVER	5	DME
	EO INHIBIT	5	DME
DISCRETE D/L HEADING	EO HEADING LEFT	5	D/L (2 sec PULSE)
	EO HEADING RIGHT	5	D/L (2 sec PULSE)

Two of these discretes are generated by the wing module to identify to PDAP the vehicle aerodynamic configuration. Three autopilot logic output signals are required as shown in Table 6 -- one to activate the fin actuators, one to activate the planar wing deployment bottle, and one to control the seeker transition line. Only the latter one is generated within the processor itself because it is controlled by autopilot logic. The other two must be generated by special dedicated components.

TABLE 6. DISCRETE OUTPUT SIGNALS

SIGNAL DESCRIPTION	DESTINATION	VOLTAGE LEVEL, volts
WINGS DEPLOY	PLANAR WING MODULE	28
TRANSITION LINE REMOVE	SEEKER	28
ACTUATOR ACTIVATE	ACTUATOR	28

A special D/L input module is another interface requirement for PDAP. This module receives the pulsed steering signals listed in Table 5 from the D/L receiver.

DIGITAL PROCESSOR REQUIREMENTS

The following digital processor requirements were determined:

- Sampling rate

- Transport lag
- Digital/analog converter quantization
- Analog/digital converter quantization
- Computer word lengths
- Computations to be performed
- Digital filter formats

Sampling rate and transport lag requirements are important since they affect autopilot stability and influence the computation speed of the processor. Sampling rate is the number of times per second that the computations are performed. Transport lag is the total time allowable for the analog signals to be sensed, the computations to be performed, and the analog outputs to be generated. By considering the sampling rate, allowable transport lag, and total number of computations to be performed, the processor speed requirements can be determined.

Analog-to-digital and digital-to-analog quantization and the computer internal word lengths control the amount of vehicle limit cycle motion that occurs, as well as the accuracy of the computations and ultimately, accuracy of guidance. The type of digital filter format is important because it can affect processing speed, program memory requirements, and growth flexibility. Each of these items will now be discussed in more detail.

Digital Autopilot Sampling Rate

A primary factor influencing the stability of a digital autopilot is the sampling rate, or the frequency that the computations are performed and the fin servo commands are updated. It is the belief at Hughes that a relatively high sampling rate is required in an autopilot to guarantee the performance and the dynamic stability. One reason for the fast sampling rate is to minimize the destabilizing effect caused by the sampling and hold process. With typical missile autopilots, the designer is always constrained by the effect of the phase lags caused by the dynamics of the hardware, particularly the actuators. He usually must compensate for the lags by using lead networks in the autopilot electronics. The amount of lead is limited by the amount of system noise that is present. In a digital autopilot, the sample and hold introduces additional phase lags which further degrade stability.

The amount of digital compensation which may be used to compensate for the added lag is limited because the compensation further amplifies system noise as well as introducing its own quantization noise. Thus, to the extent possible, the design approach followed at Hughes is to select a sampling rate high enough so as to not appreciably degrade autopilot stability, i.e., introduce additional phase shift. This is especially true in the digital implementation of the RIC autopilot where relatively stringent gain and phase criteria are specified for the individual autopilot loops.

Another reason for using high sampling rates is to implement high frequency digital filters. Experience has shown that filters (especially notch filters) can be implemented when the sampling rate is approximately six times greater than the filter frequency.

A third reason for using high sampling rates is to prevent foldover of any high frequency noise that may be present in the system. Foldover can degrade guidance and control accuracy if the noise is folded into the missile control frequencies.

Additional Phase Shift Due to Hold and Transport Lag

Figure 12 shows the amount of additional phase shift that is added to the autopilot loops as a function of input frequency and for different sampling frequencies. The effect of the 600 μs transport lag specified for PDAP is also included in these curves. The input frequency region of interest for autopilot rigid body stability is from zero to 16 Hz. Rockwell has specified to its individual vendors that any additional phase shift due to sensor filtering, demodulation, etc. should be no greater than 5 degrees for frequencies up to 100 rad/sec (approximately 16 Hz). As far as vehicle stability is concerned, the frequency region up to 10 Hz is of primary interest. An appreciable amount of added phase shift in this region would severely affect stability.

It can be seen from Figure 12 that the amount of added phase lag is much more sensitive to sampling frequency at low sample rates than at high sample rates. A point of diminishing returns is reached where increasing sampling frequency causes no appreciable reduction of phase shift. Note that a sample rate greater than 1000 Hz is needed to meet the RIC requirement of 5° at 16 Hz. Hughes feels that the requirement is unnecessarily stringent and places an unreasonable requirement on sampling rate. Analysis has shown that the autopilot design can tolerate more than 10 degrees of additional phase shift at that frequency. A better method for evaluating the effect is to determine the variation of autopilot stability margin caused by sampling as shown in Figure 13.

Rigid Body Stability

The stability of the RIC autopilot is shown in Figure 13 for a worst case high dynamic pressure flight condition. As indicated, the stability margin starts to degrade for sampling rates below 200 Hz. At rates above 300 Hz, the stability margin is very nearly that of the analog autopilot.

Considering this curve alone, the inference can be drawn that the sampling rate could be reduced to possibly as low as 200 Hz. However, two effects have not been included in the stability analysis. One is the frequency response characteristics of the actual actuator, and the variations of the frequency response due to parameter variations. An important characteristic is the torsional load resonance prevalent with pneumatic actuators. Data describing the detailed actuator dynamics is required in order to update the stability analysis. A second factor not included is the flexible

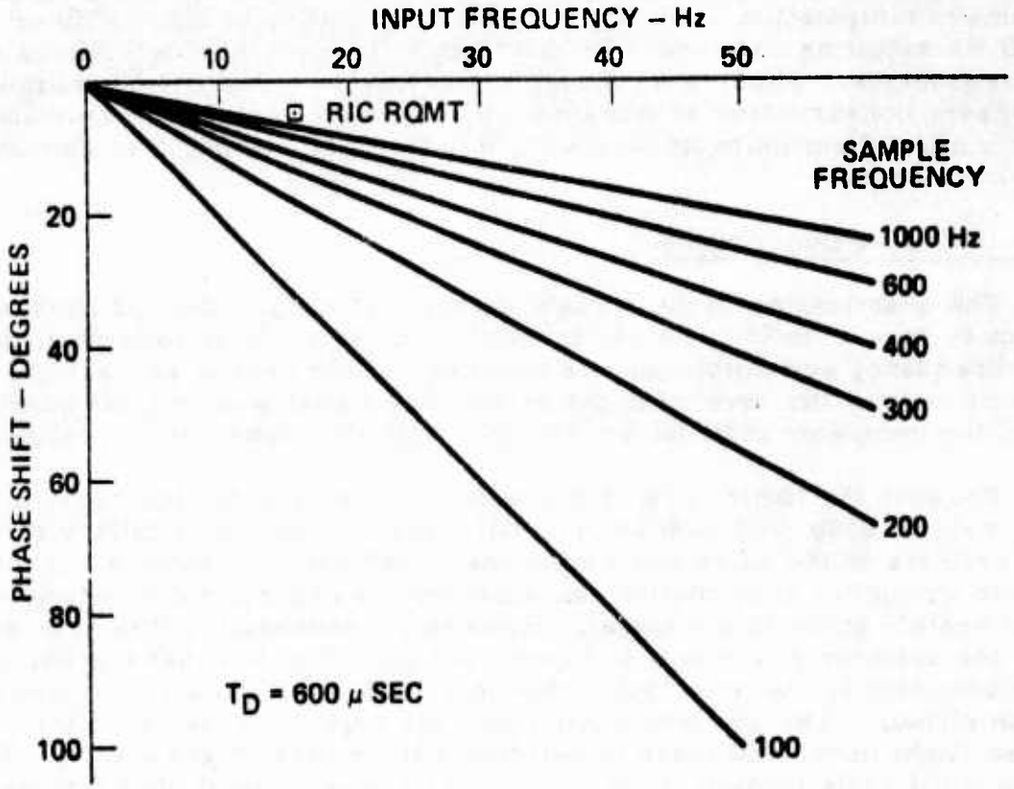

Figure 12. Additional Phase Shift Caused by Hold and Transport Lag

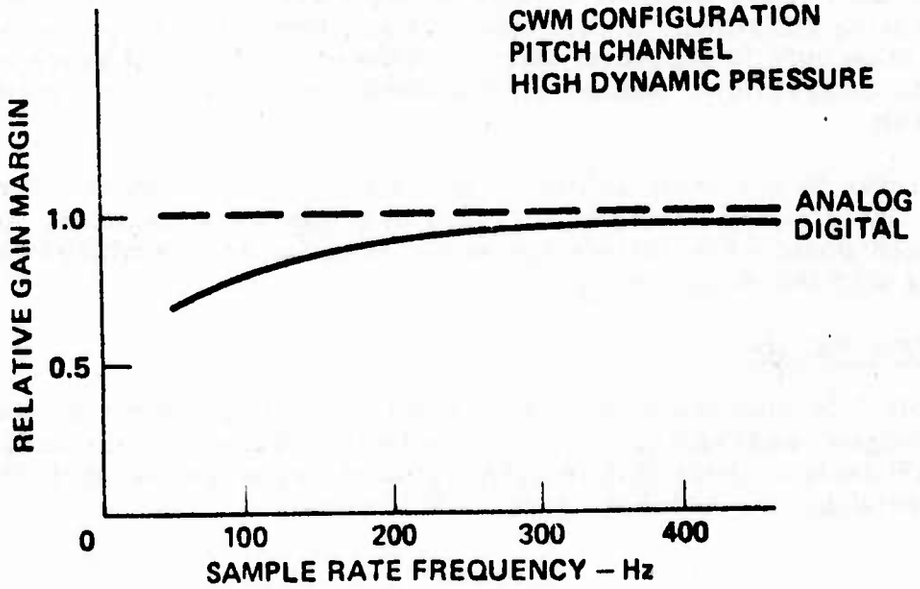

Figure 13. Rigid Body Stability

fuselage dynamics. Of particular concern are the dynamics of the planar wing. Preliminary information indicated wing bending modes as high as 50 or 60 Hz. The 400 Hz sampling rate would be required to implement notch filters at these frequencies. Thus, even though the selection of the 400 Hz sampling rate appears conservative at this time, the effects of actual actuator and flexible airframe dynamics must be analyzed before any reduction in sampling rate is considered.

Digital-to-analog Quantization

The quantization of the signals within the digital autopilot causes the autopilot to have a limit cycle oscillation. This is a closed loop phenomenon and the frequency and amplitude are functions of the vehicle and actuator dynamics as well as the level of quantization. The analog-to-digital quantization and the computer internal wordlengths will also cause limit cycling.

Because the limit cycle is a closed loop oscillation, the control fins, and the vehicle body will both be in oscillatory motion. It is difficult to assign criteria on the allowable amplitude of vehicle body motion. A considerable amount of body motion can exist during flight and the vehicle will still accurately guide to the target. However, whenever the fins are oscillating, the actuator gas supply is being used up. It is felt that the amount of gas consumption is the principal factor in specifying the maximum limit cycle amplitude. The gas bottle must provide control of the vehicle for an extended flight time, and there is relatively little margin remaining. Therefore the limit cycle motion of the fins must be small enough that it does not appreciably increase the power supply consumption rate.

However, care must be exercised so that the quantization requirements are not overspecified. This adds unnecessarily to the cost of the autopilot. Ordinarily system noise and actuator nonlinearities such as hysteresis and friction will also cause actuator motion in flight even with the infinite resolution of an analog autopilot. A cost effective solution, therefore, is to specify the quantization only to that level which matches the effects of noise and actuator characteristics. A finer quantization would result in no further improvement.

In order to precisely define the quantization requirements, a more detailed actuator model should be included in computer simulation. A preferable approach would be to include the actual actuator in a semiphysical simulation along with the digital autopilot.

Analog Output Signals

Table 7 defines the three analog output signals and their dynamic ranges as Hughes understands the requirements and has implemented them in the PDAP design. Note that an output gain is necessary on each channel to match scale factors to the fin servo electronics.

TABLE 7. ANALOG OUTPUT SIGNALS

SIGNAL DESCRIPTION	RANGE, degrees	OUTPUT GAIN	DIGITAL-TO-ANALOG RANGE, degrees
YAW/PITCH NO. 1 FIN COMMAND	15	1.8	±15
YAW/PITCH NO. 2 FIN COMMAND	15	1.8	±15
ROLL COMMAND	15	1.8	±15

Digital-to-Analog Conversion Requirements

The digital-to-analog conversion requirements are as follows:

- Number of outputs 3
- Quantization 8-9
- Allowable bias 2 percent of FS
- Gain tolerance 5 percent including droop
- Conversion time Compatible with total transport lag
- Output voltage ±9 volts

In addition to the basic requirements of quantization and voltage range, tolerances on gain and bias are specified. These tolerances are loose enough to permit a low cost design, while still being compatible with system performance requirements. The gain tolerance of 5 percent is one half the specified 10 percent gain tolerance on the closed loop fin servo. When the two are RSSed together, the combined gain variation is only 11 percent. Similarly, a 2 percent bias allowed on the digital-to-analog is 0.3 degrees, whereas each fin has an allowable bias of 1 degree. The RSS of a four fin control aileron for example, would be 0.58 instead of 0.5 degree. This is only a 16 percent increase and is acceptable, particularly when the other error sources are also included.

The possibility exists of realizing a production cost savings if an 8 bit digital-to-analog quantization could be used instead of 9. Since the actuator power consumption was not much larger for 8 than for 9 bit quantization, more detailed simulation analysis would be warranted to determine the feasibility of such a reduction.

Analog-to-Digital Conversion Requirements

Analog-to-digital conversion requirements are as follows:

- Number of inputs 16
- Quantization 12 bits

- Allowable bias — 2 percent of FS
- Gain tolerance — 3 percent of FS
- Input voltage range — 15 volts
- Preamplification — Selected channels
- Prefiltering — 150 Hz

A total of 16 signals must be converted. These signals can be time multiplexed and quantized to 12 bits (including sign) in one analog-to-digital converter. Certain input channels require preamplification before conversion. This is because some of the analog signals entering PDAP have low scale factors. The resolution of these signals would be very coarse after quantization. Prefiltering is also included on each channel to roll off high frequency noise and to allow the analog-to-digital converter to have a smooth, steady input signal during its conversion period.

Bias and gain tolerances were relaxed as much as possible to permit a low cost design. Preliminary analysis has indicated that such a relaxation is possible when other system error sources are considered. However, this conclusion should be verified by simulation analysis with detailed and updated system error sources.

Analog Input Signals

Table 8 identifies all of the known analog input signals which must be processed by the analog-to-digital converter. Also shown is the dynamic range of the analog input signal and the dynamic range actually quantized by the analog-to-digital converter. Preamplification on three channels is used to improve scale factors. The gain of 0.667 is the gain of the resistor network that drops 15 volt input signals to the 10 volt analog-to-digital level. It does not alter the signal scale factor. The unity gain is a direct connection and does not imply preamplification. The two DME input signals can also be preamplified to improve the scale factor. A factor of two will be used on these two channels.

Autopilot Programming

There are two general approaches to programming PDAP to provide the autopilots for the three aerodynamic configurations. One way is to treat each autopilot as a separate entity and to design a set of digital algorithms specifically for each autopilot/airframe configuration. With this approach separate programs would be used for each configuration (unless one long program were used). The PDAP would be programmed before flight depending on the particular GBU-15(V) configuration that was assembled. This perhaps was the concept first envisioned at the beginning of the PDAP program.

Another concept is the common autopilot approach in which all of the autopilot requirements for all configurations are integrated into one common

TABLE 8. ANALOG INPUT SIGNALS

SIGNAL DESCRIPTION	RANGE	PREAMPLIFIER GAIN	ANALOG-TO-DIGITAL RANGE
PITCH SEEKER STEERING SIGNAL	53 deg/sec	2.940	12 deg
YAW SEEKER STEERING SIGNAL	53 deg/sec	2.940	12 deg
PITCH SEEKER DERIVED RATE	45 deg/sec	0.667	45 deg/sec
YAW SEEKER DERIVED RATE	45 deg/sec	0.667	45 deg/sec
PITCH RATE GYRO	45 deg/sec	0.667	45 deg/sec
YAW RATE GYRO	45 deg/sec	0.667	45 deg/sec
PITCH ACCELEROMETER	7.5 g	0.667	7.5 g
YAW ACCELEROMETER	7.5 g	0.667	7.5 g
PITCH ATTITUDE-D/V GYRO	90 deg	0.667	90 deg
YAW ATTITUDE-D/V GYRO	90 deg	0.667	90 deg
ROLL GYRO	177 deg	2.620	45 deg
PITCH GIMBAL ANGLE	37.5 deg	0.667	37.5 deg
DME PITCH GUIDANCE COMMAND	20 g (5 v)	1	40 g
DME YAW GUIDANCE COMMAND	20 g (5 v) 30 deg	1	40 g 60 deg
ANGLE OF ATTACK SENSOR	25 deg	0.667	25 deg
PAVE TACK ROLL COMMAND	TBD	TBD	TBD

design. This would imply one PDAP program and eliminate the need for programming after vehicle assembly.

An example of separate autopilot programming is shown in Figure 14. It is assumed for illustration purposes, that four autopilot computations must be performed -- gain, compensation, limiting, and scaling. As the computer cycles through the required computations each iteration interval, it first computes the pitch channel. Then it repeats essentially the same computations for yaw because the two channels are often very similar. Finally it repeats similar calculations for roll. Since it does all of these computations serially, the processor must be fast enough to perform all of the computations within the allowed iteration interval.

When a second airframe is added another program is developed for that autopilot. There will, of course, be similarities between the two programs because the types and number of computations will be similar. An alternative to having two programs is to have one long program. This, of course, doubles the program memory size requirement.

The parallel channel approach is shown in Figure 15. This is sometimes referred to as the federated approach. In effect the pitch, yaw, and roll calculations are performed by separate processors in parallel. The control of the three channels is maintained by an executive processor. In this approach, a common autopilot configuration is often used for each channel. The executive section would then control the parameter selection in each channel based on the vehicle configuration.

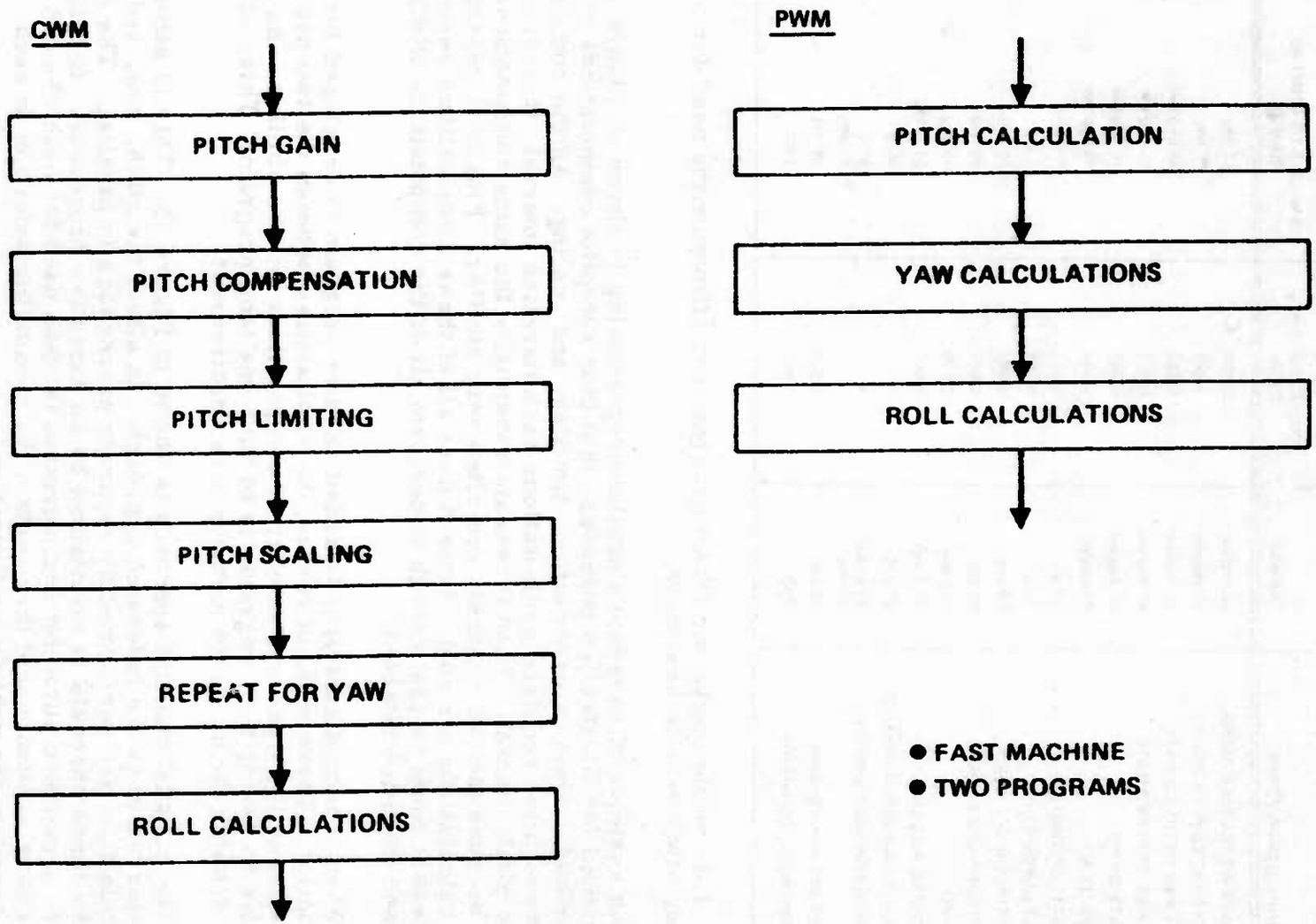

Figure 14. Separate Autopilot Programming

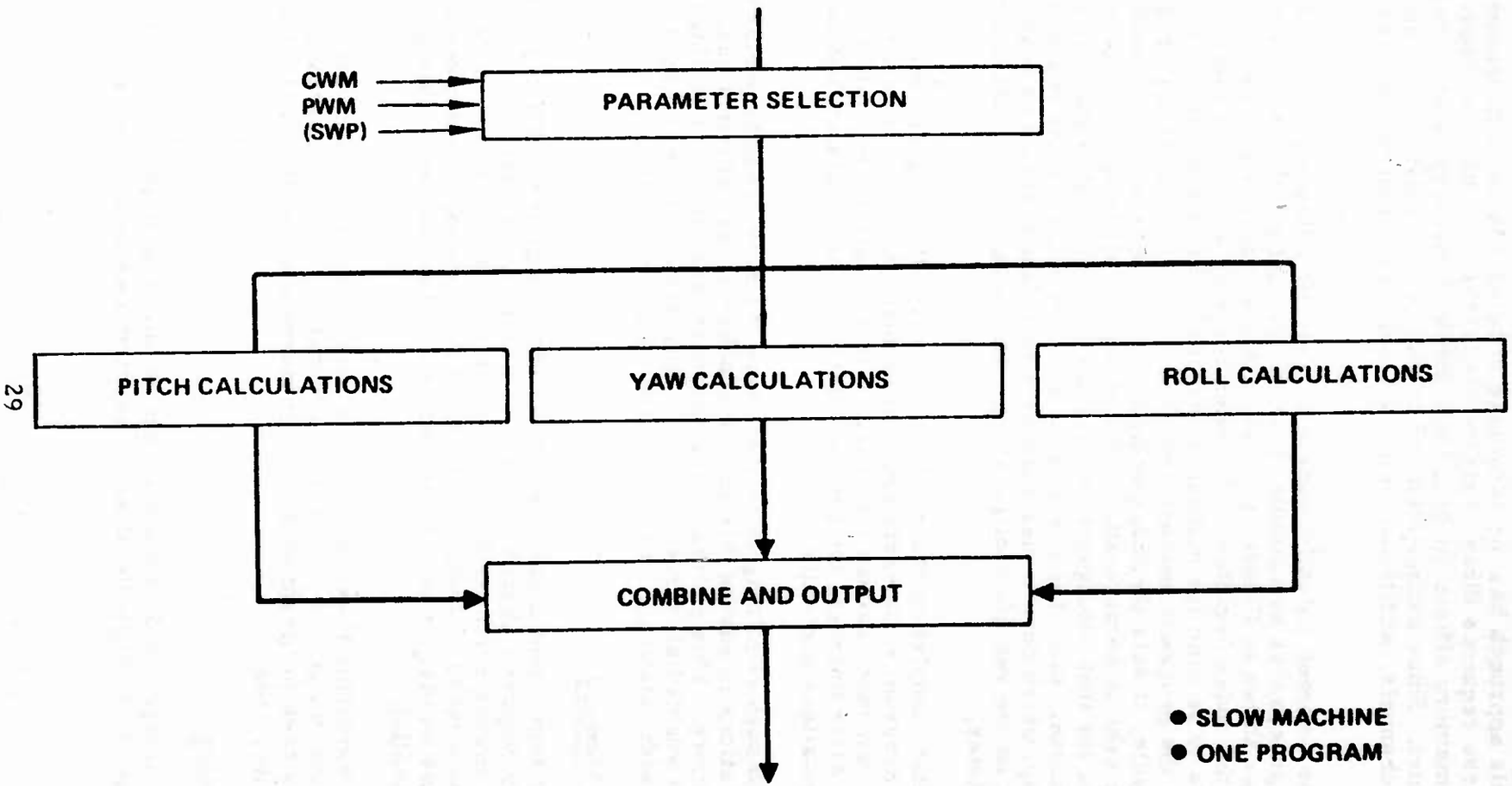

Figure 15. Parallel Channel Programming

This approach has the advantage of being adaptable to slower machines, but of course requires three separate processors. It has the disadvantage of not using memory efficiently because a block of memory must be dedicated to each channel. Since excess memory cannot be conveniently allocated across the three channels, additional memory for margin must be included in each channel.

The common autopilot approach takes advantage of some of the features of digital processors to combine all autopilot configurations into one integrated program as shown in Figure 16. Two of these features are the conditional jump and the index register. The index register allows the same program statements to be used for multiple purposes. This substantially reduces the amount of the program memory required. For example as the program begins its cycle, it sets the index registers with the index corresponding to a particular vehicle configuration. From then on all program statements operate on data for that configuration. As the program statements are executed for one channel, pitch for example, a decision point may be reached (conditional jump) which determines whether a calculation should be made or not, depending on the vehicle configuration. This jump is also controlled by the index register.

After completing the pitch calculations, the program will cycle through the same program statements again to perform the yaw computations. In this case, the yaw index causes the program to use data appropriate for the yaw channel. After finishing the yaw calculations, the program continues to the roll computations and exits.

Although requiring somewhat more machine speed to perform all of the calculations in series this approach offers a very efficient usage of program memory. This programming approach was employed by Hughes in PDAP. It enabled all three autopilot configurations to be included in one program with relatively little additional memory required.

Program Memory

To implement either the CWM (large wing) or the PWM autopilot separately requires about 650 words of program memory. By combining the two in a common software design, the total number of words increases by only 16 percent to 770 words. Adding a third autopilot increases the requirement to 844 words, or only 28 percent more than the requirement for an individual autopilot.

Considering these results, the feasibility of including all of the autopilots in one integrated program is demonstrated. This approach eliminates the necessity to program each vehicle independently after it is built up in the assembly area.

Data Memory

Two types of data memory are required to implement a digital autopilot. One is the variable data, or operand memory. This is a read/write

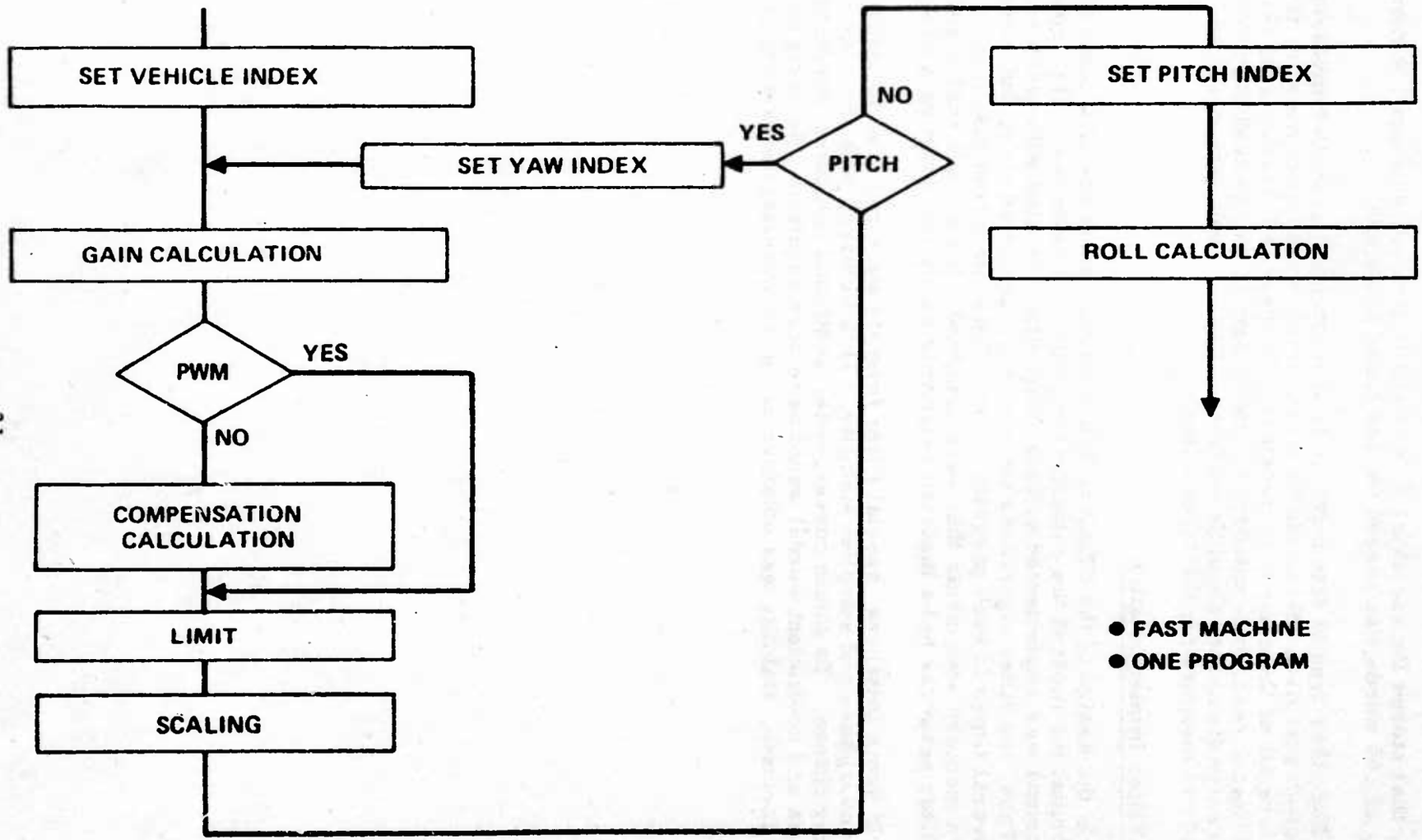

Figure 16. Common Autopilot Programming

memory that stores the variables being used in the computations. A memory capacity of 105 words was needed for the three autopilots.

The other type of data memory is the constant parameter memory. In a production autopilot, this would be a non-volatile read-only memory that would store all of the system parameters. In the PDAP brassboard, this memory was a read/write memory (actually part of the operand memory) so that design flexibility could be retained. The constant data required 264 words of memory for the three autopilots.

Digital Filter Implementation

In the design of the PDAP software Hughes made use of a common filter format for most of the autopilot compensation networks. The common filter format was implemented using a subroutine, coupled with index registers. Thus, the filter algorithms were only programmed once, but were used several times in each program cycle. This minimized the number of program memory statements that were required. It also will enable additional filter networks to be inserted relatively easily into existing software.

In some instances, special filter formats were required to obtain filter convergence and autopilot stability. This occurred with the very low frequency filters. To obtain convergence, additional computer wordlength (both data and coefficient words) would have been required. By using the special formats, stability was obtained using the wordlengths existing in PDAP.

SECTION IV

DESIGN VALIDATION

The hybrid computer design validation study included analog and PDAP trajectory comparisons for both the CWM and PWM autopilot configurations at various launch conditions. The time response of the autopilot modes (EO, DME control, D/L or DME midcourse heading commands, pitch and yaw rate gyros, or derived rate inputs, etc.) was also examined. The PDAP and analog autopilot results were similar. Word length sensitivity of the analog to digital converter, digital to analog converter, and computational bit size was also examined with regard to actuator gas consumption due to limit cycle effects. PDAP and analog autopilot noise comparison runs were made for the EO terminal mode using the CWM configuration. Gain Margin results were measured for the PWM configuration. The PDAP transport lag associated with the PWM and CWM autopilot designs were measured. The results were within the design objective of 600 μs.

SIMULATION DESCRIPTION

A functional block diagram of the hybrid simulator is shown in Figure 17. The detailed model description is included as Appendix A.

RESULTS

CWM Pitch Mode - Time History

CWM pitch channel time history comparisons of the analog autopilot representation and PDAP are depicted on Figure 18. The top figures show the CWM configuration when the pitch g-bias command is initiated. The CWM autopilot is in a rate damping mode for the first 1.75 seconds of flight. Then the acceleration loops are closed and the pitch g-bias command is initiated. This command consists of three signals (a constant input, a decaying exponential input, and pitch accelerometer information minus 1.03 g's through an integrator). The analog autopilot and the digital autopilot traces are very similar. A peak acceleration level of -45 fps^2 (-1.4 g) is achieved at the start of the g-bias input for this flight region. An acceleration level of -29 fps^2 (-0.9 g) is obtained after the transient g-bias phase of flight.

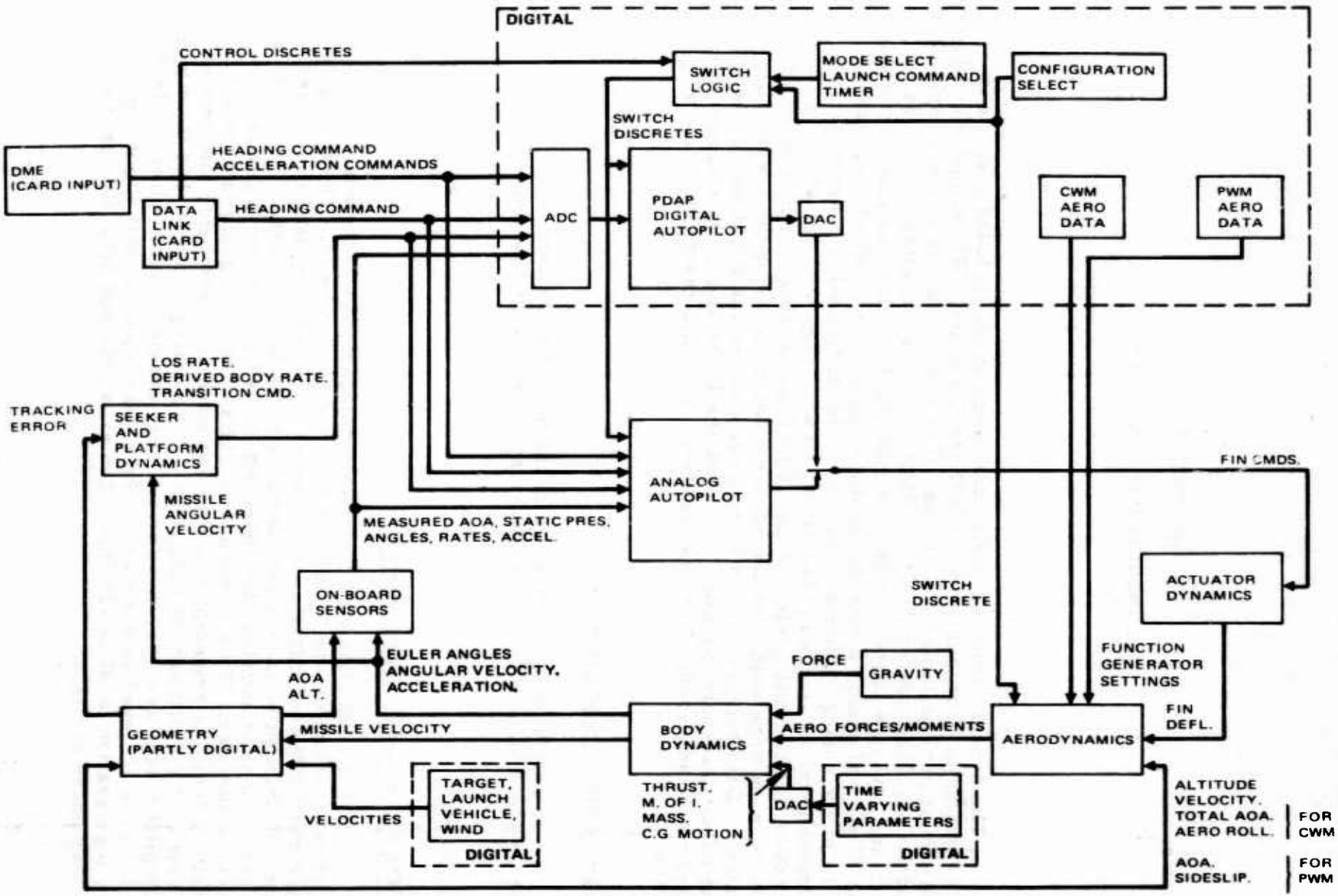

Figure 17. Simulation Functional Block Diagram

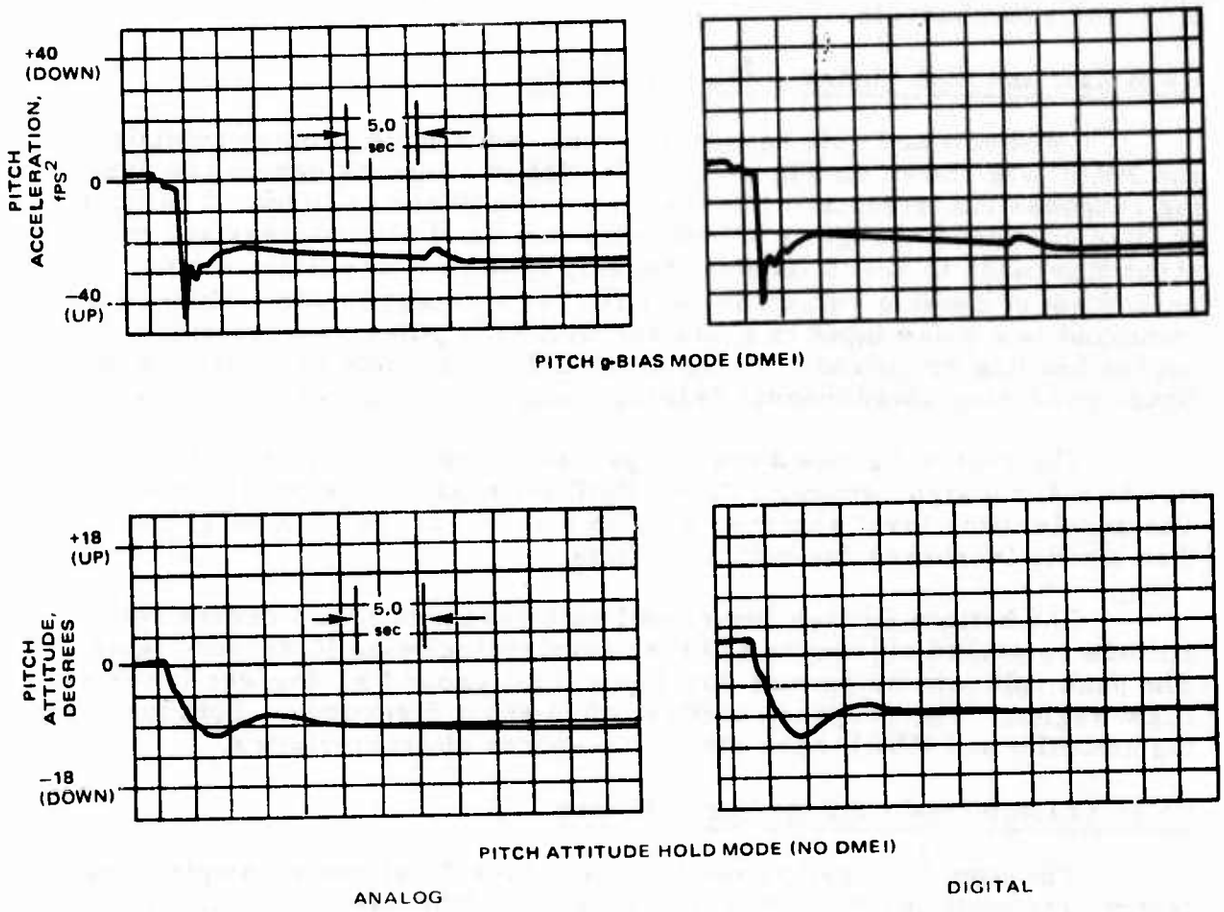

Figure 18. CWM Pitch Modes - Time Histories

The bottom figures depict the CWM pitch attitude hold mode configuration which is initiated 35 seconds after launch. These traces are similar with the analog autopilot having a smaller pitch attitude angle when this mode is initiated. Both the analog autopilot and PDAP obtain a pitch attitude angle around -9 to -10 degrees after the transient period. The pitch attitude hold configuration shown here uses derived rate information from the D/V gyros while the top two figures use rate gyro information in the pitch and yaw channels.

CWM Yaw and Roll Modes - Time Histories

CWM yaw and roll response comparisons of the analog autopilot and PDAP are shown on Figure 19. The top two figures depict yaw heading response characteristics in the midcourse phase of flight. The first heading command change is a DME step command of 5 degrees and takes about 8 seconds to reach its final heading value for this flight region. The second set of heading commands are (D/L) command inputs. Each D/L command is a pulse input to a counter with each pulse representing a 1 degree heading command. There are 5 D/L commands generated in this figure producing an additional heading change of 5 degrees.

The center figures show the yaw acceleration response characteristics to a 2.5 g step command in the DME terminal mode configuration. The acceleration level achieves a value around -21 fps^2 (-0.66 g) and then slowly increases for both autopilots.

The bottom figures depict roll rate response to a 5 degree roll attitude command clockwise and then counterclockwise 10 seconds later. The peak roll rate magnitude reaches a level around 53 deg/sec for this flight region. The response settles out in about 5 seconds. Both the analog autopilot and PDAP have similar response characteristics.

CWM Trajectories - PDAP Time History

The time history information on Figure 20 shows a complete trajectory response for the CWM configuration. The various modes include initial rate damping ($t < 1.75$ seconds), g-bias mode, pitch attitude hold, DME heading control, and EO terminal steering. This trajectory case represents a high speed launch from a high altitude. A maximum pitch acceleration level of -50 fps^2 (-1.55 g) was obtained when the acceleration loops are closed and the g-bias command is initiated. During the pitch attitude hold mode, pitch attitude reaches a value around -15 degrees. During midcourse, the DME heading commands produce a peak yaw acceleration magnitude of about 36.8 fps^2 (1.11 g). The terminal steering phase of flight produces a maximum pitch acceleration level of around -20 fps^2 (-0.62 g).

CWM LOBL Time Histories

Figure 21 depicts a low altitude lockon-before-launch (LOBL) flight condition where the pitch and yaw channels use seeker derived rate

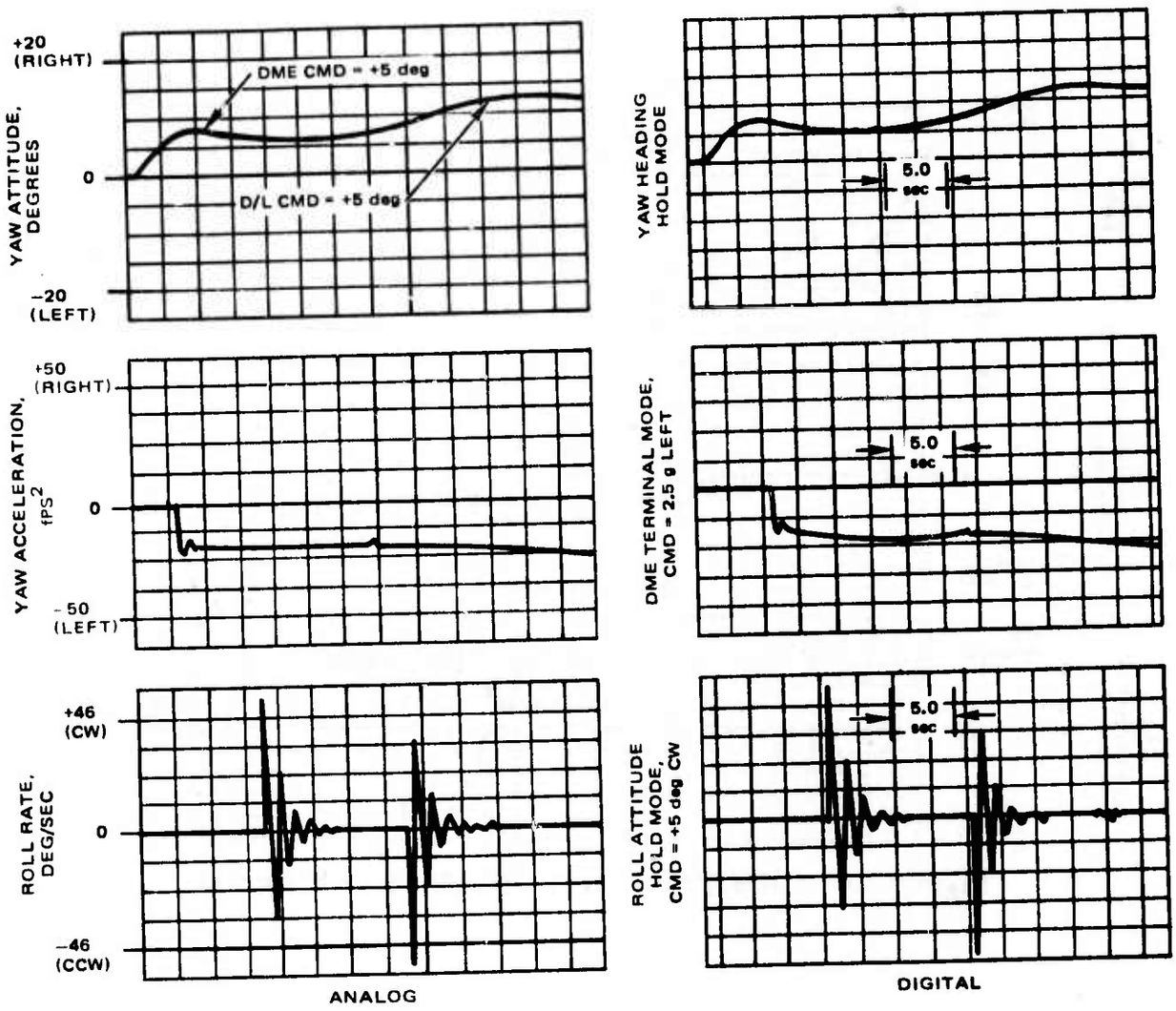

Figure 19. CWM Yaw and Roll Modes - Time Histories

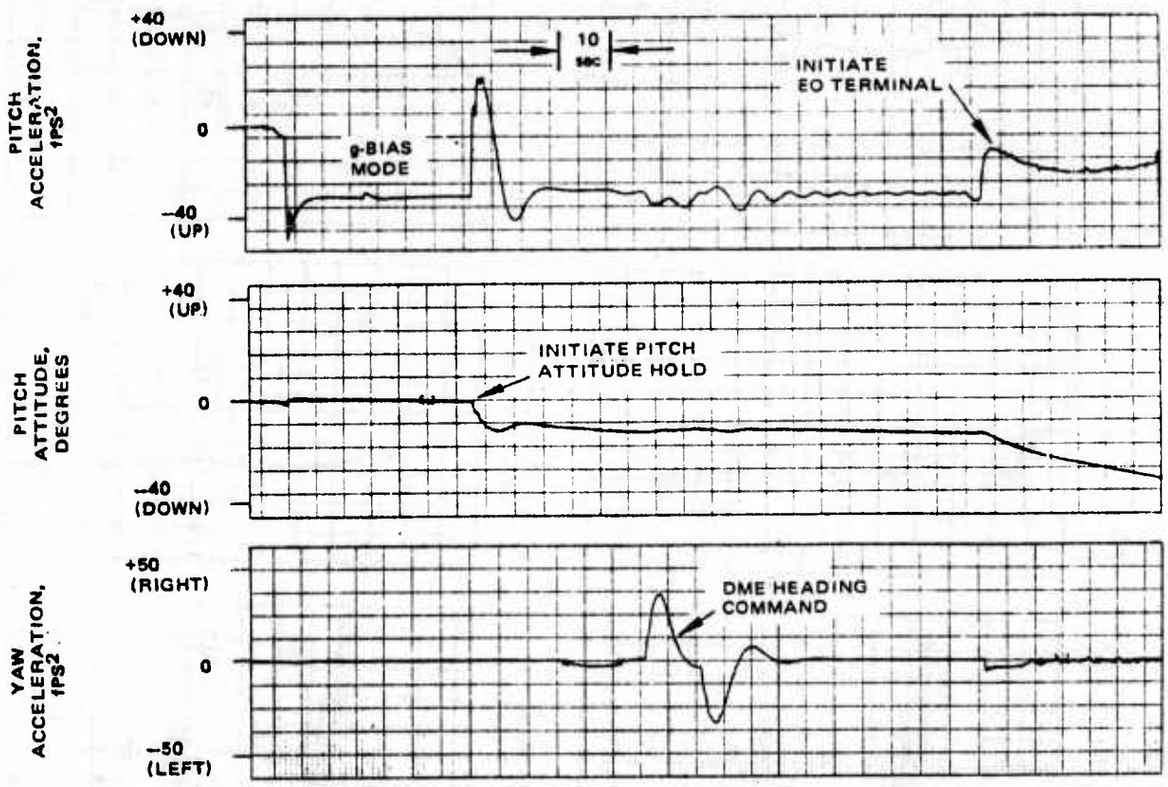

Figure 20. CWM Trajectory – PDAP Time Histories

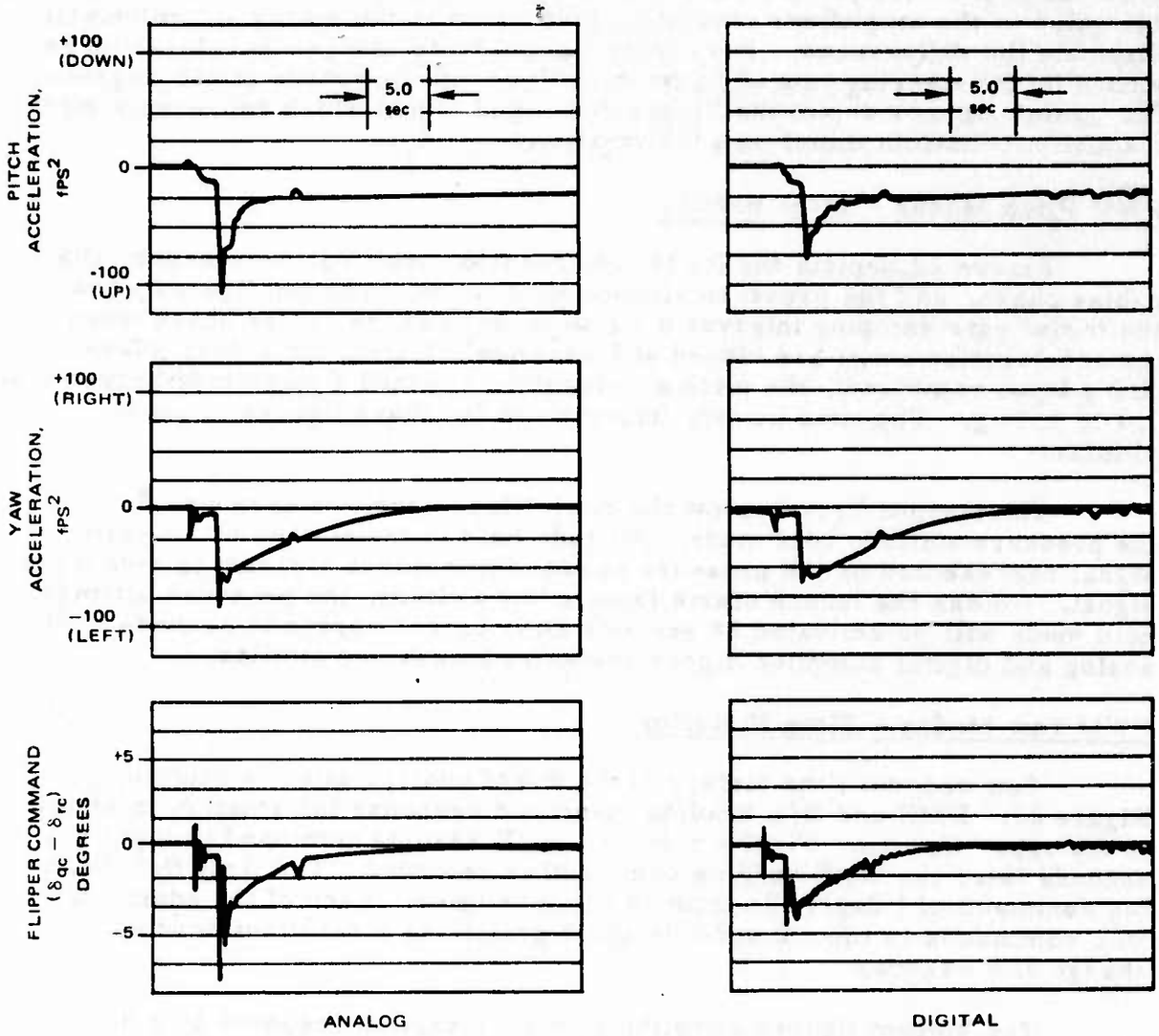

Figure 21. CWM LOBL - Time Histories

information for damping purposes. The PDAP and analog autopilot response traces are similar except for the initial transient peak which occurs 1.75 seconds after launch when the EO steering signals are activated for LOBL. This transient peak amplitude difference was explored further and was found to be due to the value of software limiting used to prevent overflow. Adjusting this value to the amplifiers saturation level used in the analog autopilot will eliminate the differences. The center figures show the yaw acceleration response to EO steering caused by an initial yaw heading value of +15 degrees. The bottom figures depict the flipper command signal which represents pitch channel information minus yaw information ($\delta_q - \delta_r$).

PWM Pitch Modes - Time History

Figure 22 depicts the PWM configuration starting from launch, the g-bias phase, and the pressure altitude hold mode. The top figures show the initial rate damping interval ($t < 2$ seconds) and the g-bias phase when the acceleration loops are closed at 2 seconds. During the g-bias phase (1.2 g input command), the pitch acceleration reached a magnitude between 1.1 to 1.24 g. The time history information for these figures is very similar.

The bottom figures show the pitch flipper position response during the pressure altitude hold mode. Altitude hold is maintained by an error signal represented by the pressure sensor input minus a pressure reference signal. Unless the launch starts from a low altitude, the pressure altitude hold mode will be activated 28 seconds after launch versus 12 seconds. The analog and digital autopilot flipper response traces are similar.

PWM Yaw Modes - Time Histories

Yaw channel time history of the PWM configuration is depicted on Figure 23. DME and D/L heading command response information is shown in the upper figures. First a 5 degree DME heading command is input, 10 seconds later the DME heading command is removed. The first D/L heading command of 1 degree is input 10 seconds later. Each of the additional D/L commands is input 2 seconds apart producing a resultant heading change of 5 degrees.

The bottom figures show the yaw acceleration response to a 0.5 g acceleration command during the DME terminal mode. The command is applied for 10 seconds and then removed. Both autopilot responses are similar and achieve an acceleration level around 0.5 g.

CWM Noise Comparisons (EO Terminal) EO Steering Noise

Figure 24 shows both a noise and noise free case for the analog autopilot and PDAP. The noise characteristics at the pitch EO steering point, $\dot{\lambda}$, has a bandwidth of 10 Hz and a standard deviation value of 0.37 degrees/second. This noise source was used as an example of a noise run but is not necessarily representative of EO steering noise. An actual EO seeker should be used with PDAP to generate the EO steering noise characteristics. The PDAP response is stable with this noise input. Because noise is a random variable, some of the noise case runs will produce slightly larger amplitudes and other noise run cases will produce smaller amplitudes. The

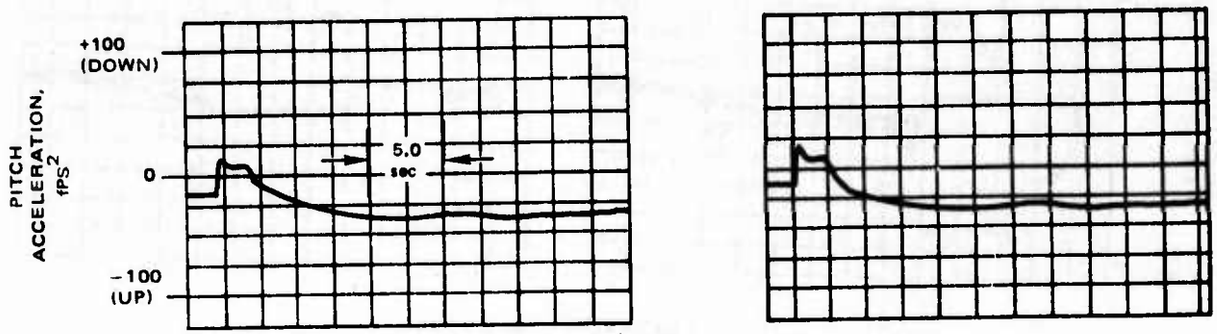

WING DEPLOYMENT MODE, 1.2 g-BIAS COMMAND

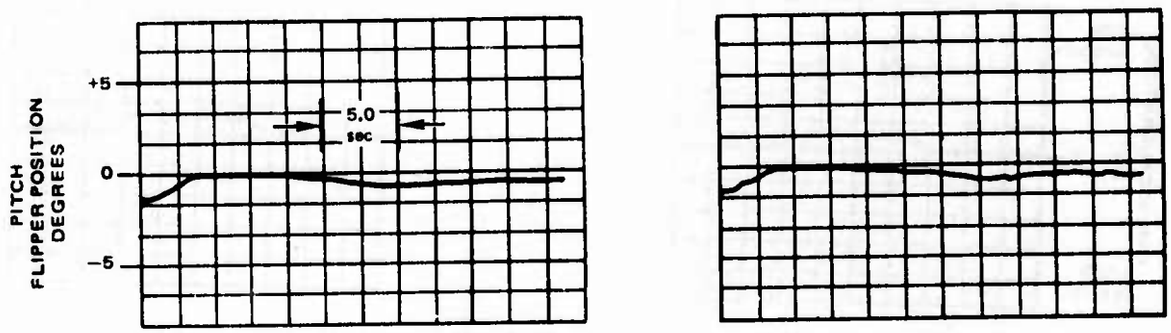

PRESSURE ALTITUDE HOLD MODE

ANALOG

DIGITAL

Figure 22. PWM Pitch Modes - Time Histories

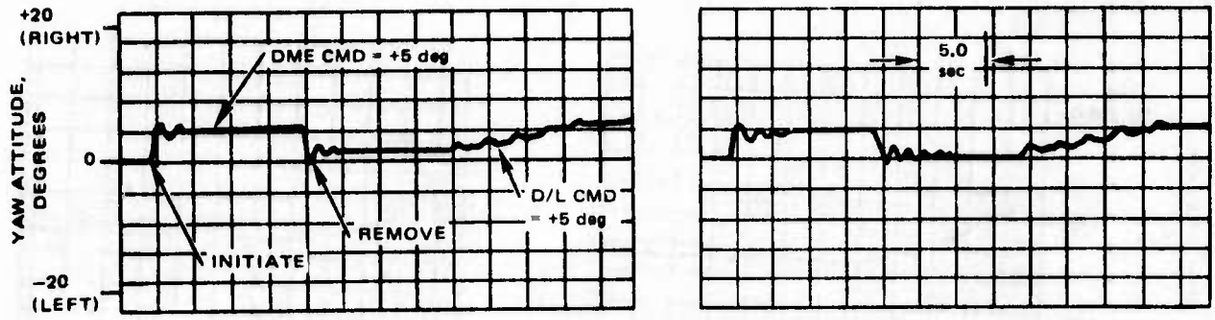

YAW HEADING HOLD MODE

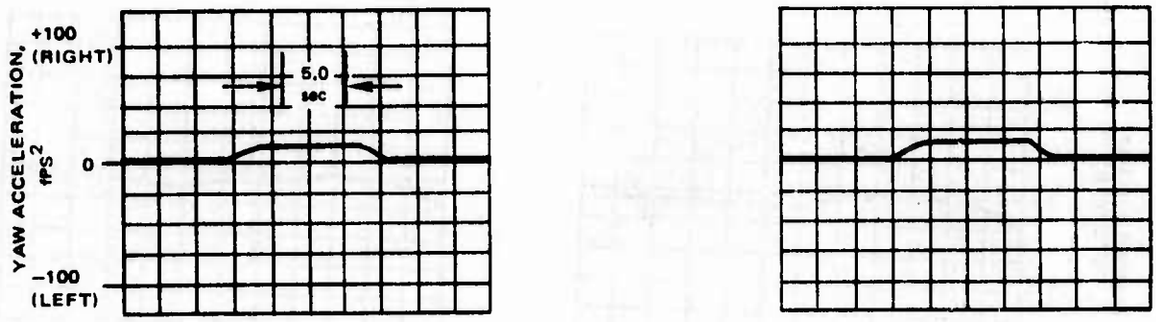

DME TERMINAL MODE, N_{Yc} = +0.5 g

ANALOG DIGITAL

Figure 23. PWM Yaw Modes - Time Histories

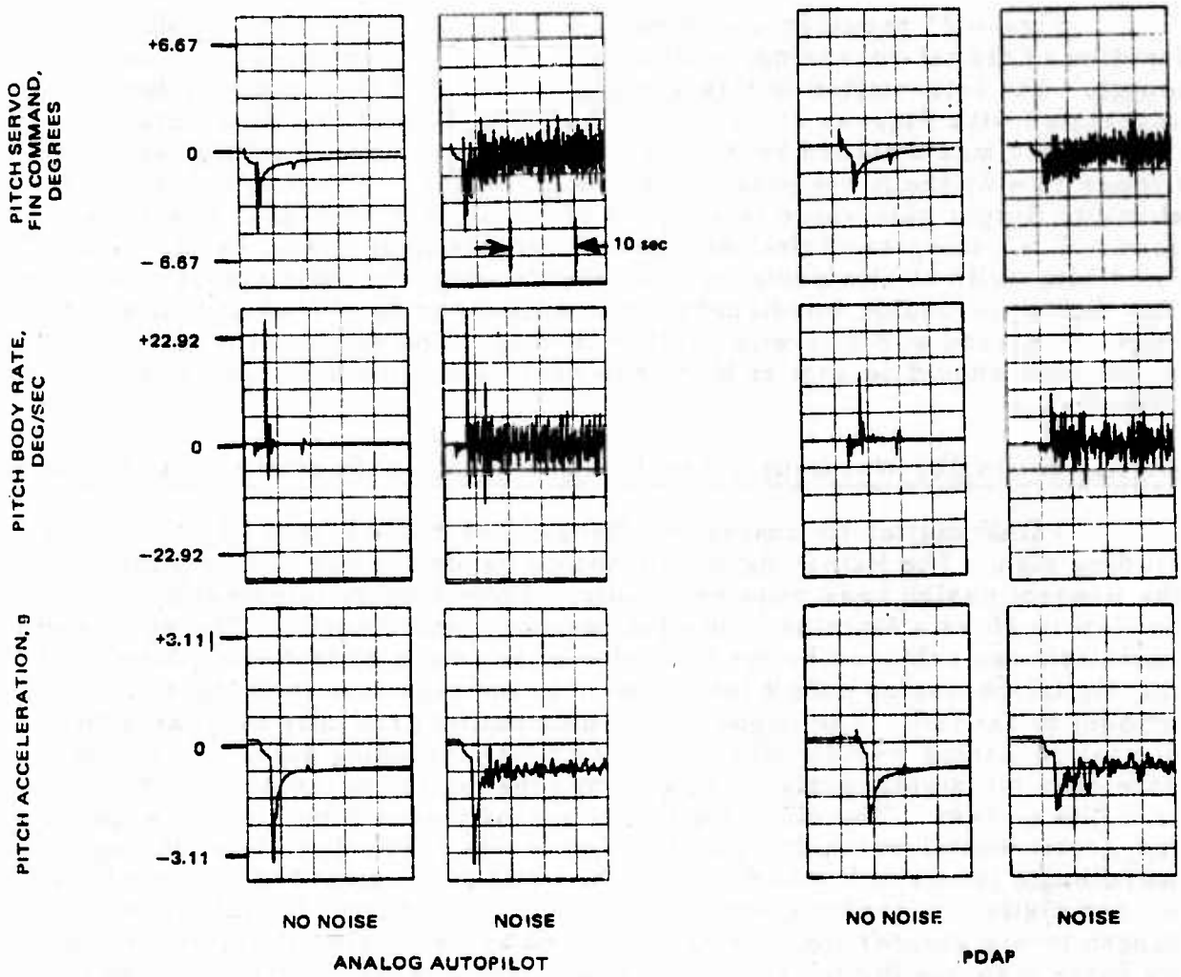

Figure 24. CWM Noise Comparisons (EO Terminal)
EO Steering Noise

PDAP steering loop has a sample rate frequency of 50 Hz and will fold noise energy above 25 Hz back into the primary frequency strip. If the representative EO steering noise inputs should produce undesired response characteristics due to folding effects, the steering loop sample rate frequency can be increased to 100 Hz with a minor software change.

PDAP Wordlength Sensitivity Summary

Figure 25 provides a summary picture of flipper rate amplitude as a function of digital-to-analog, analog-to-digital, and computational wordlength. The information in this graph was obtained from time history data associated with Figures 26, 27, and 28. The average absolute value of flipper rate was obtained by dividing the integral of the absolute value of flipper rate by the flight time value of a given run. The magnitude of the absolute flipper rate value is a figure of merit of the actuator gas supply used. The analog-to-digital wordlength requirement should be placed at 11 or 12 bits, with 12 bits preferred to provide adequate input signal resolution. The digital-to-analog wordlength requirement can be placed at 9 bits and might be placed at 8 bits with further testing. The computational computer wordlength should be kept at 16 bits to provide proper accuracy of software calculations.

Digital-to-Analog Wordlength Sensitivity - CWM Configuration (EO Terminal)

PDAP digital-to-analog wordlength was varied from 10 to 6 bits including sign. The PDAP digital-to-analog hardware has 10 bits although the present design base requires 9 bits. Time history information is shown on Figure 26 as a function of digital-to-analog wordlength. The wordlength variation was achieved by the inclusion of software statements which shift the digital-to-analog output information to the right and then the same amount to the left. The flipper rate information gradually increases for digital-to-analog wordlengths less than 9 bits including sign. Roll body rate does not significantly increase until the digital-to-analog wordlength is 6 bits or less. The pitch digital-to-analog output time history shows the actual digital-to-analog quantization levels. For digital-to-analog wordlength levels of 7 bits or less, the limit cycle amplitude is controlled by one digital-to-analog quantization level. For digital-to-analog wordlength levels greater than 8 bits, the limit cycle amplitude is controlled by more than one digital-to-analog quantization level. A figure of merit of servo gas consumption in terms of digital-to-analog wordlength variation is depicted in Figure 25.

Analog-to-Digital Wordlength Sensitivity - CWM Configuration (EO Terminal)

The PDAP analog-to-digital wordlength was varied from 12 to 9 bits. The PDAP analog-to-digital hardware has 12 bits including sign. This is the present analog-to-digital converter wordlength requirement. Flipper rate, pitch body rate, and roll body rate are shown on Figure 27 as a

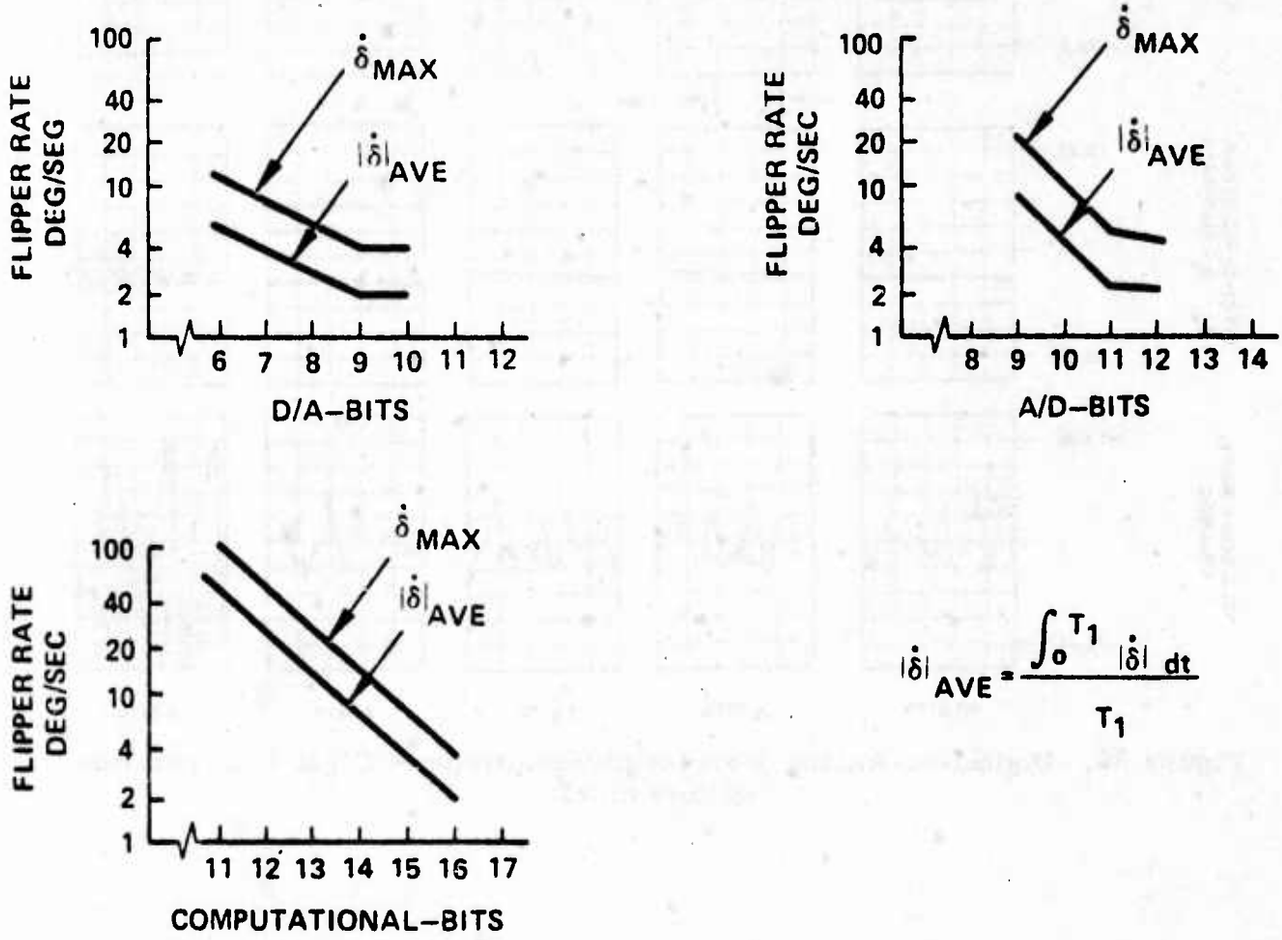

Figure 25. PDAP Wordlength Sensitivity Summary

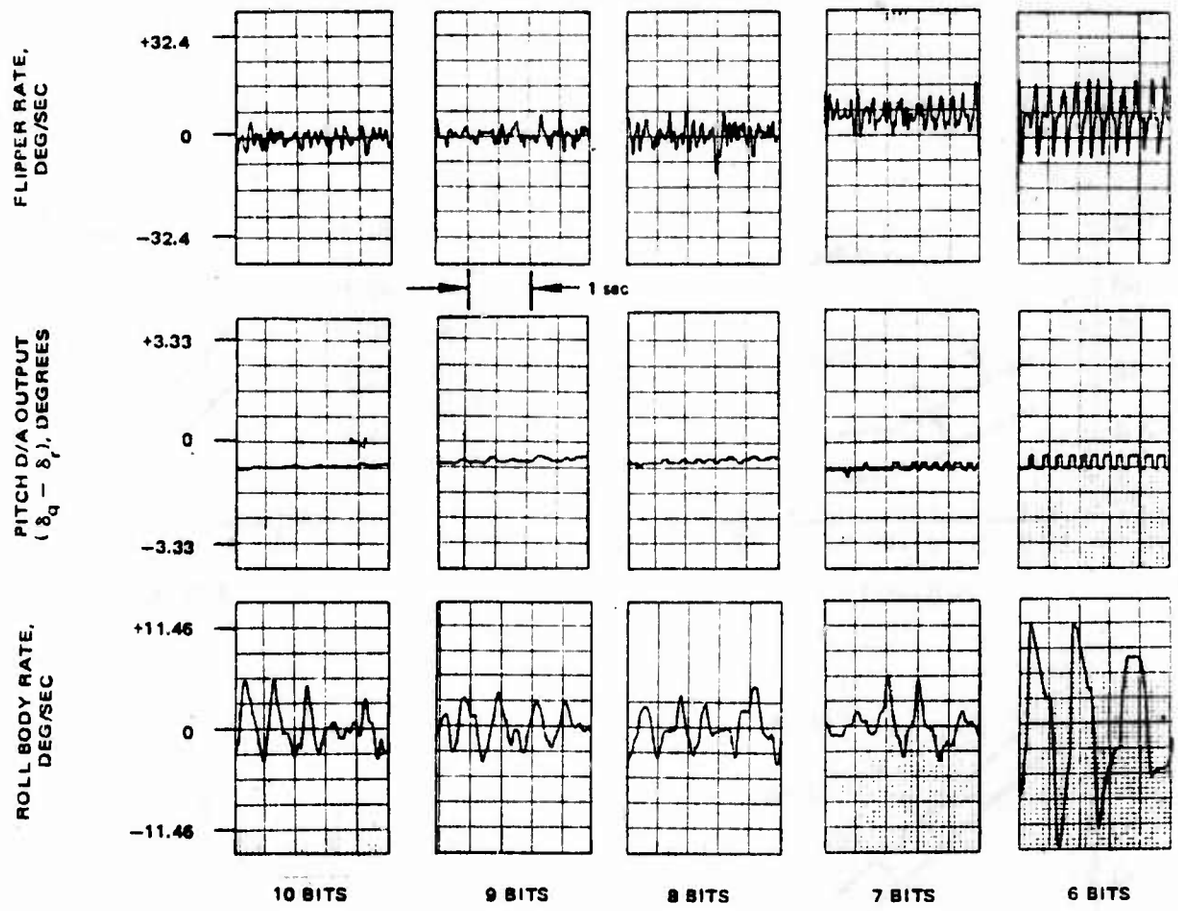

Figure 26. Digital-to-Analog Wordlength Sensitivity – CWM Configuration (EO Terminal)

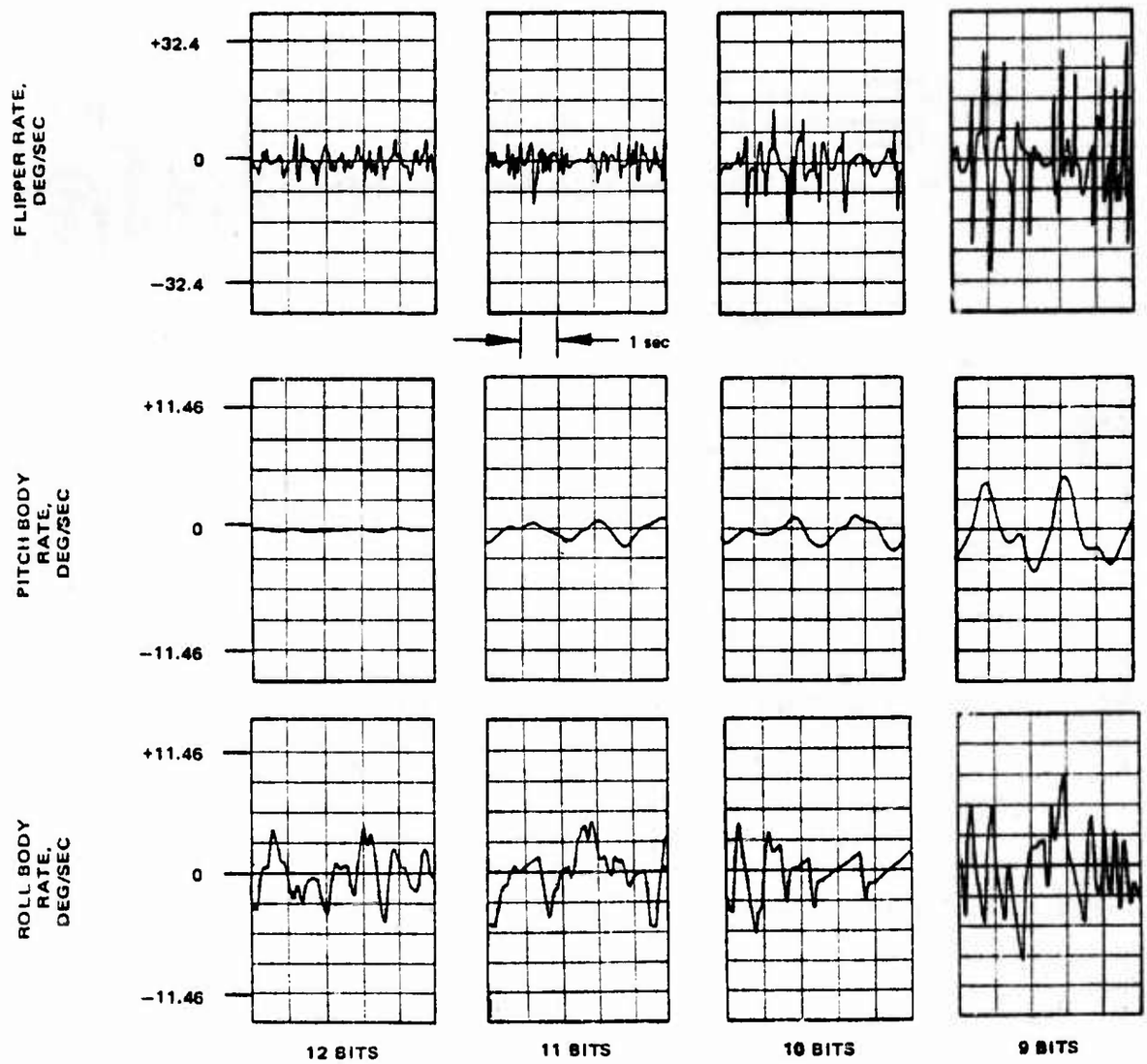

Figure 27. Analog-to-Digital Wordlength Sensitivity – CWM Configuration (EO Terminal)

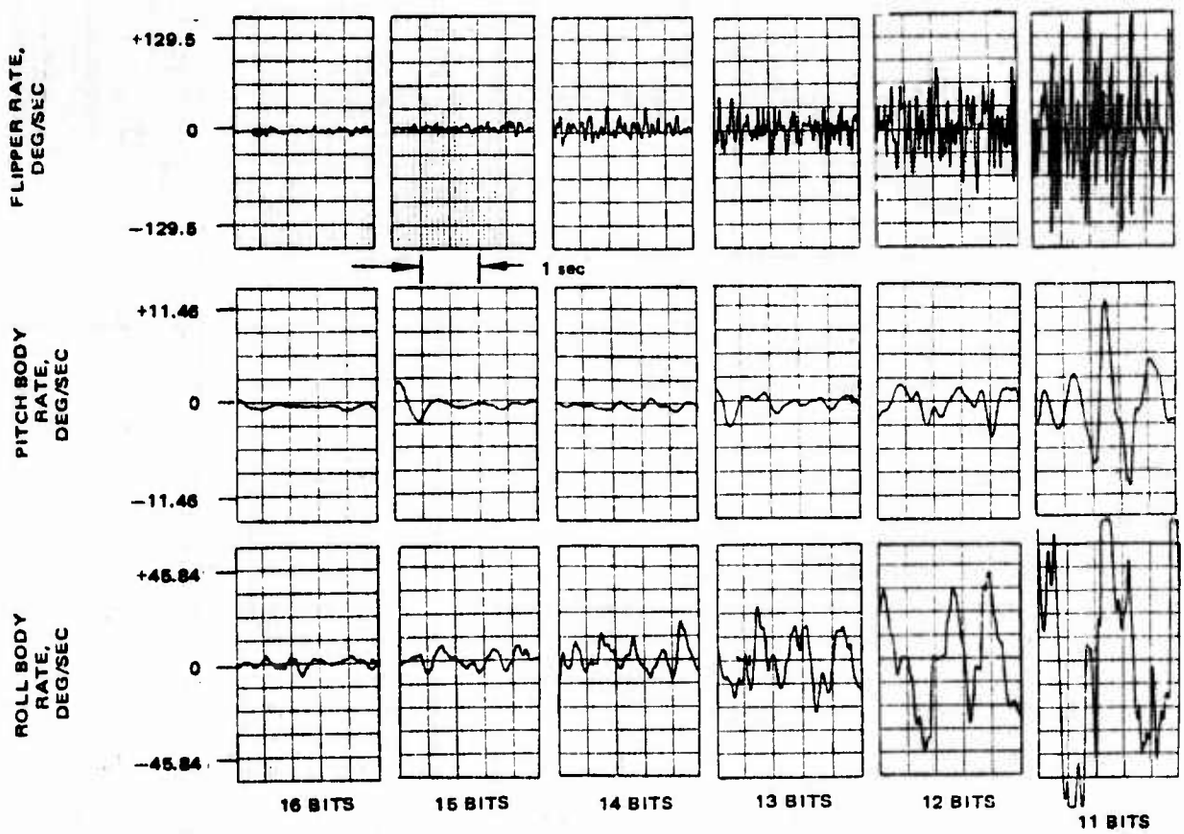

Figure 28. Computational Wordlength Sensitivity — CWM Configuration (EO Terminal)

function of analog-to-digital wordlength. The flipper rate amplitude is the same for 12 and 11 bits, but significantly increases for 10 bits or less. Pitch body rate and roll body rate amplitudes do not significantly increase until 9 bits. A figure of merit of servo gas consumption in terms of analog-to-digital wordlength variation is shown in Figure 25.

Computational Wordlength Sensitivity - CWM Configuration (EO Terminal)

Computational wordlength sensitivity of the number of bits used for multiplication results are shown on Figure 28. Both flipper rate and roll rate amplitudes increase as computational wordlength is decreased. The computational wordlength requirement is 16 bits including sign. Pitch body rate does not significantly increase until about 13 bits or less. A figure of merit of servo gas consumption in terms of computational wordlength variation is depicted in Figure 25.

PWM Gain Margin Comparison

The information in Table 9 was obtained from the AFATL hybrid simulation and provides PWM gain margin comparisons of the analog autopilot and PDAP at Mach = 0.95 and altitude = 20,000 feet. The gain margin measurements were obtained by raising the gain of a given loop until the time response becomes marginal. Forward loop gain margin refers to the margin obtained by raising the gain prior to the actuator input. Rate loop gain margin refers to the margin obtained by raising the gain just after the rate sensor. Position or acceleration loop gain margin refers to the margin obtained by raising the gain just after the attitude or accelerometer sensor, respectively. All of the gain margin differences are 11 percent or less except for one.

TABLE 9. PWM GAIN MARGIN COMPARISON

(MACH = 0.95, ALTITUDE = 20K)

	ANALOG, dB	PDAP, dB	DIFFERENCE, dB (percent)
ROLL AUTOPILOT			
• POSITION LOOP	8.46	7.78	0.68 (8)
• RATE LOOP	16.59	16.12	0.47 (5)
• FORWARD LOOP	12.87	12.04	0.83 (9)
YAW MIDCOURSE			
• POSITION LOOP	11.71	8.95	2.76 (27)
• RATE LOOP	20.98	20.00	0.98 (11)
• FORWARD LOOP	18.79	18.64	0.15 (2)
YAW DME TERMINAL			
• RATE LOOP	20.70	19.96	0.74 (8)
• ACCELERATION LOOP	16.59	16.06	0.53 (6)
• FORWARD LOOP	15.27	16.13	-0.86 (9)

Measured PDAP Damping Loop Transport Lag

The measure transport lag values of the PDAP rate damping loops are listed in Table 10. The measured transport lag value includes one or more analog-to-digital conversion time cycles, the pitch; yaw and roll rate loop calculations and one or more digital-to-analog signal generations. The design objective is to have a transport lag value of 600 μs or less in each rate loop. This objective was met. Fairly simple reorganization of the software calculations can get each rate loop transport lag value to less than 120 μs if needed. Software reorganization would be needed to implement the existing autopilot equations into a computer having a slower instruction execution time.

The transport lag measurement defines the time lag associated with the high speed rate loops (400 Hz) and does not include any time lag from the slow speed loops (50 Hz). The slow speed loops introduce Bode phase shift at the point where the slow speed loop enters a high speed loop calculation. The amount of phase shift is the same for all slow speed loop calculations (50 Hz) and is expressed by the relationship, $\emptyset = -360\,[(1 + N)/2]\, f/f_s$, where N equals the ratio of the slow speed sample rate period to the high speed sample rate period and f_s is the high speed sample frequency (400 Hz). Although this Bode phase shift term can introduce additional phase, the results of gain margin comparison data for the PWW FCS configuration show that the digital FCS design is within 11 percent of the analog FCS design for most measurements in Table 9.

AFATL Simulation Results

The AFATL PDAP/GBU-15 simulation study confirmed the Hughes results and proved that the PDAP design concepts were valid. However, there were anomalies discovered by AFATL and they are discussed in Appendix B.

TABLE 10. MEASURED PDAP DAMPING LOOP TRANSPORT LAG

	PITCH AND YAW CHANNELS	ROLL CHANNELS
PITCH AND YAW RATE GYRO INPUTS	278 TO 314 μs	411 μs (PWM) 237 μs (CWM)
SEEKER DERIVED RATE INPUTS	423 TO 460 μs	516 μs (PWM) 239 μs (CWM)
D/V GYRO DERIVED RATE INPUTS	430 TO 468 μs	342 μs

TRANSPORT LAG = ANALOG-TO-DIGITAL TIME + SOFTWARE CALCULATION + D/A TIME

DESIGN OBJECTIVE ≤600 μs

SECTION V

CONCLUSIONS AND RECOMMENDATIONS

The hybrid computer studies at Hughes Aircraft Company and Eglin Air Force Base have been evaluating the PDAP design characteristics for the CWM and PWM configurations. PDAP and analog autopilot comparison runs have been made for both trajectory runs and step response inputs. The majority of the cases have compared favorably. The PWM gain margin comparisons shown in Table 9 were all within acceptable close agreement. The present PDAP hardware has 3 autopilot configurations programmed in software which demonstrate the modular weapon capability. The input and output interface for each of these autopilot configurations is the same. The PDAP software provides the desired autopilot configuration by means of missile identification through discrete logic inputs. The PDAP wordlength sensitivity results have confirmed the input/output wordlength requirements. It is concluded that the PDAP concept has been shown to be feasible and is ready for Engineering Development.

(The reserse of this page is blank.)

APPENDIX A
PDAP SIMULATION BLOCK DIAGRAM

(The reverse of this page is blank.)

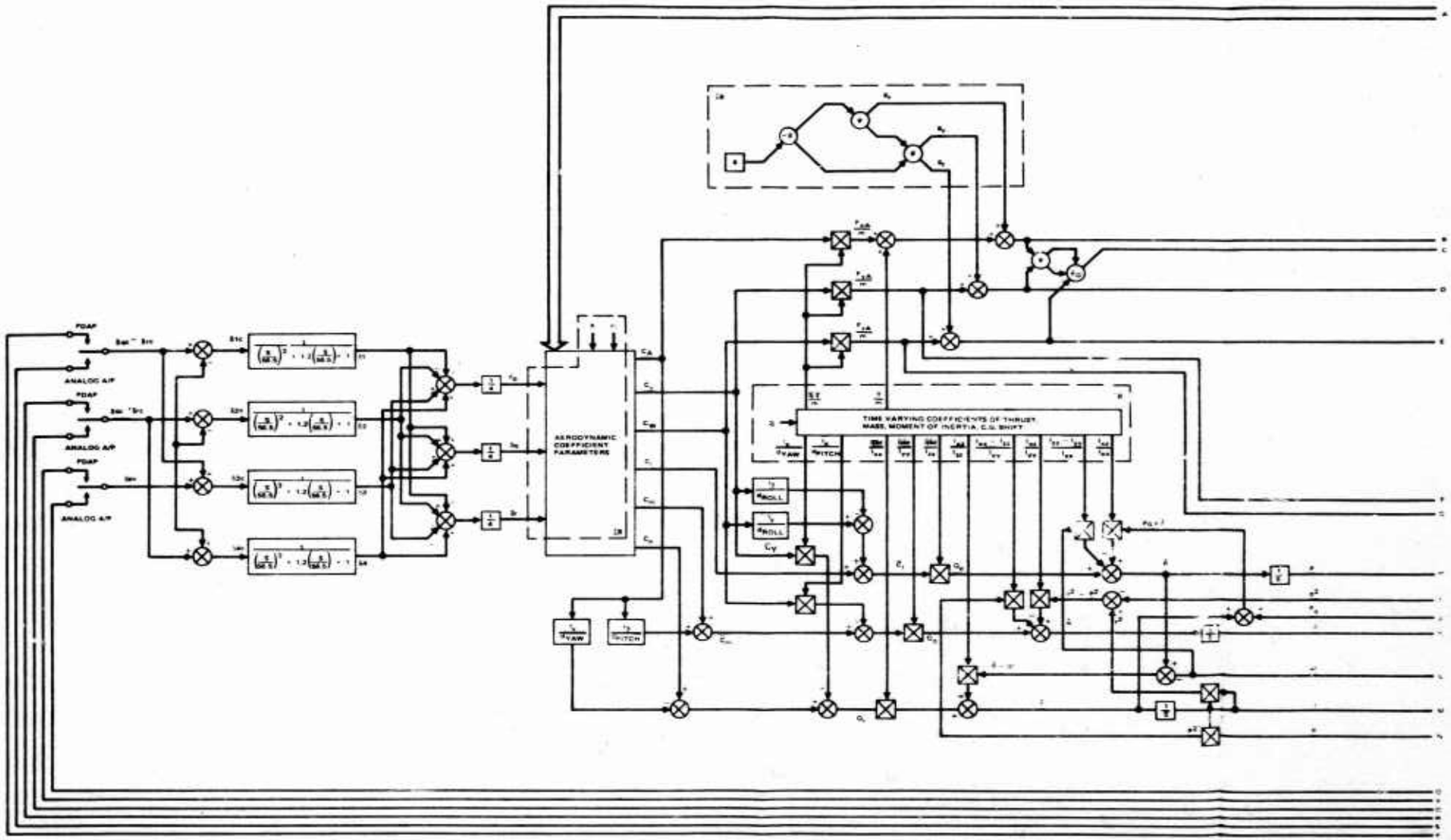

Figure A-1. PDAP Simulation Block Diagram

(The reverse of this page is blank)

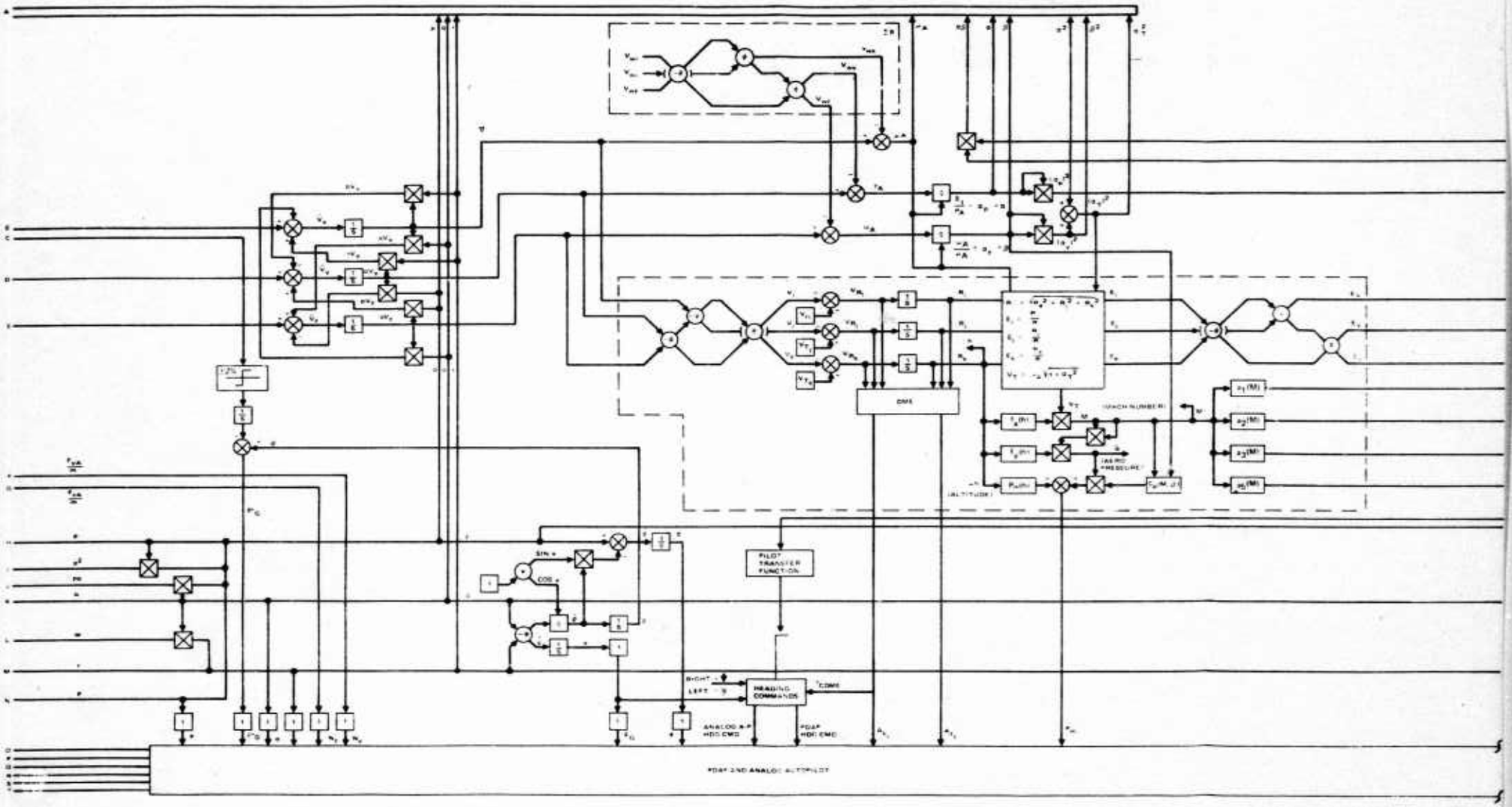

Figure A-1 (Continued).

(The reverse of this page is blan

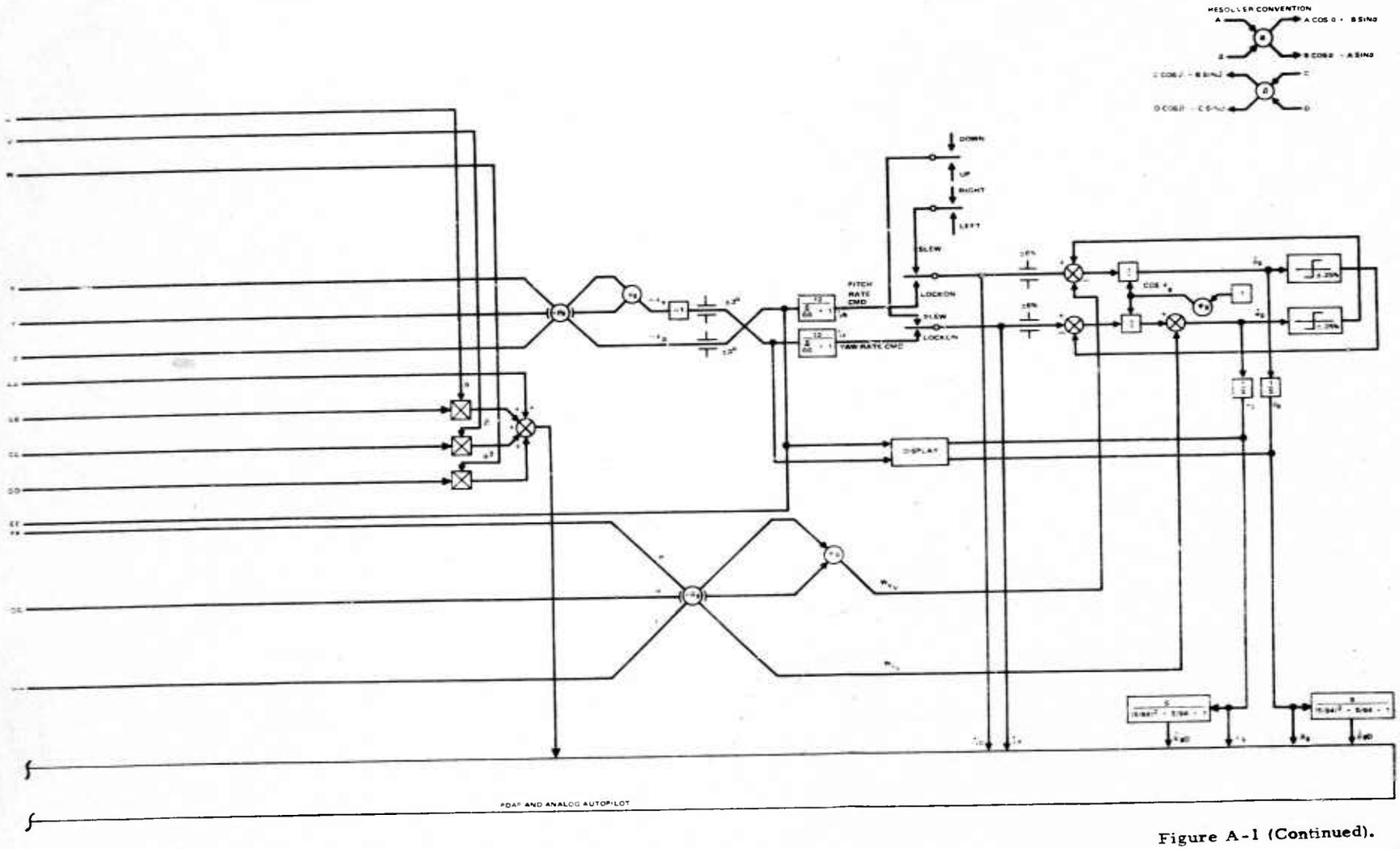

Figure A-1 (Continued).

(The reverse of this page is blank)

APPENDIX B

AFATL PDAP/GBU-15 SIMULATION (PDAP ANOMALIES)

GROUND POTENTIAL DIFFERENCE BETWEEN THE PROGRAMMABLE DIGITAL AUTOPILOT (PDAP) AND THE INTERFACE UNIT (IU)

The PDAP system exhibited a ground potential difference between the interface unit (IU) ground and the programmable digital autopilot ground. This difference is due to the fact that the signal and dc power grounds are common and large currents are required from the +5 vdc supply. Logic power (+5 vdc) for the PDAP originates from a +5 vdc power supply in the interface box (IB). (See Figure B-1a.) This power is transmitted to the PDAP via the IU. Once inside the PDAP, this power is distributed to the various cards. These cards include the three input/output (I/O) cards (Total I/O current is 1.5 A), the Arithmetic Unit (4 A), the Control Unit (5 A), the Program Memory (5.5 A), and the Operand Memory (2 A). The total current which is being supplied is 18 amperes. The power supply which is used requires 100 μfd/ampere at the remote sense point to maintain regulator stability. There is no physical space available in the PDAP or IU for the size capacitors required, therefore, remote sensing at the PDAP or IU is not used. Twenty gauge wire is the largest gauge that the connector pins will accept. Five 20 gauge wires (0.011 Ohms/foot) are used for grounds between the IU and the PDAP. Approximately two feet of wire connects the two unit grounds through two sets of contacts ($\simeq$0.01 Ohms each). The effective resistance of the five parallel paths is approximately 0.0085 Ohms. With 18 A of current flow, this produces a potential difference between the two unit grounds of approximately 153 mv.

The +5 volt power distribution and ground systems for the production PDAP will be designed to minimize ground potential differences due to line losses. (See Figure B-1b.) Features which will achieve this are:

(1) Production PDAP will require much less +5 volt power than the evaluation test units.

(2) The +5 volt regulator will be located in the PDAP chassis in close proximity to the central distribution points.

(3) Power and ground will be distributed to individual cards using minimal wire lengths.

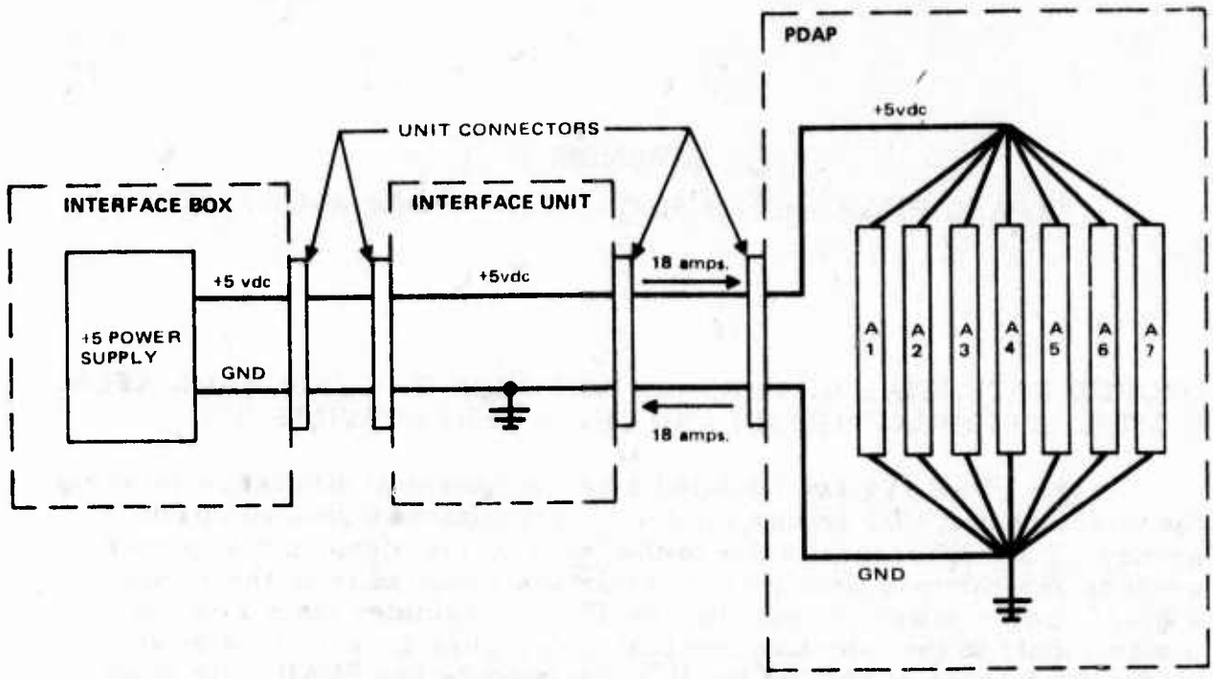

a) EVALUATION TEST PDAP GROUND AND POWER DISTRIBUTION

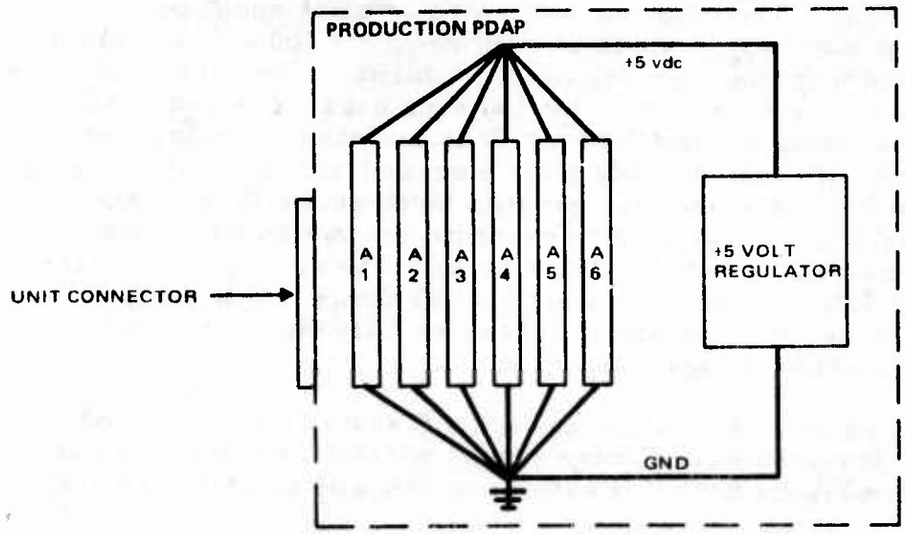

b) PRODUCTION PDAP GROUND AND POWER DISTRIBUTION

Figure B-1. PDAP Power and Ground Distribution Systems

(4) The number of series connector contacts, through which power and grounds must pass in getting from the central distribution point to the individual cards, will be held to a minimum.

PDAP PROGRAM STAYING WITHIN THE ENDLESS ANALOG-TO-DIGITAL LOOP

The PDAP software has an analog-to-digital control section which provides the analog-to-digital hardware with coded instructions used to sequence each analog to digital signal conversion. The software instructions specify which multiplexer input signal to convert and provides the analog-to-digital timing signals, sample and hold and start of conversion. These instructions are sent to the analog-to-digital hardware by the use of a dedicated operand memory word at location 1026. Figure B-2 shows a flow diagram of the software analog-to-digital functions provided to achieve analog-to-digital conversion of the PDAP input signals. After the proper sequencing of the Sample and Hold Signal and the Start of Conversion Signal have been sent to the analog-to-digital hardware, the PDAP program loops around the endless loop, assembly line numbers 296-297, until the End of Conversion flag is generated by the analog-to-digital hardware. When this flag is received, the PDAP program jumps out of the endless loop and executes other analog-to-digital software instructions for the next analog-to-digital conversion.

If, at the time the Start of Conversion Signal is sent to the analog-to-digital hardware, there should be a noise burst on the main bus which falsified the Start of Conversion code, the analog-to-digital hardware will not be able to start the conversion of the analog input signal. The analog-to-digital hardware will also not be able to generate the End of Conversion Flag. Once the PDAP program sends the start of conversion signal, the program waits in the endless loop for the End of Conversion flag. If a noise burst has falsified the Start of Conversion signal, the PDAP program will wait in the endless loop until the program is restarted, MASTER RESET.

Observation and testing of the PDAP hardware at Hughes Aircraft has not revealed this problem as yet. A special program was written to stop the PDAP software if the program remained within the endless loop for longer than 24.5 μs (the measured analog-to-digital conversion cycle time). The special test has not shown any failures. Although the number of times this problem has occurred at Eglin is small, the problem is undesirable. One failure after 100 hours of operating time corresponds to one failure after 2.304×10^9 analog-to-digital signal conversions. Because it is remotely possible to have a noise burst when the Start of Conversion signal is sent, it is recommended that the endless loop be replaced by a software timer (about 150 μs). The use of a software timer will allow the PDAP program to continue even though one analog-to-digital signal was not converted from time to time. The analog-to-digital signal will be updated during the next analog-to-digital cycle, 2500 μs later, and should

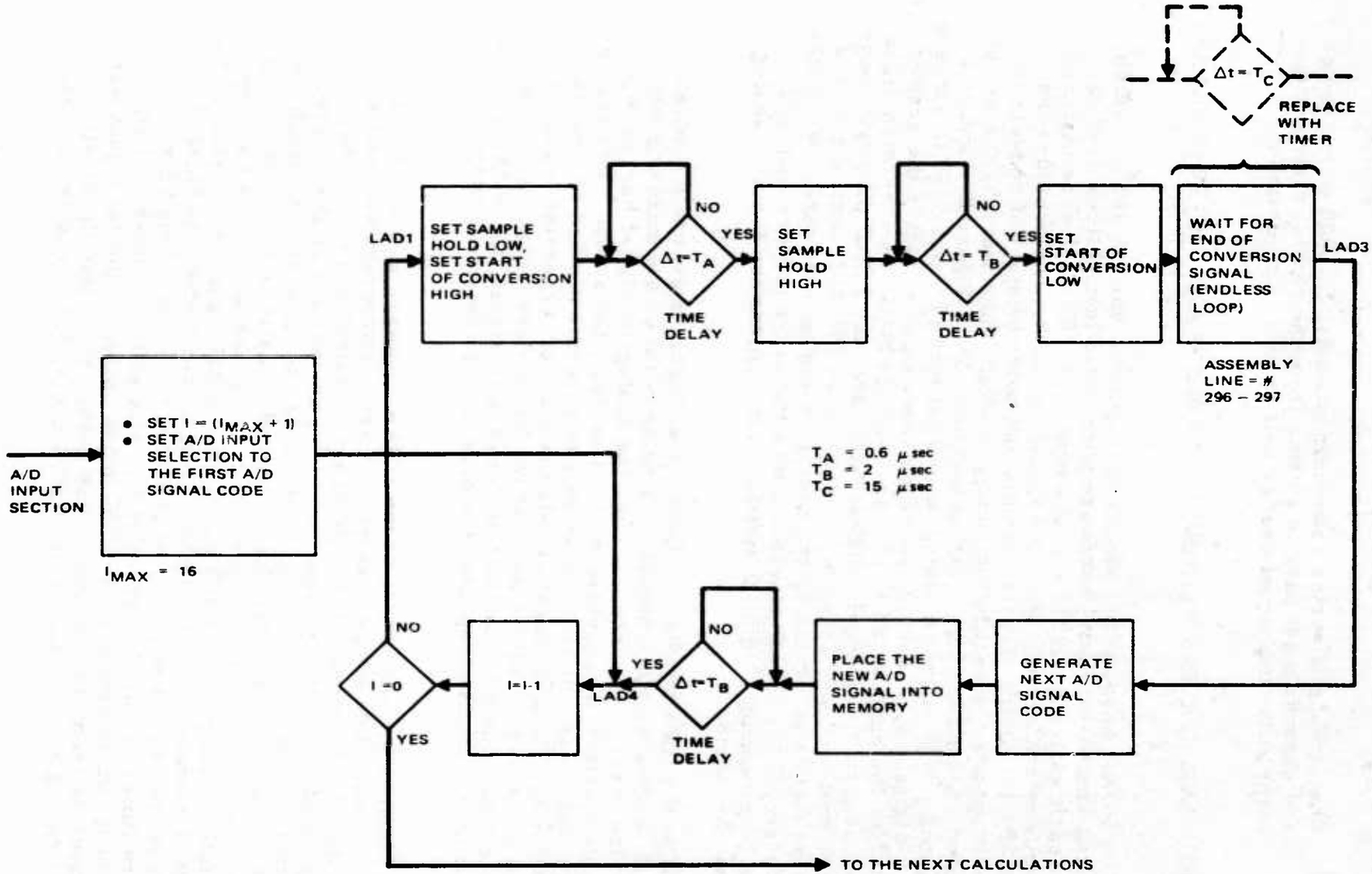

Figure B-2. Analog-to-Digital Signal Control Flow Diagram

not degrade PDAP autopilot performance. The use of endless loops (there is one in the existing PDAP program) will not be incorporated in the Production PDAP program. The software timer can be inserted into the present PDAP software program by replacing assembly line numbers 296 and 297 by the statements below. This timer will allow about 15 μs before proceeding to assembly line number 298.

REPLACEMENT FOR ASSEMBLY LINE NUMBER 296-297

SOFTWARE TIMER (ΔT = 15 μs)

```
296        ST, 23, 36
297 LAD2   IND, 23, LAD2
```

PDAP INPUT SIGNAL CROSS-COUPLING SENSITIVITY

PDAP cross-coupling can occur between the individual buffer amplifiers located within the interface unit and the analog-to-digital multiplexer circuitry located within the PDAP unit. In general, the cross-coupling amplitudes will increase with higher frequency input signals due to unwanted capacitor impedance paths that exist between electronic components. Input signal information to the multiplexer will be attenuated for frequencies above the analog pre-filter break frequency, 150 Hz. This attenuation will reduce multiplexer cross-coupling that is input signal dependent.

The PDAP A/D wordlength is 12 bits including sign. A bias level (offset value) of one least significant bit (1 LSB) in the 12 bit analog-to-digital wordlength corresponds to a value of 16(2^4) when the bias level is read in terms of the 16 bit wordlength used within the PDAP (see Figure B-3). A bias level equal to 1 percent of the analog-to-digital range (zero to the maximum position level) corresponds to a value of 328 when read in terms of the 16 bit word.

Figure B-4 shows the converted analog-to-digital signal levels read for each input channel when a 10 volt (0-P) 100 Hz sine wave was applied to one of the interface unit buffer inputs (see Figure B-5). This test was performed with each buffer input other than the driving channel capped with a 50 ohm resistor between the input pin and shield ground. All of the converted analog-to-digital signal levels in Figure B-4 are within 2 LSB levels (32) of the 12 bit analog-to-digital wordlength. Review of any column of Figure B-4 shows that the converted analog-to-digital signal level is basically the same value even though the buffer gain values are different (see Figure B-5). The values in this figure are the same values that are read when no input driving signal is applied and are the analog-to-digital bias levels. The same values as shown in Figure B-4 were obtained when the input driving signal was applied to the shielded cable input (approximately 15 feet long) connecting the analog computer to the interface unit. The conclusion drawn is that no measurable cross-coupling amplitude can be seen when a 10 volt (0-P) 100 Hz sine wave is

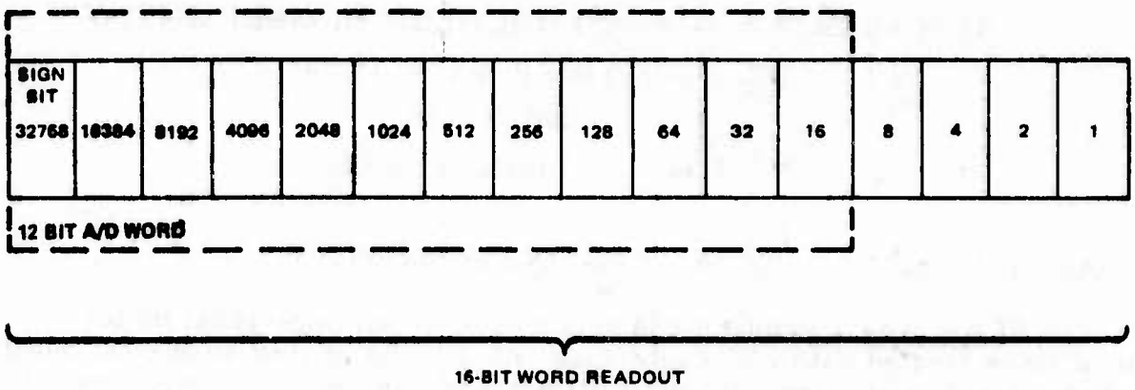

Figure B-3. Bit Location Value for a 16-Bit Word

A/D INPUT CHANNEL NUMBER AND PIN NUMBER		CONVERTED ANALOG/DIGITAL CROSS-COUPLED SIGNAL READOUT RANGE															
		0 J7	1 J8	2 J9	3 J10	4 J11	5 J12	6 J13	7 J14	8 J15	9 J16	10 J17	11 J18	12 J19	13 J20	14 J21	15 J22
0	J7	X	0 32	0	0	0	0 16	−32 0	0	0	0	16	0	0	0	0 32	32
1	J8	−32 0	X	0 16	0	0	0 32	−32 0	0	0	0	16	0	0	0	0 32	32
2	J9	−32 0	0	X	0	0	0 32	−32 0	0	0	0	16	0	0	0 16	16 32	32
3	J10	−32 0	0	0	X	0	0 32	−32 0	0	0	0	16	0	0	0 32	0 32	32
4	J11	−32 0	0	0	0	X	0 32	−32 0	0	0	0	16	0	0	0 16	0 16	32
5	J12	−32 0	0	0	0	0	X	−32 0	0	0	0	16	0	0	0 32	0 32	32
6	J13	−32 0	0	0	0	0	16 32	X	0	0	0	0 16	0	0	0 16	0 32	32
7	J14	−32 0	0	0	0	0	16 32	−32 0	X	0 32	0	16	0	0	0 32	0 32	32
8	J15	−32 0	0	0	0	0	0 32	−32 0	0	X	0	16 32	0	0	16 32	0 32	32
9	J16	−32 0	0	0	−16 0	0	0 32	−32 0	0	0	X	16 32	0	0	0 32	0 16	32
10	J17	−32 0	0	0	0	0	0 32	−32 0	0	0	0	X	0 32	0	0 32	0 32	32
11	J18	−32 0	0	0	0	0	16 32	−32 0	0	0	0	16	X	0 16	0 16	0 32	32
12	J19	−32 0	0	0	0	0	0 32	−32 0	0	0	0	16	0	X	0	0 32	32
13	J20	−32 0	0	0	0	0	16 32	−32 0	0	0	0	16	0	0	X	0 32	32
14	J21	−32 0	0	0	0	0	16 32	−32 0	0	0	0	16 32	0	0	0 32	X	32 48
15	J22	−32 0	0	0	−16 0	0	0 32	−32 0	0	0	0	0 16	0	0	0 32	0 32	X

Figure B-4. Input Cross-Coupled Readout Range Using a 10 Volt Sine Wave (100 Hz)

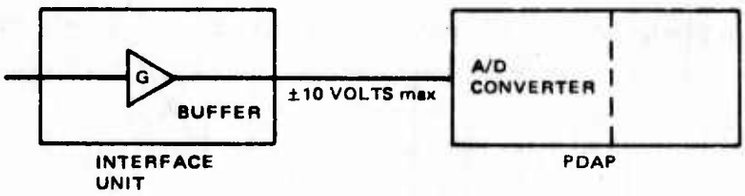

A/D INPUT CHANNEL NUMBER AND PIN NUMBER		INTERFACE UNIT GAIN, G
0	J7	0.6
1	J8	0.4
2	J9	0.2
3	J10	0.2
4	J11	0.4
5	J12	0.2
6	J13	0.4
7	J14	0.4

A/D INPUT CHANNEL NUMBER AND PIN NUMBER		INTERFACE UNIT GAIN, G
8	J15	0.1
9	J16	0.1
10	J17	0.4
11	J18	0.4
12	J19	0.2
13	J20	0.2
14	J21	0.2
15	J22	0.1

Figure B-5. Interface Unit Gain Values used with PDAP and Hybrid Simulation at Hughes

used. The same conclusion is assumed to apply for larger input signal levels. The magnitude of the high frequency information entering the interface unit when the PDAP is connected in a closed-loop configuration will be smaller than low frequency information because of attenuation by autopilot filtering and system dynamics.

PDAP GAIN MARGIN COMPARISONS

The PWM gain margin comparisons measured at Eglin are shown in Table B-1. Each of these gain margin comparisons are within 11 percent except one margin which is 27 percent low. This PDAP gain margin 8.95 dB (2.80) is adequate for the gain variations the yaw position loop will experience. The PDAP yaw heading position loop gain margin is 27 percent low because of the phase shift associated with the 50 Hz update rate of this loop calculation. The additional phase shift of this digital loop when combined with the yaw rate loop gain - phase characteristics produce a lower crossover frequency ($\angle\phi = -180$ degrees). The lower crossover frequency for this autopilot configuration has a larger Bode gain which produces a smaller gain margin. The 50 Hz update rate for other autopilot loop calculations (PWM roll attitude loop, PWM pitch attitude and acceleration loops, etc.) also produce additional phase shift over the analog design but the lower crossover frequency occurs in regions where the Bode gain is moderately flat. When the Bode gain is flat, the gain margin is relatively unchanged by additional phase shift.

TABLE B-1. PWM GAIN MARGIN COMPARISON

(MACH = 0.95, ALTITUDE = 20K)

	ANALOG, dB	PDAP, dB	DIFFERENCE, (percent)
ROLL AUTOPILOT			
• POSITION LOOP	8.46	7.78	0.68 (8)
• RATE LOOP	16.59	16.12	0.47 (5)
• FORWARD LOOP	12.87	12.04	0.83 (9)
YAW MIDCOURSE			
• POSITION LOOP	11.71	8.95	2.76 (27)
• RATE LOOP	20.98	20.00	0.98 (11)
• FORWARD LOOP	18.79	18.64	0.15 (2)
YAW DME TERMINAL			
• RATE LOOP	20.70	19.96	0.74 (8)
• ACCELERATION LOOP	16.59	16.06	0.53 (6)
• FORWARD LOOP	15.27	16.13	-0.86 (9)

Figure B-6 shows measured and theoretical yaw position loop gain margin as a function of the yaw position loop update rate. The measured data obtained from Eglin varied the yaw position loop update rate from 12.5 Hz to 400 Hz. The theoretical data tracks the measured data within 13 percent. The theoretical analog autopilot tracks the measured analog autopilot gain margin within 10 percent. Appendix C describes the method used to obtain the theoretical results. The additional phase shift of a digital loop (versus an analog loop) can be approximated by the expression, $\angle\phi = 360f\,T_2$. The transport lag, T_2, is equal to $(N + 1)/2$ times the sample rate period of the high speed loop. The variable, N, equals the ratio of the high speed update frequency to the lower speed update frequency.

Gain margin is a stability measurement of the gain variation (uncertainty) possible within a given loop before a system will go unstable. The amount of gain margin needed for a system design is a function of the parameter variation seen by a given loop. The parameter variation seen by the forward gain includes fin servo variations, aero variations, and digital-to-analog output gain variations each in series. The parameter variation seen by the rate loop includes rate gyro characteristics, the yaw rate analog-to-digital converter input, and closed-loop characteristics of the yaw position with the fin servo and aero data. The parameter variation seen by the yaw position loop includes heading sensor characteristics, and closed-loop characteristics of the yaw rate loop with the fin servo and aero data. In general, aero data and fin servo characteristics are the items having the biggest parameter variation. The gain margin to these parameters are displayed in the yaw forward loop gain margin. Because the yaw position loop sees aero data and the fin servo characteristics in a closed-loop form with the yaw rate loop, the yaw position gain margin is not a direct function of these gain variations. The yaw position loop gain margin will be a direct function of the yaw heading sensor and the yaw position analog-to-digital input gain, but these items do not have big gain variations. As mentioned before the PDAP yaw position gain margin value of 2.80 is adequate for this loop.

PWM PRESSURE LOOP RESPONSE

The PDAP PWM pressure altitude hold mode exhibits waggles in pitch body rate and angle of attack which are not readily apparent in the PWM analog autopilot configuration. This condition was observed in the hybrid simulation results at Eglin and at Hughes. The type of response seen in the pressure altitude hold mode is shown in Figures B-7 and B-8. The frequency of the waggles or limit cycle are around 0.4 Hz (2.5 second period). Although the PDAP configuration exhibits this condition, the PDAP PWM pressure altitude hold mode performs properly.

Figure B-9 shows a simplified block diagram of the PDAP pressure loop with its filter compensation. Because the PDAP PWM loops other than the pressure loop do not display this time response characteristic, the software program was also modified to allow the output of the pressure filter calculation to be sent directly to the pitch digital-to-analog input. The program was also modified to allow the converted analog-to-digital

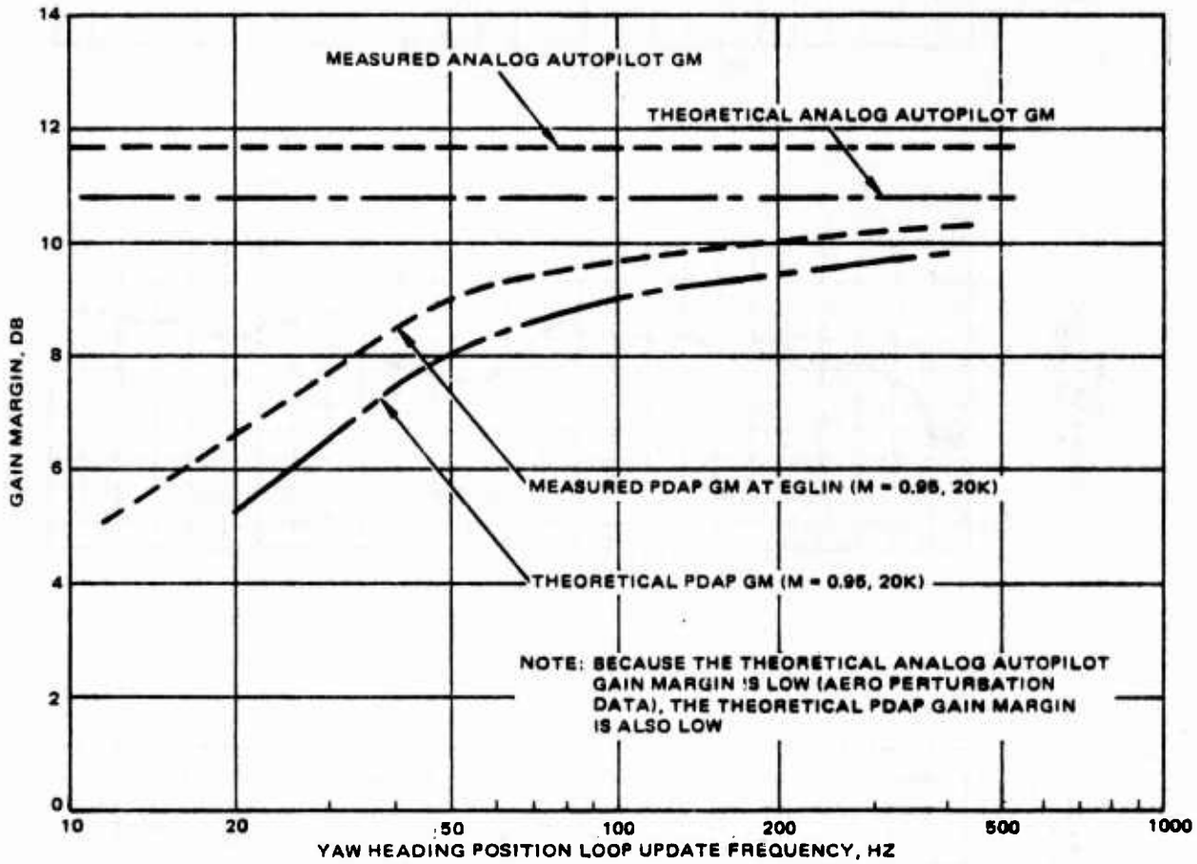

Figure B-6. PWM Gain Margin as a Function of Yaw Heading Position Loop Update Frequency

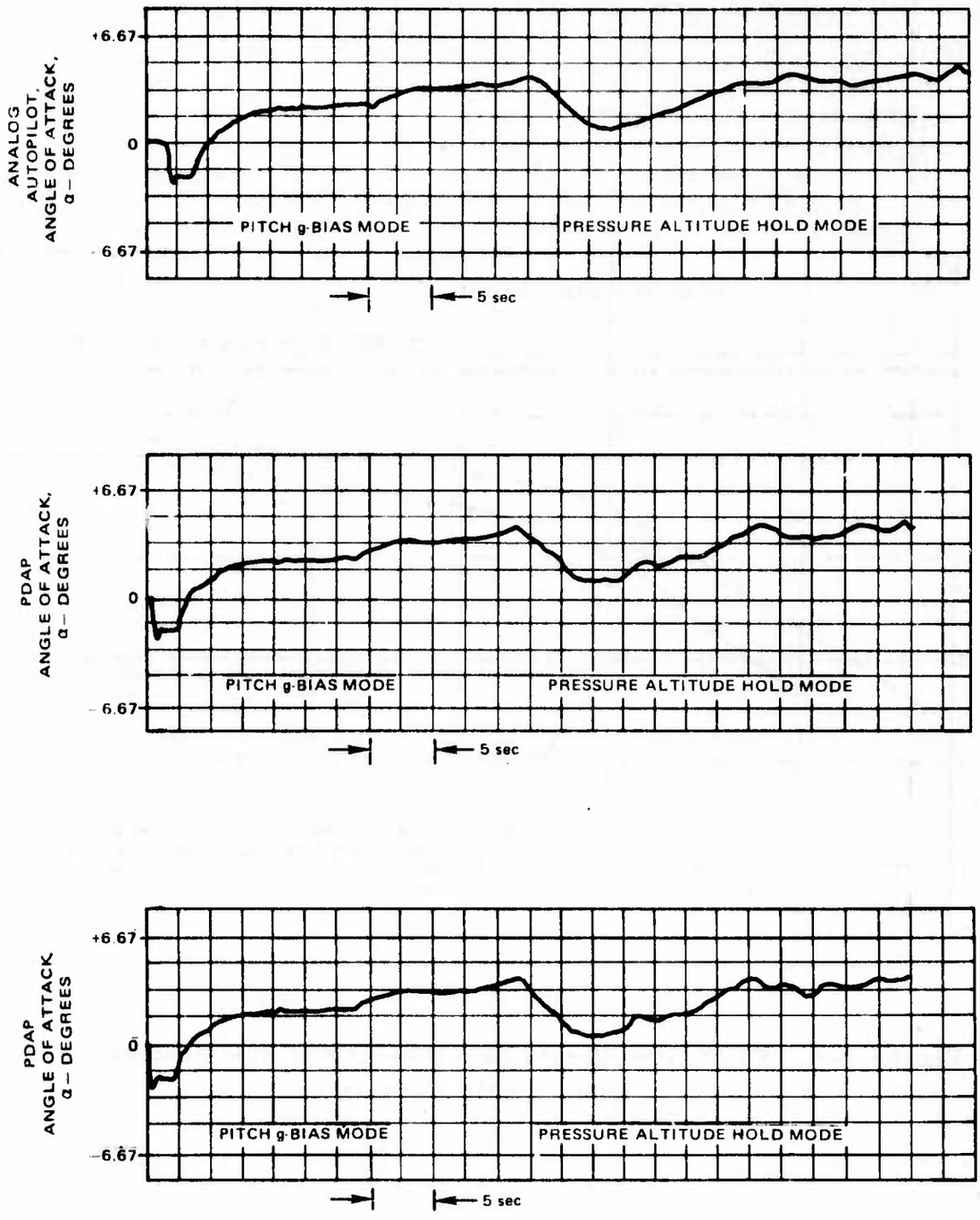

Figure B-7. PWM Autopilot Response Comparisons

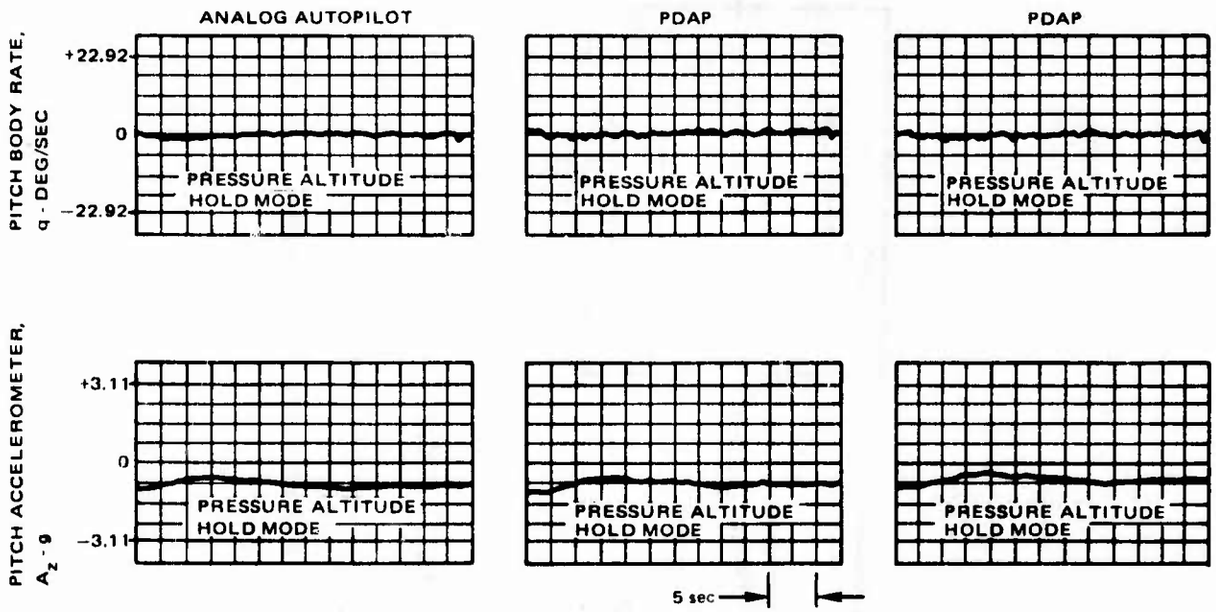

Figure B-8. PWM Autopilot Response Comparisons

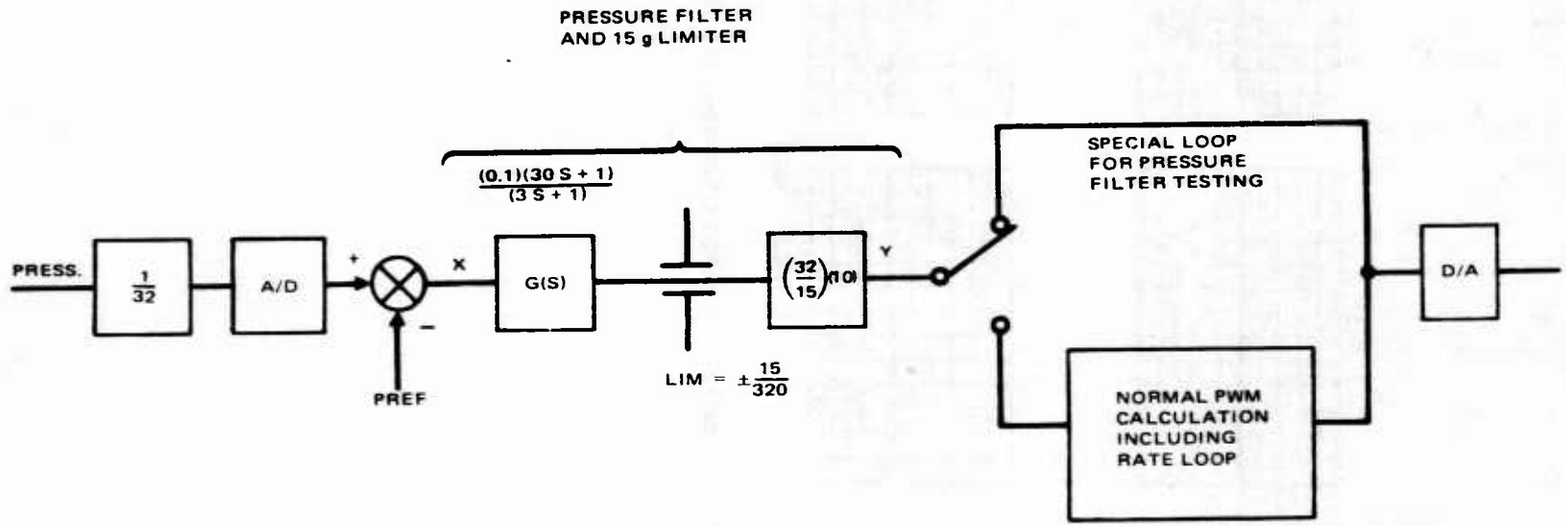

PRESSURE FILTER STEP RESPONSE

$$X(t) = \left(\frac{32}{15}\right) Y_o \left[U(t) + 9e^{-t/3}\right], \; Y_o - \text{STEP INPUT MAGNITUDE}$$

Figure B-9. PWM Pressure Filter Loop Calculation

pressure signal to be sent to the yaw digital-to-analog input. For testing purposes the pressure reference signal was set to zero.

Figure B-10 shows the time response of the pressure filter to a square wave input. The pole-zero location of the pressure filter, (30S+1)/(3S+1), produces a transient peak amplitude which is ten times larger than the steady state amplitude. The time response of the pressure filter in this figure is very clean (no waggles). Figure B-11 shows the pressure filter response to a triangular signal having an input frequency of 0.1 Hz (left side) and 1.0 Hz (right side). Some waggles are seen in the response to the 1.0 Hz input and more waggles are seen in the response to the 0.1 Hz input. Figure B-12 shows the pressure filter response to a triangular signal having an input frequency of 0.01 Hz. The response on the left side of this figure is a rerun of the response on the right using a faster recorder speed. The waggles or limit cycle condition in Figure B-12 are more pronounced because the filter response amplitude relative to the strip chart height is magnified and because the limit cycle frequency is lower. The frequency of the waggles associated with the transient filter response are the same as those seen in Figures B-7 and B-8 (0.4 Hz, 2.5 second period). The reasons for the waggles become more apparent when one correlates the analog-to-digital quantization levels in the bottom strip chart with the filter response in the center strip chart. Each time the converted pressure signal changes analog-to-digital quantization levels in the bottom strip chart (dense pin response region), the filter response output has a jump change in amplitude which is the transient response of the filter. In the region where the converted pressure signal has a constant quantization level, the pressure filter response decays to the steady state filter amplitude (one-tenth the transient amplitude). When the converted pressure signal changes amplitude again, the transient filter response is repeated. The frequency of the waggles (limit cycle) in the filter response is due to the slope magnitude of the input signal, not the frequency of the input signal. If the input amplitude in Figure B-12 is increased (larger slope magnitude), then less time will be spent at each analog-to-digital quantization level and the limit cycle frequency will be higher. The amplitude of the waggles will then be smaller and more uniform.

The pressure altitude hold mode in a closed loop configuration (the hybrid simulation) wants to hold the pressure input signal to the pressure reference signal level. The closed loop dynamics of the PWM configuration are such that the pressure signal slowly varies in a fashion which produces the waggles seen in figures B-7 and B-8. The waggles in these figures are smoothed because of autopilot filtering and system dynamics. The time derivative of the pressure input signal is proportional to the glide bomb body velocity in the Z plane $\{P = (\Delta P/\Delta h)h, \dot{P} = (\Delta P/\Delta h)V_Z\}$. If the PWM system performance is degraded by the limit cycle condition, the waggles could be minimized by adding more analog-to-digital wordlength (a cost increase), by rescaling the range of the pressure input signal to a value less than 32 PSI, or by the use of alternate or additional filtering which would smooth the pressure input signal. Since the PDAP PWM pressure altitude hold mode performance does not appear to be degraded, no change is recommended. The production PDAP design will not include a pressure altitude hold mode.

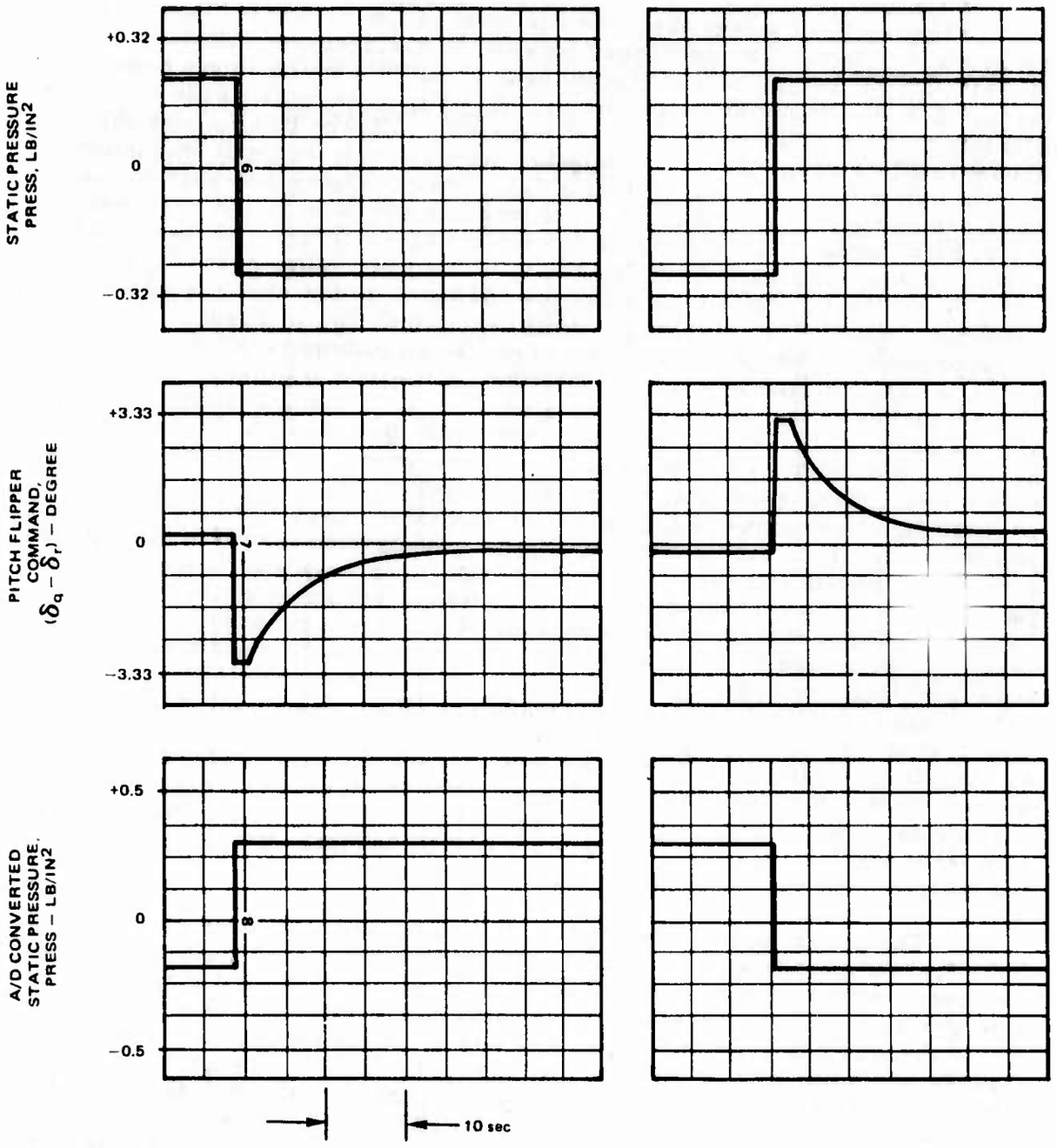

Figure B-10. PDAP Pressure Response to Square Wave Pressure Signal

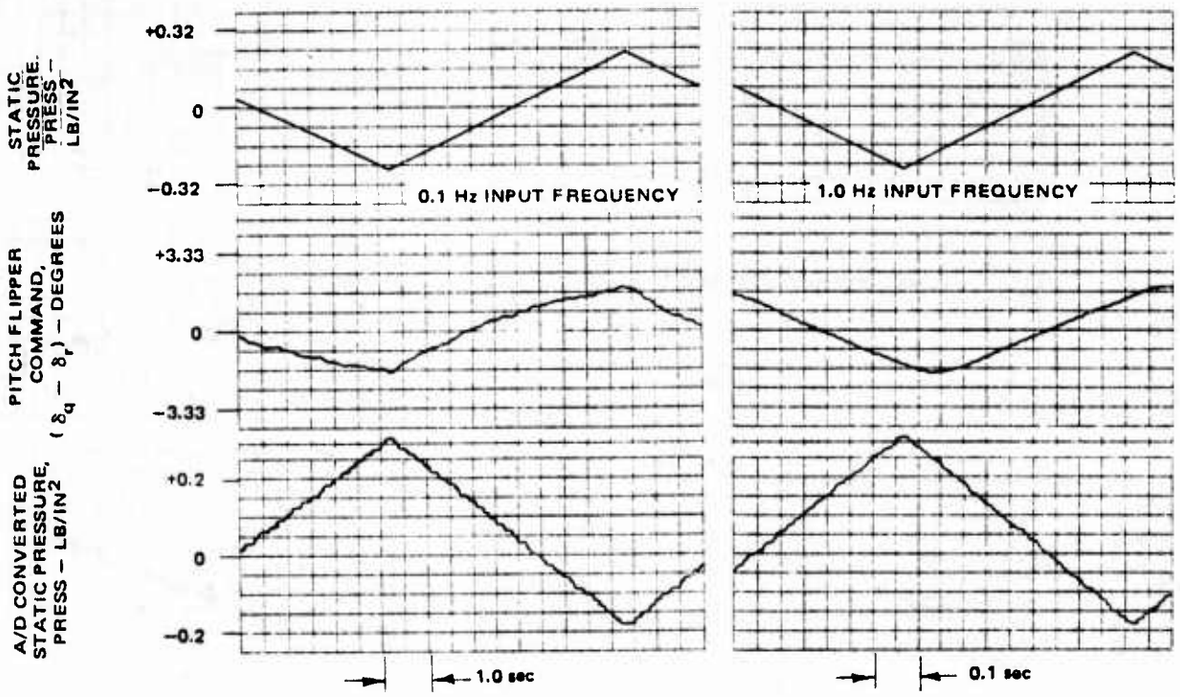

Figure B-11. PDAP Pressure Filter Response to 0.1 Hz and 1.0 Hz Pressure Signal

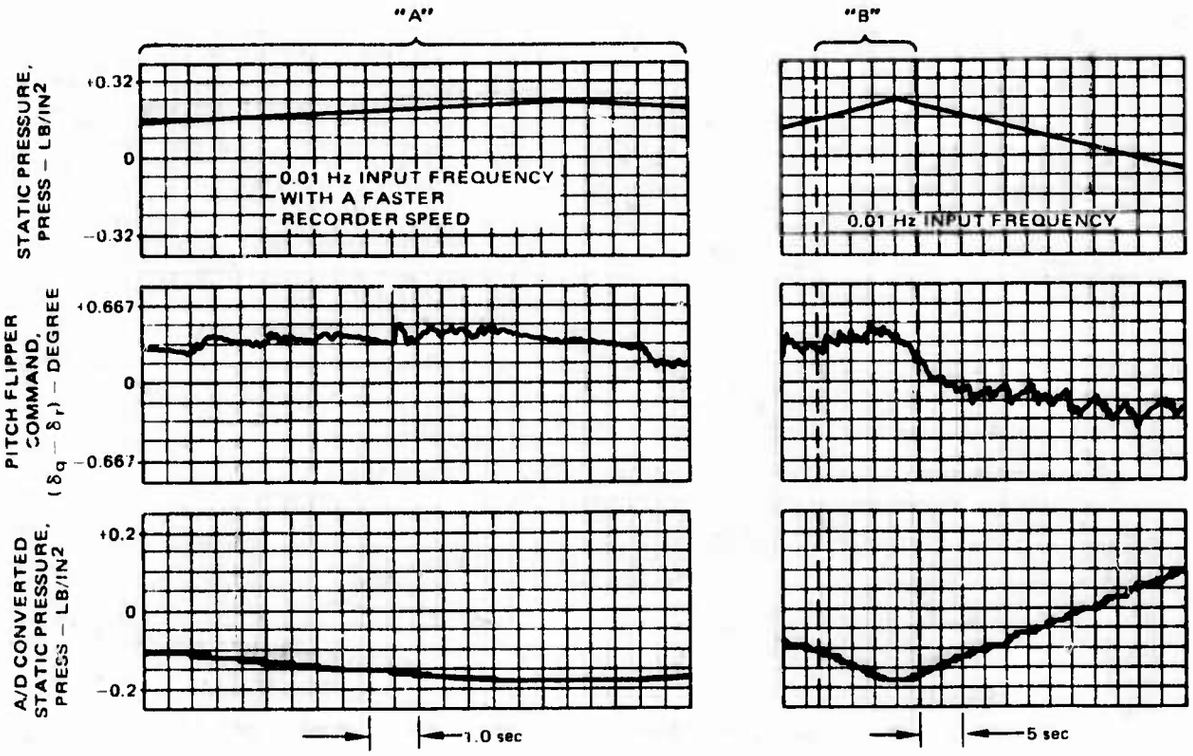

NOTE: REGION "A" DATA IS AN EXPANDED SCALE OF THE INFORMATION BETWEEN THE DASHED LINES ON THE RIGHT -- WHICH IS IDENTIFIED BY THE "B".

Figure B-12. PDAP Pressure Filter Response to 0.01 Hz Pressure Signal

PWM YAW CROSS RANGE DRIFT

The PWM autopilot study at Eglin showed that the PDAP PWM autopilot configuration produces an inertial cross range drift equivalent to 0.66 degrees of yaw heading error as depicted in Figure B-13. The equivalent PWM analog autopilot configuration (bias free) produced no noticeable inertial cross range drift. Unlike the simulated analog autopilot configuration, the PDAP hardware buffers, analog-to-digital converter circuitry, and digital-to-analog circuitry have biases (null offsets) which are within 1 percent of the full scale voltage range (± 10 volts). The PDAP biases like sensor biases, actuator offset values, etc. in a complete hardware configuration will cause attitude and acceleration signals to achieve values necessary to counteract system offset values. Part of the inertial cross range drift in Figure B-13 is a result of yaw heading position analog-to-digital circuitry bias (0.2 degrees measured) while the remaining cross range drift is primarily due to roll attitude analog-to-digital circuitry bias (0.288 degrees measured). When the PDAP roll analog-to-digital bias was nulled, the inertial cross range drift approached the yaw heading position analog-to-digital bias level.

Figure B-14 shows PWM analog autopilot cross range drift when roll attitude bias levels are added to the simulation. This figure shows the PWM analog autopilot is also sensitive to roll attitude biases in the yaw inertial plane. One of the cross range traces in Figure B-14 depicts the PDAP PWM autopilot configuration when 10 degrees of roll attitude bias is added. This PDAP cross range result is very close to the analog autopilot result having the same roll attitude bias. This comparison shows that the inertial cross range drift is not a digital problem, but a roll attitude bias condition which couples into the yaw plane through aero coupling terms for either the PDAP or analog autopilot.

Figures B-15 through B-18 describe how a roll attitude bias will produce a steady state side slip angle, B, which will contribute to inertial cross range drift. The information in these figures depicts how roll errors can generate cross range drift using simplified aero expressions. The results from these equations unfortunately do not produce the cross range magnitudes seen in simulation results. More complicated aero equations are not pursued since the observed cross-range drift is a PWM roll to yaw coupling phenomena not an exclusive PDAP coupling effect. The real analog autopilot design like the PDAP will also have bias offset values associated with operational amplifiers. The sensors associated with the glide bomb will also have bias levels. Bias errors from the operational amplifiers and/or sensors will produce cross range drift effects.

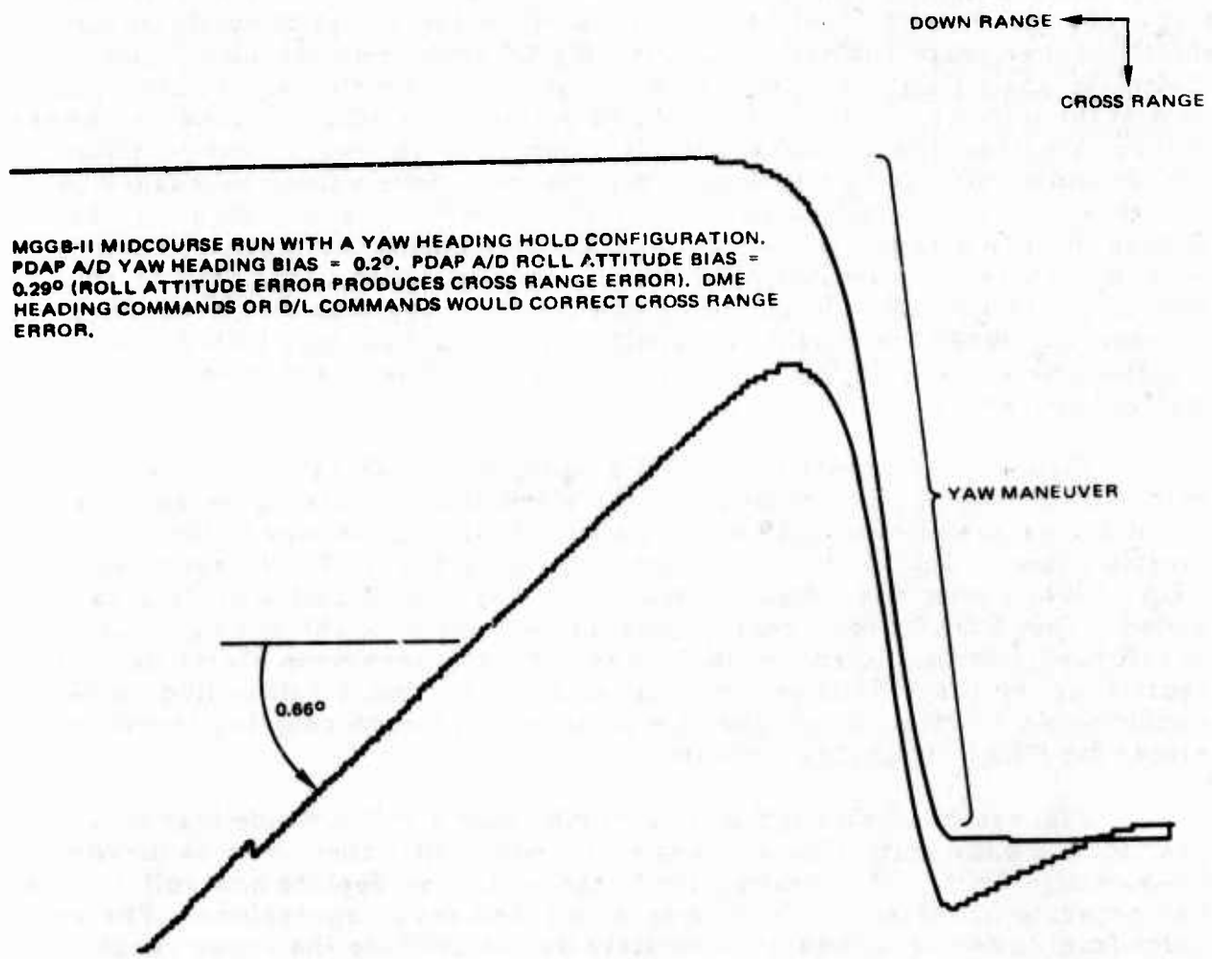

Figure B-13. Analog and PDAP MGGB-II (Phase I) Autopilot Comparison

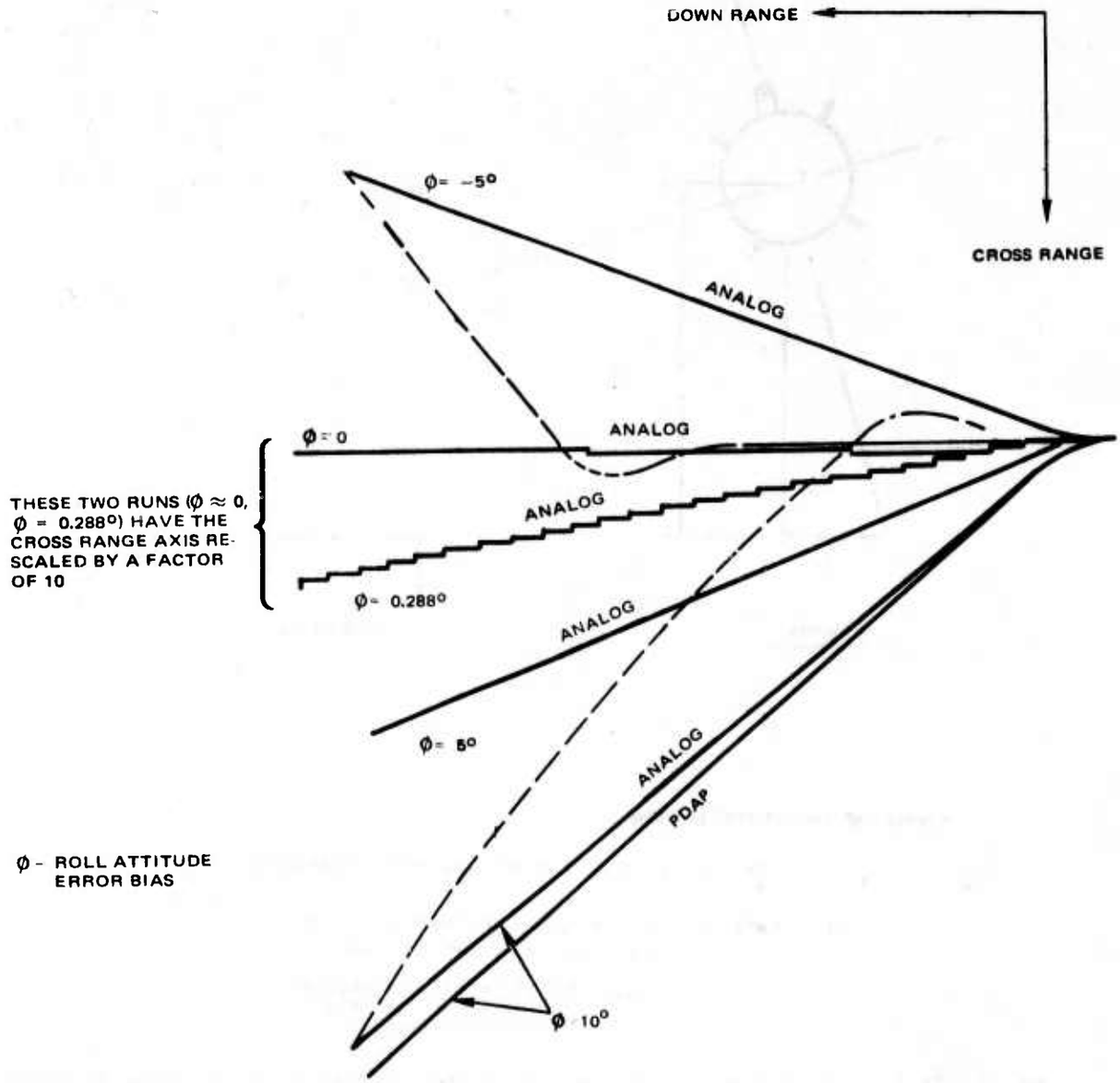

Figure B-14. Roll Attitude Error Sensitivity to Cross Range Error

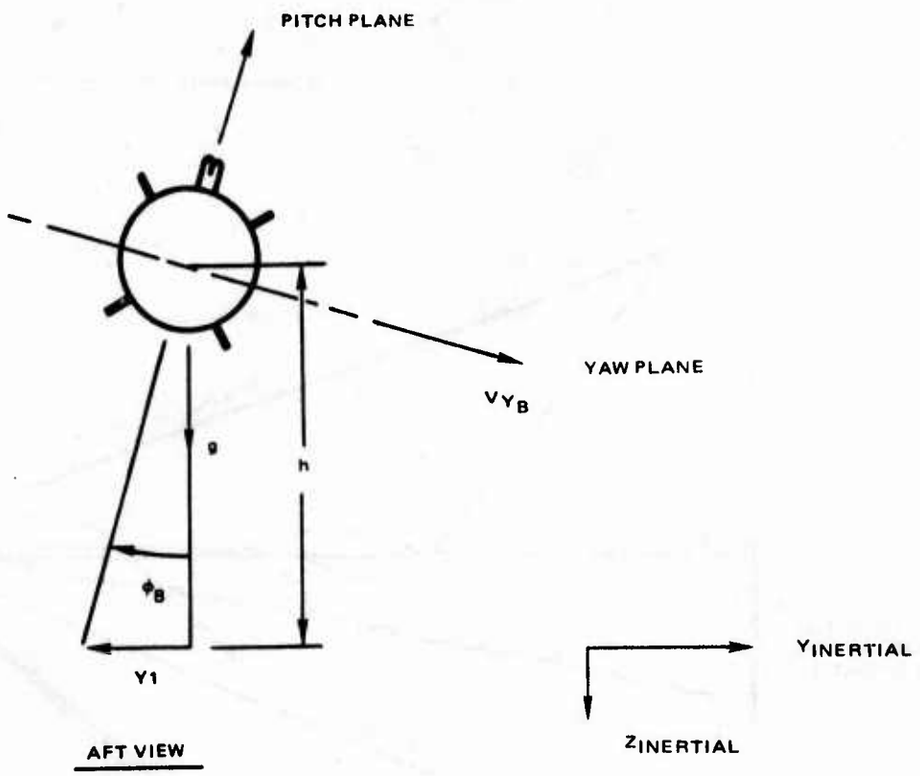

CROSS RANGE INERTIAL MOTION

$$Y = -Y_1 + \left\{V_{Y_B} \cos \phi_B\right\} t \quad \text{(SMALL } \phi_B \text{ ANGLE EQUATION)}$$

$Y_1 = h \sin \phi_B$,

h – INITIAL GLIDE BOMB ALTITUDE

ϕ_B – ROLL ATTITUDE A/D BIAS

V_{Y_B} – STEADY STATE SIDE VELOCITY GENERATED BY THE ROLL ATTITUDE A/D BIAS

Figure B-15. Cross Range Motion Equation Due to Roll Attitude Analog to Digital Bias

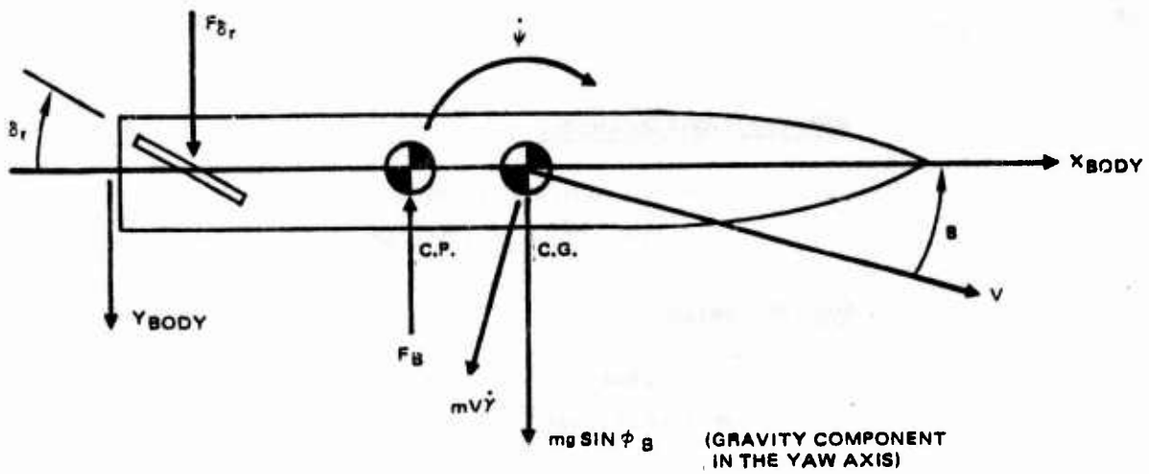

(1)

$$(q A C_{Y_{\delta_r}})_r + (q A C_{Y_\beta})\beta + mg \sin \phi_B = mV\dot{\gamma} = 0 \quad \text{(FORCE EQ)}$$

STEADY STATE AERO TERMS DUE TO β WITH FORCE $mV\dot{\gamma}$ TO ZERO FOR THE YAW HEADING HOLD CONFIGURATION

(2)

$$(q Ab C_{n_{\delta_r}})\delta_r + (q Ab C_{n_\beta})\beta = I_Z \ddot{\psi} = 0 \quad \text{(MOMENT EQ.)}$$

THE STEADY STATE YAW HEADING HOLD CONFIGURATION WILL FORCE $\ddot{\psi} = 0$, $\dot{\psi} = 0$ AND $\psi = \psi_\epsilon$ NO ASSUMED HEADING SENSOR DRIFT)

$$\beta = \frac{-mg \sin \phi_B}{qA\left[C_{Y_\beta} - C_{Y_{\delta_r}}\left(\frac{C_{n_\beta}}{C_{n_{\delta_r}}}\right)\right]}$$

$$V_{Y_{BODY}} = V \sin \beta$$

$$\delta_r = -\left(\frac{C_{n_\beta}}{C_{n_{\delta_r}}}\right)\beta, \left|\frac{C_{n_\beta}}{C_{n_{\delta_r}}}\right| < 1$$

Figure B-16. Steady State Yaw Aero Perturbation Equations

ASSUMED FLIGHT CONDITION

$M = 1.3$, ALTITUDE = 19k

$q = 1200\ lb/ft^2$, $V = 1353\ ft/sec$

MASS PROPERTIES

$A = 16.594\ ft^2$

$M = 88.27$ SLUGS

AERO PARAMETERS

$$C_{Y_{\delta_r}} = 0.435,\ C_{Y_B} = -1.566$$

$$C_{n_{\delta_r}} = -0.181,\ C_{n_B} = 0.091$$

$$\left[C_{Y_B} - C_{Y_{\delta_r}}\left(\frac{C_{nB}}{C_{n_{\delta r}}}\right)\right] = -1.3473$$

AERO EQUATION

$$\frac{B}{\sin \phi_B} = \frac{-mg}{qA\left[C_{Y_B} - C_{Y_{\delta_r}}\left(\frac{C_{nB}}{C_{n_{\delta r}}}\right)\right]} = 0.1059$$

$$V_{Y_{BODY}} = 1353 \sin B$$

Figure B-17. Yaw Heading Flight Conditions

INFORMATION OBSERVED FROM EGLIN DATA

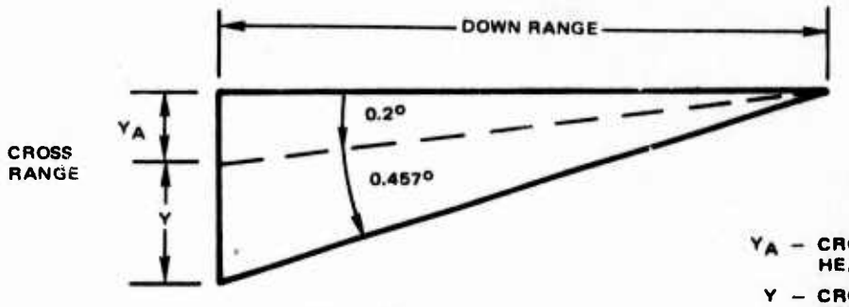

Y_A – CROSS RANGE DUE TO YAW HEADING A/D BIAS

Y – CROSS RANGE DUE TO ROLL-YAW COUPLING OF THE ROLL ATTITUDE A/D BIAS, ϕ_B

Y = 2393 ft

V_{Y_B} = 5.57 ft/sec

CALCULATED CROSS RANGE MOTION DUE TO ROLL A/D BIAS

USING THE FLIGHT TIME AND THE MEASURED ROLL A/D BIAS (0.29°) ASSOCIATED WITH FIGURE B-13, THE CALCULATED VALUE OF Y FROM FIGURE B-15 WITH THE DATA FROM FIGURE B-17 IS SIGNIFICANTLY SMALLER THAN THE OBSERVED VALUE OF Y ABOVE. A ROLL A/D ATTITUDE BIAS IN THE NEIGHBORHOOD OF 2.5° WILL PRODUCE THE CROSS RANGE MAGNITUDES OBSERVED ABOVE. MORE COMPLICATED AERO EQUATIONS (INCLUDING ROLL-YAW COUPLING TERMS) THAN THOSE SHOWN IN FIGURE B-16 COULD PRODUCE A LARGER SIDE SLIP ANGLE, B, FOR A GIVEN ROLL A/D BIAS LEVEL.

Figure B-18. Cross Range Data/Calculations

(The reverse of this page is blank)

APPENDIX C
PWM HEADING LOOP GAIN-PHASE CALCULATIONS

PDAP RATE LOOP PHASE SHIFT

PDAP HEADING POSITION LOOP PHASE SHIFT

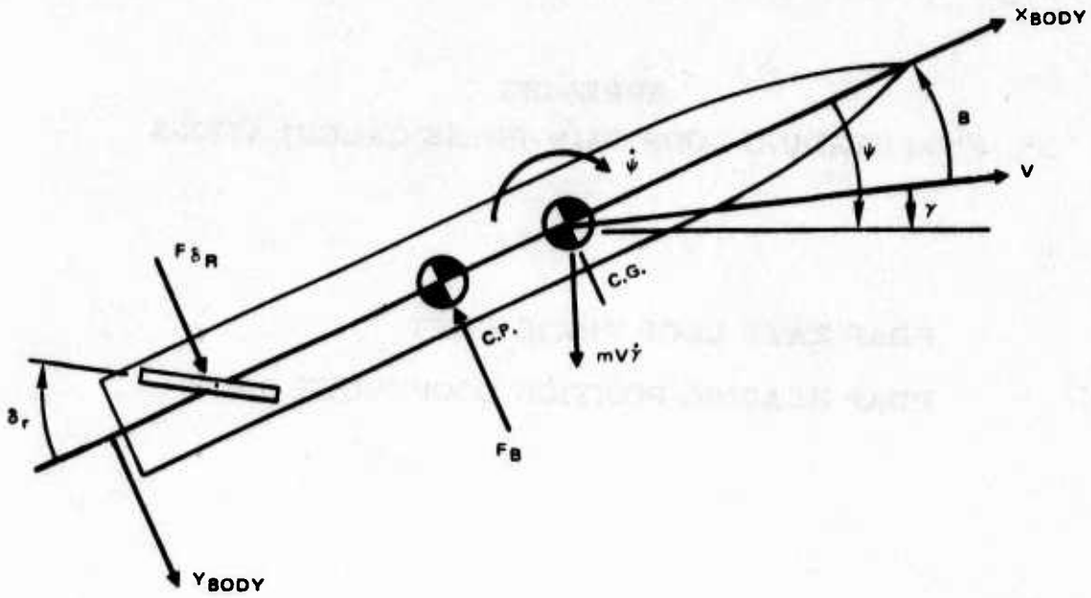

(1) $(q A C_{Y_{\delta_r}})\delta_r + (q A C_{\beta})\beta = mV\dot{\gamma}$ (FORCE EQ.)

(2) $(q Ab C_{n_{\delta_r}})\delta_r + (q Ab C_{n_\beta})\beta = I_Z\ddot{\psi}$ (TORQUE EQ.)

(3) $\psi = \gamma - \beta$

$N_{Y_{\delta_r}} = q A C_{Y_{\delta_r}}/mV \geq 0, N_{Y_\beta} = q A C_{Y_\beta}/mV \leq 0$

$N_{\delta_r} = q Ab C_{n_{\delta_r}}/I_Z \leq 0, n_\beta = q Ab C_{n_\beta}/I_Z \geq 0$

$$\frac{\dot{\psi}}{\delta r} = \frac{-\left[-Sn_{\delta_r} + (N_{Y_\beta} n_{\delta_r} - N_{Y_{\delta_r}} n_\beta)\right]}{S^2 - N_{Y_\beta} S + n_\beta}$$

Figure C-1. Yaw Aero Perturbation Equations

FLIGHT CONDITION, $M = 0.95$, ALT = 20k

$q = 614.9\ lb/ft^2$, $V = 1036.9\ ft/sec$

MASS PROPERTIES, $m = 88.3$ SLUGS

$I_z = 765\ SLUG\text{-}ft^2$

$A = 16.59\ ft$

$b = 11.33\ ft$

AERO PARAMETERS, $C_{Y_{\delta_r}} = 0.768$, $C_{Y_\beta} = -1.857$

$C_{n_{\delta_r}} = -0.346$, $C_{n_\beta} = 0.1785$

AERO PERTURBATION EQUATION

$$\frac{\dot{\psi}}{\delta_r} = -\frac{[52.21S + 8.498]}{[S^2 + 0.207S + 26.97]} = \frac{-0.3151[6.14S + 1]}{Q_{2\pi 0.827}^{0.02}}$$

FIN SERVO MODEL

$$\frac{\delta_r}{\delta_C} = \frac{1}{\left[Q_{2\pi 9}^{0.7}\right]^2}$$

AUTOPILOT COMPENSATION

$$G(S) = \frac{1}{\left(\frac{S}{400} + 1\right)^2}$$

YAW RATE GAIN

$$K_{\dot{\psi}} = 0.11$$

Figure C-2. PWM Yaw Heading Configuration Parameters

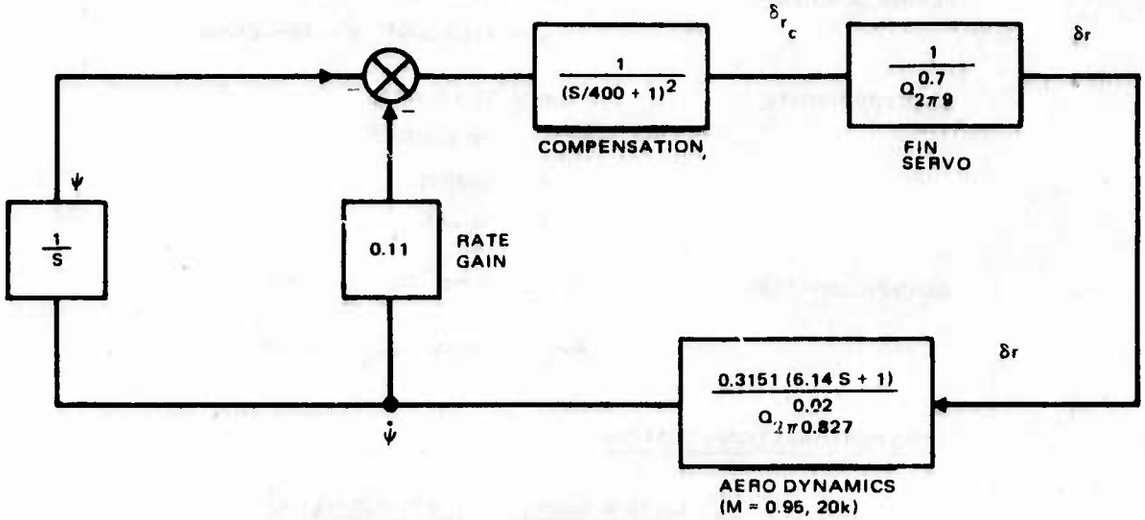

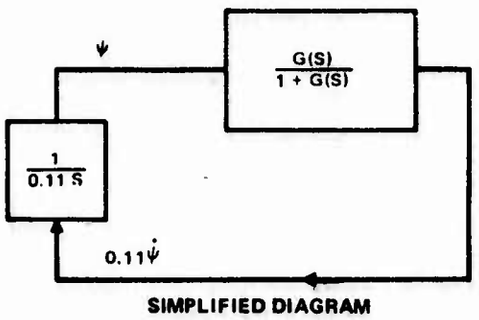

$$G(S) = \frac{\{(0.11)(0.3151)\}\ (6.14\,S+1)}{(S/400+1)^2\ Q^{0.7}_{2\pi 9}\ Q^{0.02}_{2\pi 0.827}}$$

Figure C-3. PWM Yaw Heading Block Diagram

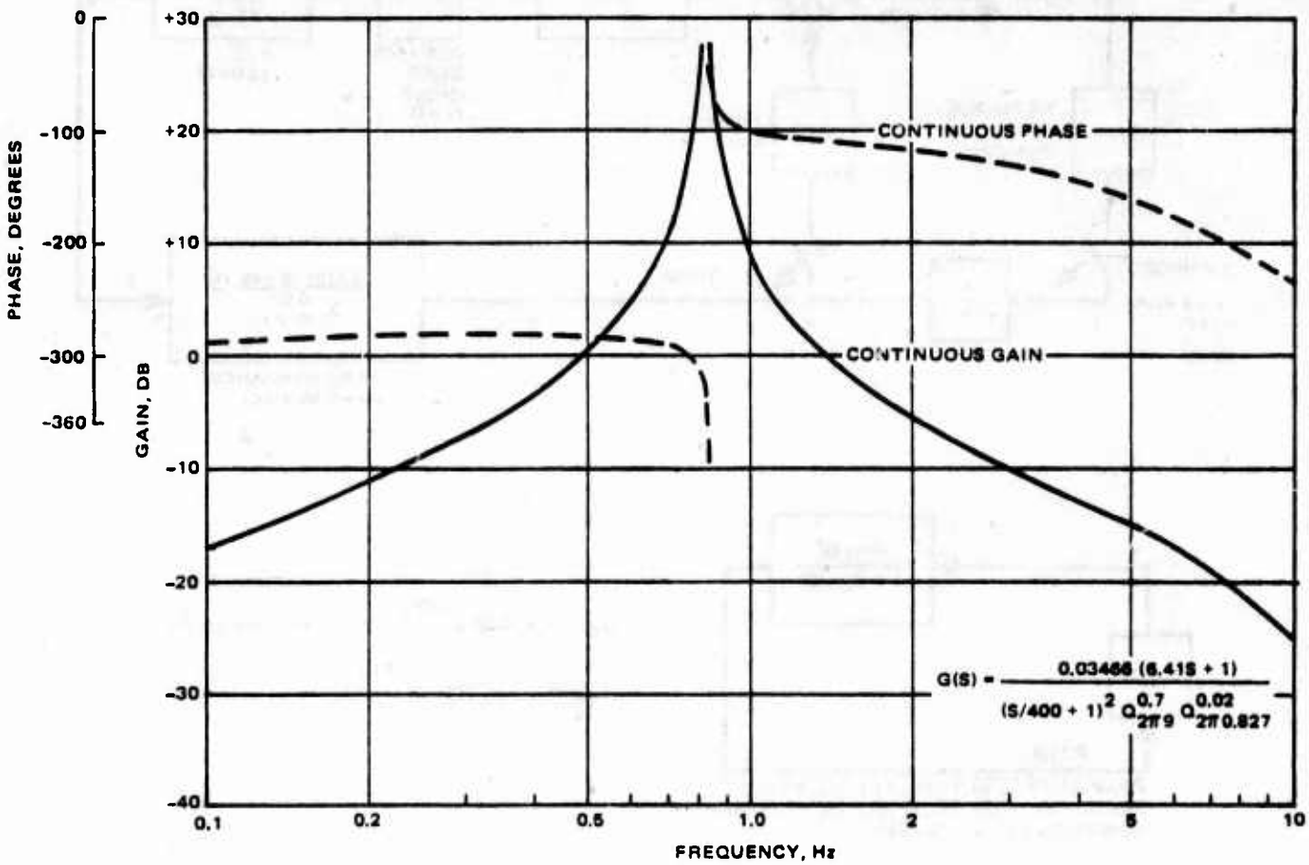

Figure C-4. PWM Yaw Heading Rate Loop Gain-Phase Characteristics (M = 0.95, 20K)

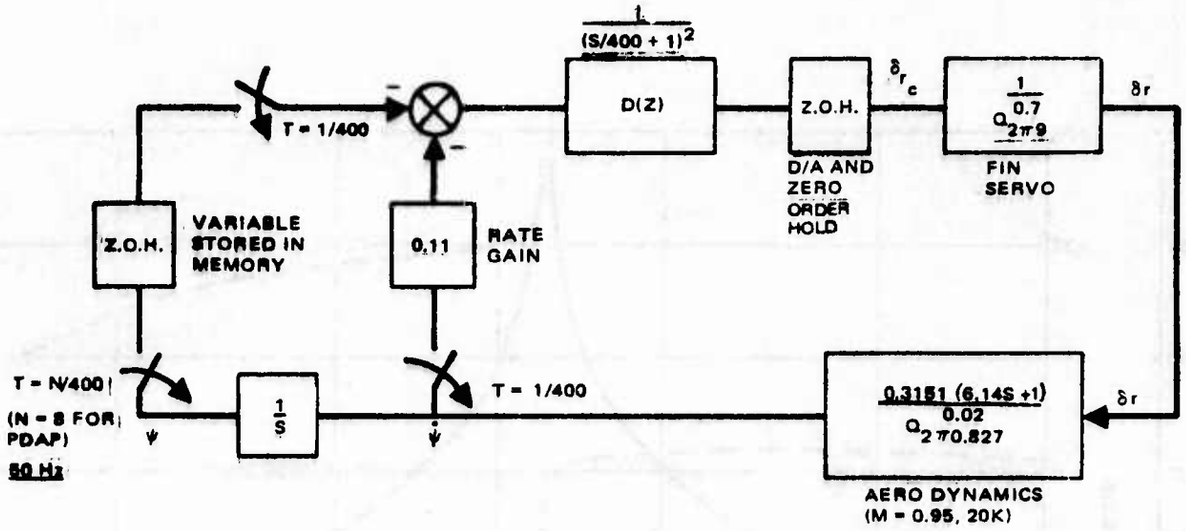

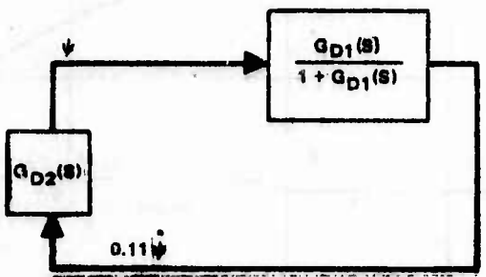

$G_{D1}(S) = G(S)\, e^{-ST_1}$, G(S) – SEE FIGURE A3

$G_{D2}(S) = \left\{\frac{1}{0.11S}\right\} e^{-ST_2}$

Figure C-5. PDAP PWM Yaw Heading Block Diagram

$$\left[G_{D1}(S)\right]_{\substack{\text{PDAP}\\\text{RATE}\\\text{LOOP}}} = \left\{\left[G(S)\right]_{\substack{\text{CONTINUOUS}\\\text{RATE LOOP}}}\right\} \text{ TIMES } \left\{e^{-ST_1}\right\}$$

WHERE

$$T_1 = (T_{Z.O.H} + T_D)$$

$$T_{Z.O.H.} = \frac{1}{2}\left[\frac{1}{f_s}\right], \; f_s = 400 \text{ Hz}$$

$$T_D = 300\ \mu\text{sec, DESIGN OBJECTIVE} \leq 600\ \mu\text{sec}$$

DIGITAL RATE LOOP GAIN-PHASE CHARACTERISTICS

$$\left[G_{D2}(S)\right]_{\substack{\text{PDAP}\\\text{HEADING}\\\text{POSITION}\\\text{LOOP}}} = \left\{\frac{1}{0.11S}\right\} \text{ TIMES } \left\{e^{-ST_2}\right\}$$

WHERE

T_2 IS THE EFFECTIVE TRANSPORT LAG OF THE YAW HEADING POSITION LOOP RELATIVE TO THE UPDATE RATE OF THE YAW RATE LOOP (400 Hz)

$$T_2 = \left[\frac{\sum_{i=1}^{N} i}{N}\right] T_S, \; T_S = \frac{1}{400}$$

CONTINUOUS PHASE APPROXIMATION OF THE DIGITAL OUTER LOOP GAIN-PHASE $\longrightarrow$ $T_2 = \left(\frac{N+1}{2}\right) T_S$

N – RATIO OF RATE LOOP UPDATE FREQUENCY TO THE YAW POSITION LOOP UPDATE FREQUENCY

DIGITAL HEADING POSITION LOOP GAIN PHASE CHARACTERISTICS

Figure C-6. Digital (PDAP) Gain-Phase Characteristics Using Continuous Transfer Function Relationships

TRANSPORT LAG FUNCTION	CONTINUOUS FUNCTION	YAW HEADING POSITION UPDATE RATE			
		400 Hz	100 Hz	50 Hz	25 Hz
RATE LOOP TRANSPORT LAG, T_1 – sec	0	300×10^{-6}	300×10^{-6}	300×10^{-6}	300×10^{-6}
EFFECTIVE POSITION LOOP LAG, T_2 – sec	0	2.5×10^{-3}	6.25×10^{-3}	11.25×10^{-3}	21.25×10^{-3}

GAIN AND PHASE CHARACTERISTICS		G(S)	$\frac{1}{0.11S}$	$\left[\frac{G(S)}{1+G(S)}\right]\frac{1}{0.11S}$	DIGITAL HEADING POSITION GAIN-PHASE			
					400 Hz $\left[\frac{G_{D1}(S)}{1+G_{D1}(S)}\right] G_{D1}(S)$	100 Hz $\left[\frac{G_{D1}(S)}{1+G_{D1}(S)}\right] G_{D1}(S)$	50 Hz $\left[\frac{G_{D1}(S)}{1+G_{D1}(S)}\right] G_{D2}(S)$	25 Hz $\left[\frac{G_{D1}(S)}{1+G_{D1}(S)}\right] G_{D2}(S)$
(2 Hz INPUT)	GAIN	0.5502	0.7234	0.4190	0.4237	0.4237	0.4237	0.4237
	PHASE	-111.33^{o}	-90	-168.68^{o}	-171.47^{o}	-174.17^{o}	-177.77^{o}	-184.97^{o}
(2.5 Hz INPUT)	GAIN	0.40907	0.5787	0.2656	0.2657	0.2657	0.2657	0.2657
	PHASE	-117.10^{o}	-90	-182.98^{o}	-186.67^{o}	-190.05^{o}	-194.55^{o}	-203.55^{o}

Figure C-7. Transport Lag and Gain-Phase Characteristics

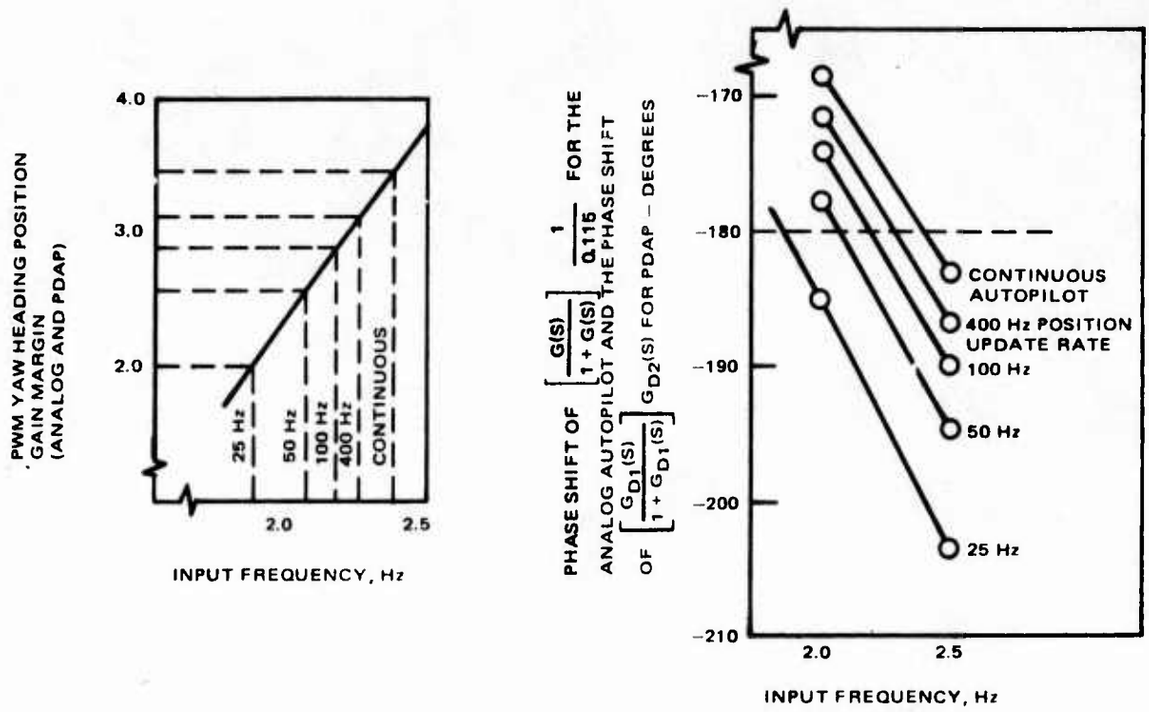

Figure C-8. PWM Yaw Heading Position Gain Margin

(The reverse of this page is blank)

INITIAL DISTRIBUTION

Hq USAF/RDPA	1	CG USAMICOM/AMCPM-CT-E	1
Hr USAF/RDQRME	1	DDC	2
Hq USAF/XOOFA	1	AFATL/DLJA	1
AFSC/INA	1	AFATL/DLJF	1
AFSC/SDA	1	USAF Academy	1
AFSC/DLCAW	1	ASD/SD-65	1
ASD/YFEI	1	AUL (AUL-LSE-70-239)	1
ASD/YFEA	1	ASD/ENFEA	1
ASD/YPEX	1	Hq USAF/SAMI	1
ASD/SD	1	Ogden ALC/MMWM	2
AFFDL/FEI	1	AFIS/INTA	1
AFAL/RW	2	Hq TAC/DRA	1
ASD/ENA	3	Hq USAFE/DOQ	1
TAC/DRAI	2	Hq PACAF/DOO	1
TAC/XPSY	1	Redstone Ars/DRDMI-TGG	1
AFAL/AAI	1		
ASD/YHEV	1		
ASD/XRG	2		
NAVAIR SYS COMD/AIR 360E	1		
NWC/Code 143	4		
NWC/Code 533	1		
AFFDL/FGL	1		
ATC (XPQS)	1		
NAVAIR SYS COMD/AIR-5323	1		
NAVAIR SYS COMD/AIR-5324	1		
OSD, ODDR&E/TST&E	1		
DARPA/TIO	1		
ADTC/PP	1		
ADTC/ADE	1		
TAWC/DT	1		
TAWC/TEFA	1		
TAWC/FTS	1		
ADTC/XR	2		
TRADDC/ADTC/DO	1		
AFATL/DL	1		
AFATL/DLB	1		
AFATL/DLA	1		
AFATL/DLMA	1		
ADTC/SD15	1		
AFATL/DLMT	1		
AFATL/DLMM	15		
AFATL/DLY	2		
ADTC/SD-7	1		
TAWC/TRADOCLO	1		
AFATL/DLOSL	9		
Redstone Sci Info Center	2		
Off Naval Research/Code 211	1		

(The reverse of this page is blank)